University of Naples "Federico II"

International PhD program
NOVEL TECHNOLOGIES FOR MATERIALS, SENSORS AND IMAGING
School of doctorate in Industrial Engineering

PHD THESIS

Engineering of Microfluidic Devices For Cell Hydrodynamic Manipulation

Stefania Torino

Supervisor:
Dr. Ivo Rendina
Institute of Microelectronics and Microsystems
National Council of Research

XXVII Cycle

If you can dream it,
you can do it.
(W. Disney)

Abstract

In the recent years microfluidic technology has affirmed itself as a powerful tool in medical and biological research. Micro-flowcytometers, micromixers, cell sorters and cell analyzers are only few examples of the developed devices. Among these different applications, cell manipulation in microfluidics has been widely investigated. Various methods for cell manipulation have been proposed, such as hydrodynamic, magnetic, optical, mechanical, and electrical, in this way categorized according to the manipulating force employed. In particular, in manipulating cells by hydrodynamic forces, since there is no needing of applying external forces, the design and fabrication phases of the device are simplified, and at the same time undesired effects on the biological sample are avoided. This thesis has been focused on the design, fabrication and testing of microfluidic devices that allow to make a complete cell characterization by only exploiting hydrodynamic effects.

The worldwide used technology for cell sample analysis is flowcytometry. Since cells focusing is the key point for the correct operation of a flowcytometer, several efforts have been made in order to reproducing it in a proper way on a micro-chip. In most cases, the traditional hydrodynamic focusing mechanism employing sheath fluid has been translated to the micro-scale. The main drawback in the approaches proposed till now, is that multiple inlets are needed. This brings to a high complexity if parallelization has to be introduced into the device. However, conventional flow cytometry measurements lose some information, if we consider that for the fluorescent signal only the information related to the total intensity is collected. This means that it is not possible to know the fluorescent signal distribution on the cell surface. This limitation has been recently overcome by introducing a new procedure, known as imaging flow cytometry, that allows to image each cell at high speed and therefore make available also the fluorescent distribution. Nevertheless, the traditional approach used for imaging cells in microfluidic systems allows to image cells by a single point of view. A way in which cells can be imaged by different sides, without the needing of moving the acquisition system, is to induce cell rotation as they flow through the channel.

My doctoral research activity has been mainly performed at the Naples Department of the Institute for Microelectronics and Microsystems (IMM) of the Italian National Research Council (CNR). Based on the problematics discussed before, my work has been focused on the design, fabrication, and characterization

of novel microfluidic devices for cell hydrodynamic manipulation.

Regarding the design phase, numerical simulations (COMSOL Multiphysics) have been used in order to find the most suitable geometry for the desired application. In order to realize the designed microfluidic chip, I have acquired the technical skills for the realization of microfluidic devices by using the PDMS replica molding technique. The device fabrication and testing have been performed respectively in the Clean Room and in the optical laboratory facilities at the IMM of Naples. Moreover, part of my doctoral thesis has been carried out during the period that I spent in the Optofluidic Cytometry Lab at the Rowland Institute at Harvard University, in collaboration with Dr. Ethan Schonbrun.

As discussed before, in most of the microfluidic devices for hydrodynamic focusing multiple inlets are needed, and this is a limitation if you want to introduce more parallel channels. Starting from

this consideration, the first part of this thesis has been related to the realization of a microfluidic device that allows to integrate hydrodynamic focusing and parallelization in a single device thanks to the fact that only one inlet is required. This is achieved by introducing a cross-filter region at each one of the parallel channels. On the second hand, in this thesis a microfluidic device that allow to control cell rotation by only taking advantage of hydrodynamic forces has been realized. The basic idea started from the consideration that, in a pressure driven flow, the velocity profile is parabolic. In particular, the velocity is minimum at the channel walls and reaches its maximum value at the center of the channel. This means that, if a cell is close to a channel wall, it will experience a velocity gradient on its surface, and therefore a rotation will be induced. A microfluidic device that allows to focus cells at the channel wall has been developed, and the correct device operation in inducing cell rotation has been tested by using asymmetrical shaped cells.

It is important to take in consideration that lab-on-chip technology introduced a breaking point in the design of bio-technological instrumentations, since there is not anymore interest in expensive benchtop instruments able to perform multiple analysis, but in small, cheap and disposable devices ad hoc for a single purpose. For this reason, in this work, it was necessary to define the cellular target, considering that since the optimization of the designed geometry mainly depends on the cell dimension. In particular, in this thesis the microfluidic devices have been designed in order to be suitable for analysis of Acute Lymphoblastic Leukemia (ALL) B-cells.

Acknowledgments

A great thanks goes to the Naples Department of the Institute for Microelectronics and Microsystems, where I have carried out most of my doctoral research activities. I would also like to acknowledge Techno System Developments (TSD) S.r.l. and Ste.Bi. S.r.l. for their support and the contribution in the development of my thesis project. Furthermore, I would like to express my gratitude to Dr. Ethan Schonbrun for the collaboration, and for allowing me to spend part of my doctoral activities in his lab at the Rowland Institute at Harvard.

Contents

1. Introduction

Microfluidics is a novel research field that has been rapidly spreading in the last two decades. Its development is related to the considerable progress done in the field of miniaturization.

Nowadays, it is effectively possible to integrate miniaturized fluidic, mechanical, thermal and opto-electronic systems on a chip. In 1980s, this perspective gave rise to a new field known as MEMS (micro-electro-mechanical systems), aimed at extending the capability and functions of microelectronics well beyond the traditional data elaboration and storing.

The first microfluidic device appears in the period when silicon-based MEMS began to take off. It was a miniaturized gas chromatography system, and it was created in the mid-seventies. This remarkable device circulated gas through microchannels etched in silicon. Anyway, it was only after 1991 that the advantages of miniaturization were thrust into the spotlight, and then all sorts of microfluidic systems began to be fabricated [1].

The main advantage of microfluidics is that at the micro-scale, microscopic amount of fluid can be handled. Since microfluidic channel dimensions stay in a range that goes from few microns to few millimeters, the required quantity of fluid is in the picoliters-nanoliters range. Therefore, scaling down in size allows to reduce the costs for sample and reagents, and at the same time it leads to the development of more sensitive and fast devices capable of isolating and analyzing minute quantities of sample in shorter times.

The perception is that microfluidics could have a revolutionizing impact on chemical analysis and synthesis, similar to the impact of integrated circuits on computers and electronics.

Microfluidic devices could change the way companies do business. Instead of selling a few expensive systems, companies could have a mass market of cheap, disposable devices. Making analysis instruments, tailored drugs, and disposable drug dispensers available for everyone will secure a huge market similar to that of computers today[2].

At the beginning of the microfluidic technology, in order to promote a widespread use of microfluidic devices in biology, all the scientific community agreed on the fact that a faster, less expensive, and less specialized method for device fabrication was needed. A first significant step forward was due to the researchers of Bell Labs in 1974, who developed a technique of molding a soft (elastomeric) material from a lithographic master [3-4]. Since then, soft lithography was used to pattern surfaces via stamping, and fabricate microchannels using molding and embossing. Anyway, the way in which soft lithography is used in microfluidics was completely revolutionized by Whitesides and co-workers [5-7] with the introduction of the poly(dimethylsiloxane) (PDMS) as material for the microdevices fabrication (see fig.1). The use of PDMS elastomer for miniaturized microfluidic bioassays has numerous advantages over silicon and glass. PDMS is inexpensive, flexible, and optically transparent down to wavelength of 230 nm, and therefore compatible with many optical methods for detection. Moreover, this polymer is compatible with biological studies because it is impermeable to water, nontoxic to cells, and permeable to gases. A final, major advantage of PDMS over glass and silicon is the easiness with which it can be fabricated and bonded to other surfaces[8].

The optimism surrounding microfluidics was well warranted. Microsystems are already revolutionizing the biomedical research. In the near future, we will see a growing trend towards the production of tailored microfluidic devices satisfying particular needs, which may be clinical, pharmaceutical, or biotechnological. Moreover, the integration of photonics in microfluidics is greatly extending the capabilities of microsystems, creating a new technology platform, often referred to as optofluidics [9].

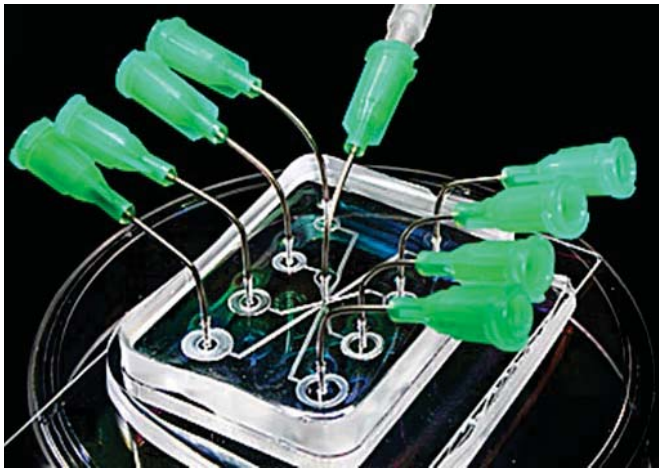

Figure 1: A microfluidic chip in polydimethylsiloxane (PDMS).

As electronic integrated circuits have transformed the world of electronics, integrated microfluidic and photonic circuits hold the promise to revolutionize the field of biomedicine. In spite of the rapid advances in microfluidics and photonics, however, the field is admittedly still in its embryonic stage. A target application is needed to guide the technology development: a bio-microsystem that could not only be the workhorse for the industry, but also a test vehicle to assess and benchmark the technology. The flow cytometer is a good candidate to meet these requirements [10-12].

Cytometry is a process in which physical and chemical characteristics of single cells, or by extension of other biological or no biological particles in roughly the same size range, are measured. In flow cytometry the measurements are made as the cells or particles pass through the measuring apparatus in a fluid stream [14].

A flow system brings cells one by one through an interrogation point, where they are illuminated by a light beam. The illuminated cell scatters the light with a characteristic directional intensity distribution. Further, fluorescently tagged antibodies are often used to mark and identify cells. Thus, both scattered and fluorescent light (made of one or more colors) is measured, providing a number of parameters to yield statistics about sample sub-populations. Flow cytometry is routinely used in the diagnosis of health disorders, and it has applications in a number of fields, including molecular biology, pathology and immunology. In this wide range of application fields, there is the need of developing devices that can substitute the traditional flow cytometry instrumentation, reducing costs and increasing portability. Lab-on-chip and microfluidic technology allows to have automating complex diagnostic procedures that are normally performed in a centralized laboratory into a hand-held microfluidic chip.

A Lab on chip device would have to perform reliably under the constraints of low cost, absence of trained workers, lack of electricity, poorly equipped laboratories, and transportation and storage in unrefrigerated conditions. The development of this novel technology could meet the urgent need in developing countries for new health-related technologies, and specifically, new technologies for health diagnostics [15].

The great interest in developing small-footprint flow-cytometers integrated on a chip by exploiting microfluidic technologies requires to address three main issues:

a) Cell focusing in the microfluidic channel;
b) miniaturization of the fluid-handling components;

c) miniaturization of the interrogations optics.

So, the first important requirement in order to correctly analyze particles is that they must be focused. This means that each particle must be isolated in some way so that it can be interrogated individually within a precise detection region. For this purpose, the fluidic system of a flow cytometer consists of two fluid streams, *viz*., the sample stream and the sheath stream. In operation, the sample stream flows constantly and is managed by regulating the air pressure in the sample chamber. Another pressure regulator acting on the sheath reservoir controls the flow rate of the sheath stream. Alternatively, a finely tuned syringe pump can be used to precisely control the flow rates of sample and sheath fluids for setting the optimum flow condition. As the velocities of the two streams are adjusted to attain laminar flows, the sheath stream is essentially cell-free fluid surrounding the center sample stream, so holding aligned in a single line (focusing) the cells transported by the sample stream (see fig.2).. The associated phenomenon is referred as *hydrodynamic focusing*[13-14].

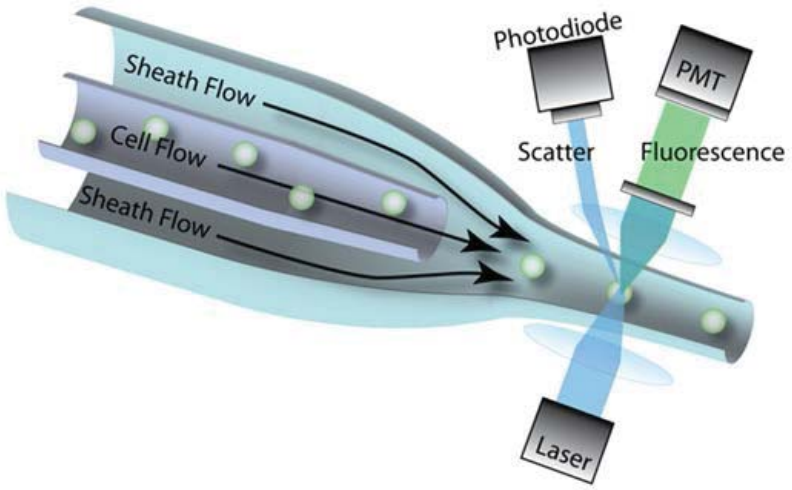

Figure 2: Schematic of a flow cytometer (D. Heikali et al. 2010 51)

The hydrodynamic focusing is a crucial condition to be fulfilled for reliable optical analysis of cells, and it is an important issue in the development
of microfabricated flow cytometer channel systems. As a matter of fact, in lab-on-a-chip development, cell focusing is still an open problem. Anyway, in principle microfabricated channel structures with multiple laminar flow configurations could be capable of stably delivering samples to a detection area with higher accuracy and better flow control compared to conventional glass capillary-based fluidic systems. Moreover, the advantages of using microfabrication include the ability to create desired structures rapidly and inexpensively, and to obtain optimized channel geometries that are difficult or impossible to fabricate using conventional glass machining techniques.

Concisely, hydrodynamic focusing can be defined as the confinement or the redirection of a slower flowing stream by a faster flowing stream. In general, the cross-sectional area of a focused stream can be predicted by the relative flow rates of the two streams. Achieving a precise control of the focused sample stream width is crucial in various applications. For example, in cell counting and sorting applications performed in micromachined-based flow cytometers, the width of the focused cell stream should be of the same order of magnitude as that of the cell size. In diffusion-based mixers [15] the characteristic time required to achieve mixing via diffusion effects depends on the diffusion characteristic length, which in turn depends on the width of the focused stream. In practice, the diffusion time reduces as the width of the focused stream decreases.
Actually, it has to take in consideration that not only the velocities at the inlets, but also the geometry of the microfluidic device has a high impact on the characteristics of the focused stream.
Predicting the forces that control the focused stream is more complex than simply calculating the ratio of the relative flow rates. Concerning this point, the scientific community agrees that numerical simulations of fluid flows through the microdevices, will facilitate in the derivation of the better design. This is not a novel approach, since numerical methods have been adopted for long now, to solve physic and engineering problems.

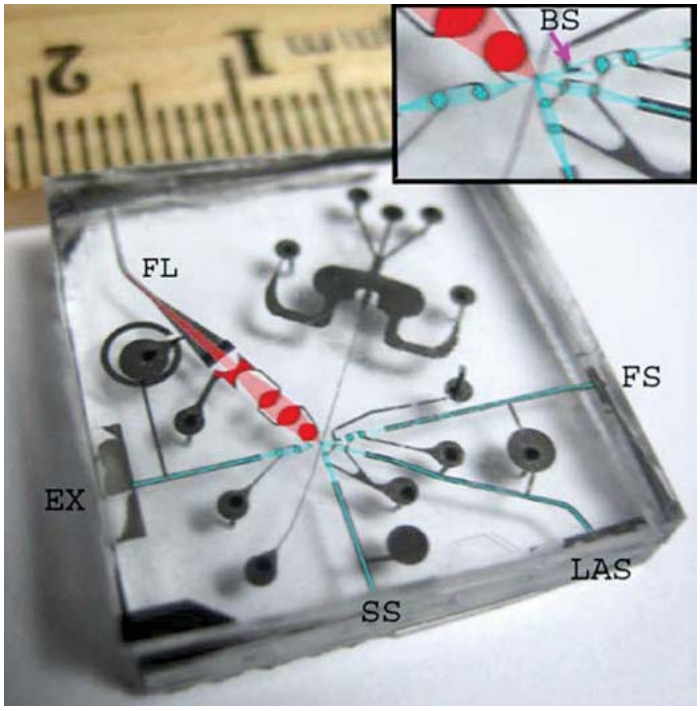

Figure 3: Early prototype of a microfluidic cytometry chip including waveguides and lenses for an excitation source (EX), a forward scatter collection line (FS) including a beam stop (BS), a side scatter collection line (SS), a large-angle scatter collection line (LAS), and a line for fluorescence collection (FL) (unpublished). The seamless integration of fluidic and photonic elements is accomplished by simple microfabrication techniques [25].

Starting from the development of microfluidic flow-cytometers [16], several scientists have focused their work on the use of hydrodynamic forces for different purposes [17]. Hydrodynamic effects have been used in order to manipulate

cells [18], DNA [19] and droplets [20]. Moreover, hydrodynamic methods have been adopted for performing label-free cells separation and sorting [21]. Hydrodynamic methods for cells separation include flow fractionation [22], hydrodynamic filtration [23], and deterministic lateral displacement [24].

Particles and cells manipulation based on fluid flow control introduces several advantages on the other existing methods. It is possible to realize microfluidic devices in which observation and analysis of target particles are performed in an environment free from electro-magnetic and acoustic force fields.

The work of this thesis has taken inspiration from this scientific background, and it has been devoted to the engineering of microfluidic devices that allow to manipulate particles or cells by taking advantage of hydrodynamic effects.

My research activity has been covered the following three areas:

1. Design;
2. Fabrication, and
3. Characterization

of novel microfluidic devices for hydrodynamic cells manipulation.

Regarding the design phase, numerical simulations have been used in order to support the choice of the right microfluidic geometry. The use of numerical analyses for design evaluation can help in understanding the behavior and characteristics of the system. Indeed, in microfluidics, effective control of the fluid properties depends on how it behaves under the applied conditions and on the micro-channel shape.

In this work, each microfluidic device was analyzed by using the software Comsol Multiphysics. Comsol is a versatile and flexible high-level software for solving partial differential equations in different fields of the physical sciences. Within the Comsol modules, Microfluidics Module brings tools for the study of microfluidic devices. This module is designed for researchers, engineers, and experimentalists working on applications in the field of lab-on-chip devices, digital microfluidics, biosensors, electrokinetic and magnetokinetic devices, inkjet technology, and vacuum system design.

By coupling the Microfluidic Module and the Particle Tracing one, it has been possible to predict the behavior of the flowing objects. By solving the Navier-stokes equations, the velocity profile of the fluid could be obtained. From this results, the drag forces and its effect on driving particles motion could be estimated.

Therefore, Comsol simulation has been an useful support in the evaluation of the better microfluidic design, according to each particular application.

After the consolidation of the design phase, I started the second step necessary to complete the work, and hence I passed to the fabrication of the designed micro-devices. This activity has been done in the clean room facility at the Institute for Microelectronics and Microsystems (IMM – Department of Naples) of the Italian National Research Council (CNR).

The microfluidic chips have been realized using the standard PDMS replica-molding technique, already described previous in this chapter. The negative master of the designed pattern was realized in the photolithography laboratory, within the clean room facility. For this process, depending on the features resolution required for each design, a chromium or a film mask have been used. Negative photoresists from the SU-8 (Microchem) series have been used. The permanent sealing of the PDMS samples with the glass substrates have been achieved through an oxygen plasma treatment, performed in a Reactive Ion Etching (RIE) chamber.

After the chips have been realized, I passed to the characterization phase. The device operation was tested in the optical laboratory facility, by adopting a traditional set-up for looking into microfluidic devices (Figure 4).

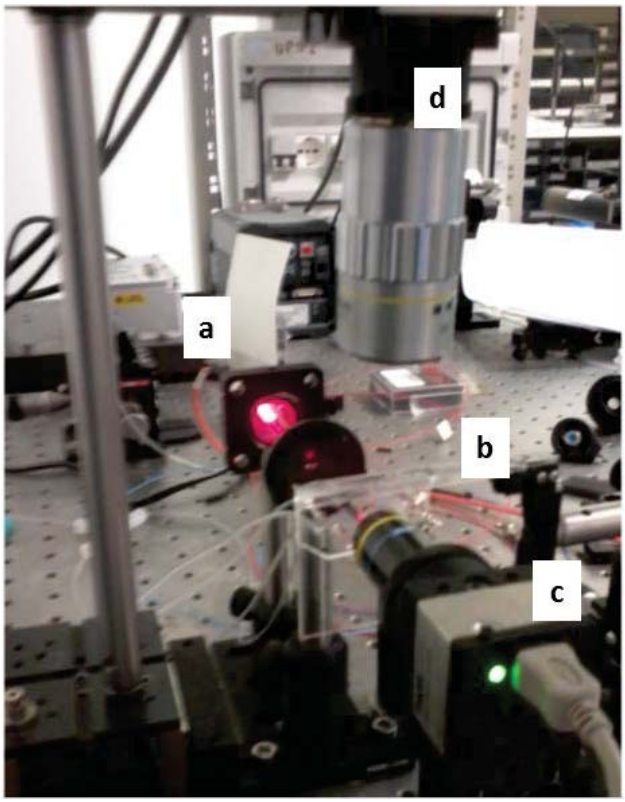

Figure 4: Optical Set-Up for characterization of the microfluidic devices. (a) Laser Illumination Source. (b) Microfluidic Chip. (c) Camera for imaging the fluid flow from a frontal point of view. (d) Camera for imaging the fluid flow from a lateral point of view.

As discussed before, the first microfluidic applications, related to hydrodynamic effects to control cells or particles position, have been focused on the development of a micro-flow cytometer.

The main effort in this research stream concerns the achievement of an hydrodynamic focusing that exactly repeats the one of a traditional flow cytometer. The main problem in the achievement of this aim is due to the fact that microfluidic devices are based on two-dimensional patterns. This makes difficult to control the particles position in the vertical (out-of-plane) direction.

Applications of two-dimensional [26] (in-plane) hydrodynamic focusing in cell/particle counting in planar micro-flow cytometers have been proposed. In these devices, it could happen that cells or particles may not pass the focused stream one by one even though the focused stream width is focused to the same order of magnitude as that of the cell size. This is because they may be located at different depths in the microchannel, as their size is smaller than the channel height. It will affect the detection performance of such flow cytometers.

Various microfabricated devices for the achievement of 3D hydrodynamic focusing (both in the in-plane and out-of-plane directions) have been reported [27-29]. In most of these studies, 3D focusing is achieved by delivering sheath flows from both vertical and horizontal directions using multi-layer 3D microfluidic devices. Multi-step photolithography and assembly protocols have been developed for fabricating the 3D microfluidic structures needed for 3D hydrodynamic focusing. However, such methods require either tedious assembly of individual

components or multiple alignments and exposures during mold fabrication. These limitations inevitably increase the cost and complexity of the device and ultimately hinder their applicability.

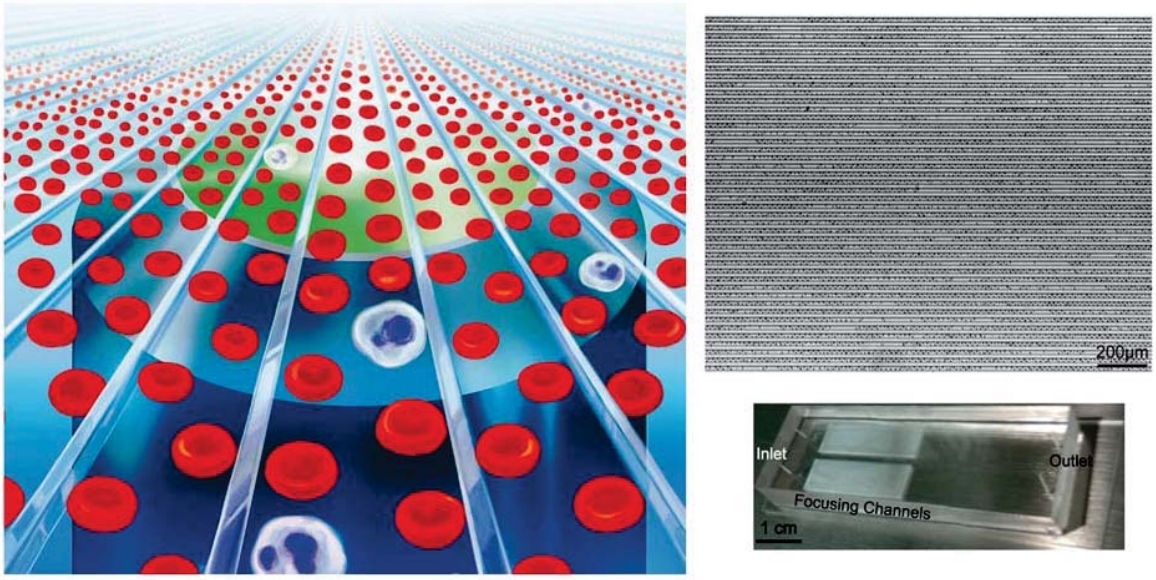

Figure 5: Inertial effects for sheath-free, parallel-flow cytometry with extreme throughput for rapid and accurate cell differentiation. In the 256 parallel channels cells are aligned at the center of the channel as they reach the region closer to the outlet (SC Hur et al. 2009 [32])

One of the main complexity is introduced by the needing of multiple inlets for the sample and the sheath fluids. Therefore, if we want to introduce parallelization in the device, the design of really complex microfluidic networks is required.

Parallelization [33-35] is one of the most advantages of using microfluidic technology. In a parallelized configuration, there are multiple microfluidic channels working simultaneously. One of the introduced advantages is the possibility to increase the throughput of the device, without the need of increasing the fluid flow velocities. Since there is the possibility to work at moderate flow velocities, the imaging of flowing objects is allowed without the necessity of high performance acquisition systems. Moreover, parallelization helps in extending the operation time of the device. Everyone working in microfluidics knows that a main cause of chip failure is the clogging of the fluidic channel. If you have parallel channels, even if one or two of them get clogged, the experiment can be continued.

Part my doctoral research activities have been focused on the development of a parallel microfluidic device that allows getting hydrodynamic focusing, without needing high-complicated designs.

I started this project during the period that I spent at the Rowland Institute at Harvard University, where I have collaborated with the Dr. Ethan Schonbrun, P.I. of the Optofluidic Cytometry Lab.

In the solution that we found out, there is only the need of one inlet for the sample fluid. A cross-filter is introduced at each channel. In a cross (or tangential) filter, the fluid flows parallel to the pores membrane. This allows having a better filter efficiency than a traditional dead-end filter. In the developed device, the design has been optimized in

order that when the sample fluid arrives at the filter region, only the buffer can cross the filter barrier. In this way particles are forced at the center, and they get focused in the region where they are recombined with the lateral fluid (Figure 6).
Examples of microfluidic applications of the cross-filtration method have been proposed for different purposes: separation of red blood cells (RBCs) from white blood cells (WBCs) [36]; separation of blood cells from plasma [37]; compartmentalization of culturing chamber in order to generate shear stresses of varied magnitudes [38]; separation of particles or cells of a specific size within a continuous flow system [39].

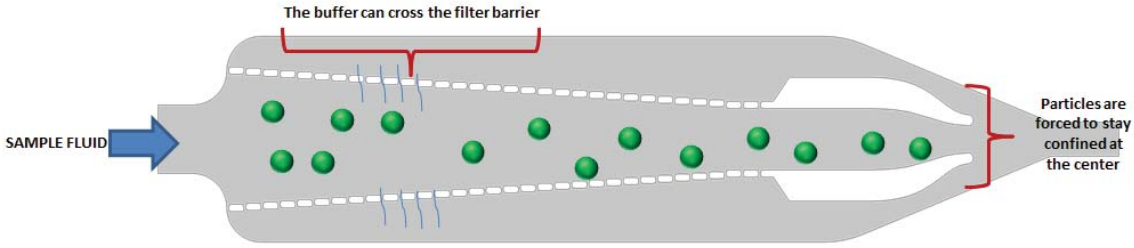

Figure 6: Operating principles of the cross-filtration for generate a self-hydrodynamic focusing in a parallel microfluidic device.

Our idea of integrating a cross-flow filter on the chip, allows combining hydrodynamic focusing and parallelization in the same device. It is a promising configuration for the development of a parallelized microflow cytometer.
As already explained, flow cytometry is one of the most used technique for cells analysis. It is also a powerful tool for analyzing multiple fluorescent signals from a large number of cells flowing [40-41] in suspension.
However,, conventional flow cytometry uses the total fluorescent signal from the entire cell to characterize the sample, and averages over the local distribution and morphology of the signal. Recent advances in imaging flow cytometry enable the collection of fluorescent images of each cell at high speed, and therefore add the fluorescent distribution to the available information.
However, such systems use extended depth-of-field imaging to compress the cell into a 2D image based on the orientation of the cell and of the imaging system, which in most cases is uncontrolled and random. Such systems allow some insight into the distribution of the signal, but due to the three-dimensional nature of the sample, are limited in their capabilities.
By controllably rotating the cell as it passes through the flow system, it would be possible to reconstruct the 3D distribution using tomographic methods, and gain further insight into the system [42] .
Moreover, precise translation and rotation of biological entities, such as cells, are two fundamental manipulation requirements in applied biotechnological research [43-45]. During the period that I have spent at the Rowland Institute, I also worked on the development of a microfluidic device that induces cells rotation by taking advantage of hydrodynamic forces.
In microfluidics, for a driven pressure flow, the velocity follows a parabolic profile [46], and the maximum value is achieved at the center of the channel, whilst the minimum at the walls. If a cell is focused at a channel wall, the two

opposite sides of its surface, one close to the wall and the other closer to center, experience two different velocity values. Due to this effect a rotation is induced [47] (Figure 7).

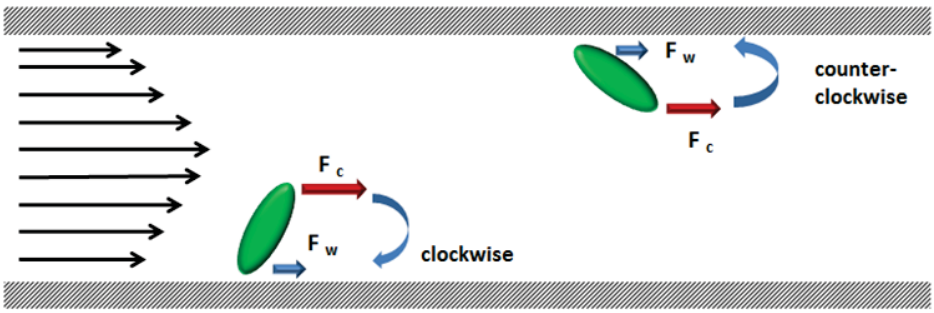

Figure 7: Objects focused at the walls in a channel characterized by a parabolic velocity profile. The velocity difference that they experience on their surface induces a rotation.

In this way it could be possible to do a more complete cellular analysis, by having the accessibility to look at cells by multiple point of views.

By coupling flow-cytometric measurement with imaging analysis, a whole characterization of the biological samples can be obtained.

As already mentioned, the objective of microfluidic technology is the realization of cheap, disposable, small devices suitable for a particular application.

Microchannel geometries need to be optimized according to the target cellular topology. This kind of approach well fits the needs of the market interested into the production of cheap and disposable microfluidic devices for the point-of-care diagnostics. No more expensive instrumentations dedicated to multiple applications, but cheaper devices ad hoc for a particular analysis.

In this work, the size of the target cells played a crucial role in the choice of the values for the geometrical parameters of each micro-device.

The principal aim of thesis has been the engineering of parallel microfluidics device that could allow to make both cytometric measurements and 3D imaging of lymphocytes. Therefore, the target object size was around 8-10 µm. There are two main applications in which we have been interested on: $CD4^+$ and $CD4^+/CD8^+$ counting , for HIV and AIDS diagnosis; and blast cells identification, for leukemia diagnosis.

Just think of the possibility to have disposable and easy transportable devices that could allow to make these analysis in all the places in which is not possible to use traditional instrumentation.

This will satisfy a new market that expresses the need of novel micro-devices for point of care diagnostics [48].

Thanks to these promises, microfluidic technology has been spreading more and more in the last years.

The development of the lab-on-a-chip brings about possibilities of handling very small volumes, bringing about the opportunity to analyze samples that were previously beyond our reach. In addition, it has proven to have the capacity to increase both speed and sensitivity. It also facilitates automation of experimental processes, which increases speed, precision, accuracy and reproducibility relative to equivalent procedures performed by hand.
Other benefits include rapid device prototyping and disposability. These qualities combined with the fact that this is a tool on the same scale as the single cell and many of the fundamental biological processes makes the lab-on-a-chip a well suited means for investigating and manipulation of these very processes.
Significant effort becomes necessary in the design phase, in order to optimize the way in which cells or particles are manipulate, and simplify the chip fabrication process as much as possible.
The results achieved in this thesis demonstrate the possibility to engineer the fluid flow in microfluidic devices, suitable for each required application, by taking advantage of the hydrodynamic effects.
In this way position, orientation and trajectories of cells or particles can be controlled without the needing of additional external physical forces [49-50].

References

1 Tabeling P., Introduction to Microfluidics, 2005, Oxford University Press

2 Nam-Trung Nguyen, Steven T. Wereley, fundamentals and applications of microfluidics, 2nd edition, 2006 ARTECH HOUSE, INC.

3 David J. Beebe, Glennys A.Mensing, and Glenn M.Walker, Physics and applications of microfluidics in biology, Annu. Rev. Biomed. Eng. 2002. 4:261–86

4 Aumiller G, Chandross E, Tomlinson W, Weber H. 1974. Sub-micrometer resolution replication of relief patterns for integrated optics. J. Appl. Phys. 45:4557–62

5 Xia Y, Whitesides GM. 1998. Soft lithography. Annu. Rev. Mat. Sci. 28:153–184

6 Duffy D, McDonald J, Schueller O,Whitesides G. 1998. Rapid prototyping of microfluidic systems in poly (dimethyl siloxane). Anal. Chem. 70:4974–84

7 Whitesides GM, Ostuni E, Takayama S, Jiang XY, Ingber DE. 2001. Soft lithography in biology and biochemistry. Annu. Rev. Biomed. Eng. 3:335–73

8 Samuel K. Sia, George M. Whitesides, Microfluidic devices fabricated in poly(dimethylsiloxane) for biological studies, Electrophoresis 2003, 24, 3563–3576

9 Y. Fainman, L. Lee, D. Psaltis, C. Yang, Optofluidics: Fundamentals, Devices, and Applications, McGraw-Hill, Inc. New York, NY, USA ©2010

10 Jessica Godin, Chun-Hao Chen, Sung Hwan Cho, Wen Qiao, Frank Tsai andYu-Hwa Lo, Microfluidics and photonics for Bio-System-on-a-Chip: A review of advancements in technology towards a microfluidic flow cytometry chip, 2008, Journal of Biophotonics, 5: 355–376

11 Huh, D., Gu, W., Kamotani, Y., Grotberg, J. B., Takayama, S., Microfluidics for flow cytometric analysis of cells and particles, Physiol. Meas. 2005, 26, R73–R98.

12 Taek Dong Chung and Hee Chan Kim, Recent advances in miniaturized microfluidic flow cytometry for clinical use, Electrophoresis 2007, 28, 4511–4520

13 H.M. Shapiro, Practical Flow Cytometry: Parameters and Probes, 3rd Edn (Wiley-Liss, New York, 1994).

14 M. Ormerod, Flow Cytometry: A Practical Approach, 3rd Edn (Oxford University Press, Surrey, U.K., 2000).

15 Knight J B, Vishwanath A, Brody J P and Austin R H 1998, Hydrodynamic focusing on a silicon chip: mixing nanoliters in microseconds Phys. Rev. Lett. 80 3863–6

16 S. Chung, S. J. Park, J. K. Kim, C. Chung, D. C. Han, J. K. Chang, Plastic microchip flow cytometer based on 2- and 3-dimensional hydrodynamic flow focusing, Microsystem Technologies 9 (2003) 525–533

17 PAK KIN WONG, YI-KUEN LEE AND CHIH-MING HO, Deformation of DNA molecules by hydrodynamic focusing, J. Fluid Mech. (2003), vol. 497, pp. 55–65

18 Khalili, A.A., Basri, M.A.M., Ahmad, M.R., Single cell trapping in microfluidic channel via hydrodynamic manipulation, IEEE International Conference on Control System, Computing and Engineering (ICCSCE), 2013, 596 - 601

19 Yannick Viero, Qihao He and Aurélien Bancaud, Hydrodynamic Manipulation of DNA in Nanopost Arrays: Unhooking Dynamics and Size Separation, Small, 24: 3508–3518

20 Chun-Guang Yang, Zhang-Run Xu, Jian-Hua Wang, Manipulation of droplets in microfluidic systems, Trends in Analytical Chemistry, Vol. 29, No. 2, 2010

21 Gossett DR, Weaver WM, Mach AJ, Hur SC, Tse HT, Lee W, Amini H, Di Carlo D., Label-free cell separation and sorting in microfluidic systems, Anal Bioanal Chem. 2010 Aug;397(8):3249-67

22 Takagi J, Yamada M, Yasuda M, Seki M (2005) Continuous particle separation in a microchannel having asymmetrically arranged multiple branches, Lab Chip 5:778

23 Yamada M, Seki M (2005) Hydrodynamic filtration for on-chip particle concentration and classification utilizing microfluidics, Lab Chip 5:1233–1239
24 Inglis DW (2009) Efficient microfluidic particle separation arrays, Appl Phys Lett 94:013510–013513
25 J. Godin, V. Lien, and Y. Lo, Integrated fluidic photonics for multi-parameter in-plane detection in microfluidic flow cytometry, in 19th Annual Meeting of the IEEE Lasers and Electro-Optics Society, 2006, 605–606.
26 Claire Simonnet and Alex Groisman, Two-dimensional hydrodynamic focusing in a simple microfluidic device, Appl. Phys. Lett. 87, 114104 (2005)
27 N. Sundararajan, M. S. Pio, L. P. Lee and A. A. Berlin, Three-dimensional hydrodynamic focusing in polydimethylsiloxane (PDMS) microchannels, J. Microelectromech. Syst., 2004, 13, 559–567.
28 Yu-Jui Chiu, Sung Hwan Cho, Zhe Mei, Victor Lien, Tsung-Feng Wu, and Yu-Hwa Lo, Universally applicable three-dimensional hydrodynamic microfluidic flow focusing, Lab Chip. May 7, 2013; 13(9): 1803–1809
29 Chih-Chang Chang, Zhi-Xiong Huang and Ruey-Jen Yang, Three-dimensional hydrodynamic focusing in two-layer polydimethylsiloxane (PDMS) microchannels, J. Micromech. Microeng. 17 (2007) 1479–1486
30 Xiaole Mao, John Robert Waldeisen and Tony Jun Huang, ‘‘Microfluidic drifting’’—implementing three-dimensional hydrodynamic focusing with a single-layer planar microfluidic device, Lab Chip, 2007,7, 1260-1262
31 Claire Simonnet and Alex Groisman, High-Throughput and High-Resolution Flow Cytometry in Molded Microfluidic Devices, Anal. Chem. 2006, 78, 5653-5663
32 Soojung Claire Hur, Henry Tat Kwong Tse and Dino Di Carlo, Sheathless inertial cell ordering for extreme throughput flow cytometry, Lab Chip, 2010,10, 274-280
33 E. Schonbrun, S. S. Gorthi, and D. Schaak, "Microfabricated multiple field of view imaging flow cytometry," Lab Chip, 12, 268-273 (2012)
34 Hur SC, Tse HTK, Di Carlo D. Sheathless inertial cell ordering for extreme throughput flow cytometry, Lab on a Chip 2010; 10:274-280
35 Hur SC, Mach AJ, Di Carlo D. High-throughput size-based rare cell enrichment using microscale vortices. Biomicrofluidics 5, 022206 (2011)
36 Xing Chen, Da Fu Cui, Chang Chun Liu, Hui Li, Microfluidic chip for blood cell separation and collection based on crossflow filtration, Sensors and Actuators B 130 (2008) 216–221
37 Virginia VanDelinder and Alex Groisman, Separation of Plasma from Whole Human Blood in a Continuous Cross-Flow in a Molded Microfluidic Device, Anal. Chem. 2006, 78, 3765-3771
38 X. Zhang, D. J. Huk, Q. Wang, J. Lincoln, and Y. Zhao, A microfluidic shear device that accommodates parallel high and low stress zones within the same culturing chamber, BIOMICROFLUIDICS 8, 054106 (2014)
39 Sean C. Gifford, Angela M. Spillane, Seth M. Vignes and Sergey S. Shevkoplyas, Controlled incremental filtration: a simplified approach to design and fabrication of high throughput microfluidic devices for selective enrichment of particles, Lab Chip. 2014 Dec 7;14(23):4496-505
40 E. Schonbrun , R. Malka , G. Caprio , D. Schaak , and J. M. Higgins , Quantitative absorption cytometry for measuring red blood cell hemoglobin mass and volume, Cytometry, Part A. 85(4), 332–338 (2014).
41 Michael J. Rosenbluth, Wilbur A. Lam, and Daniel A. Fletcher, Analyzing cell mechanics in hematologic diseases with microfluidic biophysical flow cytometry, Lab Chip. 2008 Jul;8(7):1062-70
42 Thorsten Kolb, Sahradha Albert, Michael Haug, and Graeme Whyte, Optofluidic rotation of living cells for single-cell tomography, J. Biophotonics 1–8 (2014)
43 Y. L. Liang, et al., Cell rotation using optoelectronic tweezers. Biomicrofluidics, 2010. 4(4): p. 43003.
44 C. Leung, et al., Three-dimensional rotation of mouse embryos. IEEE Trans Biomed Eng, 2012. 59(4): p. 1049-56
45 C.-H. Chiou and G.-B. Lee, A micromachined DNA manipulation platform for the stretching and rotation of a single DNA molecule. Journal of Micromechanics and Microengineering, 2005. 15(1): p. 109.

46 Stone, H. A. and Kim, S. (2001), Microfluidics: Basic issues, applications, and challenges. AIChE J., 47: 1250–1254.
47 D. S. Clague, and P. J. Cornelius, The hydrodynamic force and torque on a bounded sphere in Poiseuille flow, Int. J. Numer. Meth. Fluids 2001; 35: 55–70
48 Frank B. Myersa and Luke P. Lee, Innovations in optical microfluidic technologies for point-of-care diagnostics, Lab Chip, 2008,8, 2015-2031
49 S. I. Han, Y. D. Joo, and K. H. Han, An electrorotation technique for measuring the dielectric properties of cells with simultaneous use of negative quadrupolar dielectrophoresis and electrorotation. Analyst, 2013. 138(5): p. 1529-37.
50 Junjie Zhu, Xiangchun Xuan, Dielectrophoretic focusing of particles in a microchannel constriction using DC-biased AC flectric fields, Electrophoresis 2009, 30, 2668–2675
51 Daniel Heikali and Dino Di Carlo, A Niche for Microfluidics in Portable Hematology Analyzers, Journal of Laboratory Automation August 2010 vol. 15 no. 4 319-328

2. Microfluidic and Lab-on-Chip Technologies

In the recent years Microfluidics has established as a research field which is spreading faster and faster. The possibility to realize hand-handle devices, that allow getting the same results obtained by traditional instrumentation, has kept the interest of a wide scientific community. The small length scale of these systems introduces many simplifications in the theoretical equations that describe their behavior. The improvements that have been done in microfabrication allowed making easier the realization of these lab-on-chip devices.
Applications that involve microfluidic technology have interested a wide range of fields, although the most are related to biomedicine.

2.1 What is Microfluidics?

Microfluidics has been defined as ***"the science and technology of systems that process or manipulate small (10^{-9} to 10^{-18} liters) amounts of fluids, using channels with dimensions of tens to hundreds of micrometers"*** [1].
Switching from standard laboratory setups to systems that are in the micron and millimeter scale introduces several advantages. A direct consequence of the previous definition is that the use of micro-devices allows to significantly reduce the fluid quantity needed for system operation.
According to a second highly diffused definition, ***"microfluidics is the science and engineering of systems in which fluid behavior differs from conventional flow theory primarily due to the small length scale of the system"***.
This means that scaling down dimensions, the physical effects to consider are different to what happens on a "macro"-domain. Hence, in order to characterize the fluidic behavior in the micro-world, the standard equation from fluid dynamics are used, but some assumptions and simplifications are adopted due to the small size of the system.

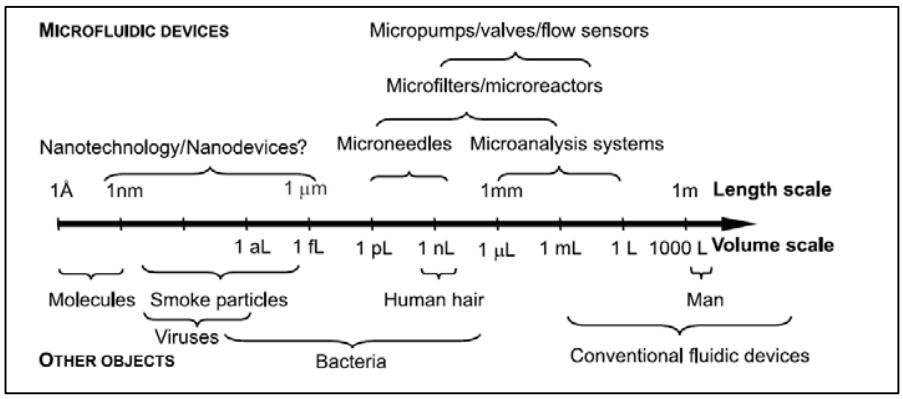

Figure 1: Characteristic sizes for macro- ad nano-devices.

2.2 Theoretical basis for Microfluidics

From the point of view of fluid mechanics, all matter consists of only two states, fluid and solid. The difference between the two is perfectly obvious, a solid can resist a shear stress by a static deformation; a fluid cannot. Any shear stress applied to a fluid, no matter how small, will result in motion of that fluid. The fluid moves and deforms continuously as long as the shear stress is applied.

We can think of a fluid as a continuous medium made up of small fluidic elements. A fluid element is made of millions of molecules, but can be considered homogeneous enough to have physical properties like density, viscosity and volume, and can also be moving, i.e. have a velocity (and possibly an acceleration) associated with it.

Two types of forces may act on a small fluid element: body forces and surface forces. Body forces like gravity and electromagnetism are forces that act at a distance and influence the whole body of the fluid element. For example the force of gravity will tend to pull any fluid element downwards. From elementary physics we know that this fluid element would accelerate, if it were not for some opposing force. The opposing forces are surface forces that act on surfaces. They can take on two forms: either the force can be normal to the surface or tangential to it.

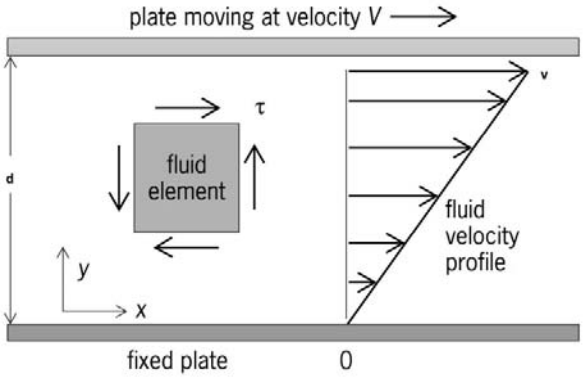

Figure 2: Schematic of the Newton experiment to determine the viscosity of the fluid

The normal force per unit area, pressure, can compress or dilate the fluid; the tangential force per unit area called shear, tends to deform the fluid body. When we go down to the microfluidic scale, these surface forces gain in importance as the size scale reduces.

A key property to take in consideration when you are working with a fluid is the viscosity μ. It is defined as the property of a fluid that determines its resistance to shearing stresses. It is a measure of internal fluid friction which exerts resistance to flow, it is primarily due to cohesion and molecular momentum exchange between fluid layers which appears as shearing stresses between the moving layers of the fluid when the flow takes place.

Newton described the viscosity of a fluid through a simple experiment, by using two parallel plates separated by a distance *d*, and with a fluid in between. If the plate on the bottom is kept fixed, the force required to move the top plate forward is obtained by the following formula:

$$\frac{F}{A} = \mu \frac{v}{d} = \mu \tau$$

Here *F* is the force, *v* the velocity of the plate, *A* the area of the plate and *d* the distance between the plates, μ the viscosity, and τ is the shear stress.
For many fluids the coefficient of viscosity is nearly independent of velocity. These are called Newtonian fluids. For some fluids, the viscosity can vary in many interesting ways, for instance depending on the velocity or past history.
Fluids can be shear thinning or shear thickening, and can have complicated time dependent effects, many of which are not completely understood.
The fluid flow inside a microfluidic channel is determined by applying the same equation that is used in fluid dynamics for modeling fluidic behavior [2]:

$$\rho \left(\frac{dv}{dt} + v \cdot \nabla v\right) = -\nabla \mathrm{p} + \mu \nabla^2 v + f$$

and it is the well-known ***Navier-Stokes equation***, written for a non-compressible fluid. In the previous statement ρ refers to the fluid density, *v* the velocity field, *p* the pressure drop across the channel, μ the fluid viscosity, and *f* the volume forces.
Conceptually, the equation can be considered as a balance of the forces acting on each single fluid element:

$$\overrightarrow{net\ inertial\ force} = \overrightarrow{net\ pressure\ force} + \overrightarrow{net\ viscous\ force}$$

In most of the microfluidic devices, the inertial forces are negligible. This means that the previous equation can be simplified as a balance between pressure forces and viscous forces:

$$\overrightarrow{net\ pressure\ force} = -\overrightarrow{net\ viscous\ force}$$

Or in another form

$$\nabla p = \mu \nabla^2 v$$

The ratio between the inertial and viscous forces defines a dimensionless number that is used in fluid-dynamics to characterize the fluid behavior:

$$Re = \frac{inertial\ forces}{viscous\ forces} = \frac{\rho v L}{\mu}$$

Re is known as Reynolds number. **It is used to classify a fluid flow as laminar or turbulent**. If the ***Re* < 2000** we are in laminar dominated regime, whilst if ***Re > 2000*** we are in a turbulent dominated regime.
In a laminar flow all the fluid elements remain parallel to each other. No vortex can generate as usually happens in turbulent flows.
In a microfluidic environment, due to the small length of the system (*L*), the Reynolds number assumes really low values. It stays in a range 1-100, according to the fluid velocity. So, in microfluidics we can assume that the flow is always laminar.

For the case of a circular tube, at low *Re* the flow regime is known as ***Hagen-Poisuelle flow***. The Navier Stokes equations can be solved in this case to reveal that the flow profile is parabolic with the velocity at the center being the highest and the velocity at the boundary being zero. For a given mass flow rate *Q*, the pressure drop is inversely proportional to the fourth power of the radius:

$$\Delta p = \frac{8\mu L Q}{\pi r^4} = R_F\, Q$$

This is called parabolic flow, and the flow rate *Q* is proportional to the pressure difference Δp, with the constant of proportionality, the fluidic resistance R_F of the system.
As it is showed by the equation, the resistance scales as the negative fourth power of radius and can become enormous, as the radius is reduced.
Let's now consider a channel with a rectangular cross-section, that is the typical condition for the standard microfluidic devices. For a geometry where the width *w* is much larger than the height h, the proportionality, to the first order, is wh^3. The actual dependence is a complicated formula but the zero-th order approximation is given below:

$$R_F = \frac{12\,\mu L}{wh^3}$$

Since the inertial forces are negligible, the viscous forces have the major role in the particles or cells motion. The velocity of the flowing objects is due to the drag force:

$$F_D = 6\pi\mu a v$$

where *a* is the particle radius and *v* the fluid flow velocity.
Another important dimensionless number used in fluid-dynamics is the ***Péclet number*.** In microfluidic devices, there is competition between convectional flow and diffusion, which gives rise to two mass transport processes. Convectional flow tends to move matter in the direction of flow, whereas diffusion tends to equalize concentration gradients. The Péclet number compares the two tendencies:

$$Pe = \frac{diffusion\ time}{convection\ time} = \frac{vL}{D}$$

Where *L* is the distance traveled by the particle: $L \approx vt$ and $L \approx (Dt)^{1/2}$, respectively for convection and for diffusion processes. *D* is the diffusion coefficient, and it is defined by the Stokes-Einstein law:

$$D = \frac{K_B\, T}{6\pi\mu a}$$

and it is a function of the temperature, fluid viscosity and target particles diameter.
For high Péclet numbers we are in a convection dominate regime. For low Péclet numbers diffusion happens much faster than convection. This latter one is the typical condition in microfluidics.

2.3 Fabrication techniques for microfluidics

The domain of microfabrication typically involves scales of the order of 0.1-100 micrometers, and can be divided into two categories: *hard* and *soft* technologies, the latter using materials like elastomers or plastics.
Figure 3 shows different types of micro-technologies currently used in microfluidics.

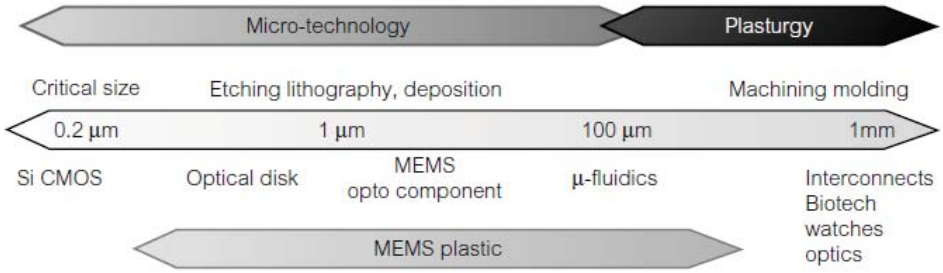

Figure 3: Different types of micro-technologies (Tabeling, Introduction to Microfluidics, Oxford 2005)

Technologies based on etching/lithography/deposition can be applied in the range of scales between 0.2 and 500 micrometers. These are the *hard* technologies, because they use hard materials such as glass or silicon. The combination of etching, lithography, and deposition techniques makes it possible to obtain complex microfluidic devices that are open or closed, contain evaporated electrodes, and allow access to the exterior.
Plastic MEMS occupy a domain between 0.5 and 500 µm. These are the *soft* or *plastic* technologies.
Depending on the material, plastic MEMS are made using a direct method (for example, laser ablation) or by replication methods.
It is important to note that while silicon technology is mature, microfabrication technologies based on plastics and polymers have only appeared more recently and are still evolving.
The first microfluidic devices were fabricated using silicon and glass, these materials being the traditional ones used for MEMS fabrication. Anyway, even if silicon has always been the optimal material in micro-electronics, it is often not the ideal material for microfluidic applications due to optical opacity, cost, and surface characteristics that are not well suited to biological applications. About glass, it was first introduced as a possible alternative material to silicon for microfluidic chip fabrication. However, also for this material, as for silicon, elaborate fabrication processes are required.
In order to promote widespread use of microfluidic devices in biology, a faster, less expensive, and less specialized method for device fabrication was needed. Elastomeric micromolding was first developed at Bell Labs in 1974 when researchers developed a technique of molding a soft material from a lithographic master.
The concepts of soft lithography have been used to pattern surfaces via stamping and fabricate microchannels using molding and embossing. Several advances were made in Japan in the 1980s that demonstrated micro-molded microchannels for use in biological experiments.
The turning point has been had with the introduction of the use of a soft-polymer called polydimethylsiloxane (PDMS) . The idea started from the Whitesides [3] group, and has completely revolutionized the microfluidic field.

Soft lithography is faster, less expensive, and more suitable for most biological applications than glass or silicon micromachining [4].

This technique allows a rapid prototyping of the devices. The sample is fabricated as a replica of a mold, obtained by a photolithography process. It consists of lighting through a mask, a photosensitive emulsion, called photoresist, that has been deposited on a substrate. Two different types of mask can be used: a transparent glass plate with metal (chromium) patterns on it or mask printed on a plastic transparency film by high-resolution image.

During a photolithographic process, the mask is placed on the top of the substrate covered with the photosensitive polymer, and then exposed to a uniform optical beam. In this way dark and light regions appear on the photoresist, forming the same pattern that had been designed on the mask. This step is known as the *transfer* step of the pattern. The photosensitive polymer is deposited in a thin layer on a solid substrate of silicon or glass. The deposit is made using a spin-coater. This piece of equipment consists of a disk that turns at high velocities (typically between 1000 rpm and 10 000 rpm) and allows for the spreading of a drop of liquid initially deposited at the center of the disc. The thickness h of a film obtained in this way is uniform; the following empirical expression accurately models the height:

$$h = kC\left(\frac{\mu}{\omega^2}\right)^{\frac{1}{3}}$$

where C is the initial concentration of polymers in solution, k is a constant, ω is the angular rotation velocity, and μ is the viscosity. While the resist spreads on the substrate, the solvent evaporates, and the film reassembles a soft solid. However, once the step is over, the resist still typically consists of about 15% solvent. If this solvent is not removed, cracks or fissures appear once the film is completely reticulated. To completely eliminate the solvent, the
resist is heated slightly, before the exposure step.

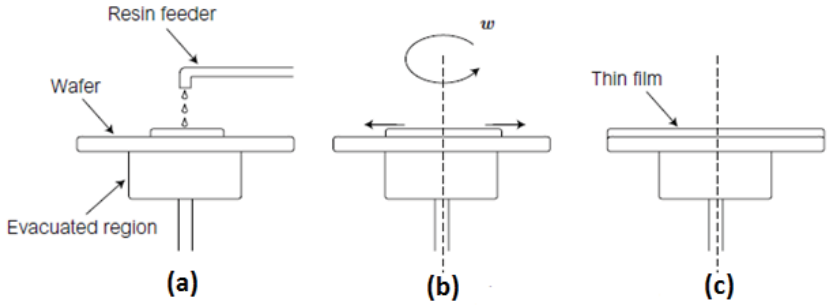

Figure 4: Deposition step of the resist on a spin-coater (spin coating). (a) The resin/resist is deposited; (b) The rotation of the disk support induce the spreading of the resin/resist; (c) The resist film is deposited on the substrate. (Tabeling, Introduction to Microfluidics, Oxford 2005)

It is worth noting that the thickness of the photoresist patterns on the master determines the depth of the microfluidic channels. So, the choice of the type of photoresist depends upon each own need.

In the last years, many efforts and studies have been dedicated to solve the multiple problems related to the fabrication for structures characterized by a high aspect ratio [5-6].
After the spin-coating step, the photosensitive polymer and its substrate are placed in an aligner whose precision is of the order of 1 µm. The film is thus exposed to a luminous flux produced by a source crossing the photolithographic mask. The source is most often a mercury vapor lamp that delivers substantial luminescent power (10 to 20 mW in strength), in wavelengths between 300 and 450 nm. Basically, the luminous flux initiates physico-chemical reactions in the polymer, which modify the solubility in certain solvents.
There are two types of resists:

- Positive resist: the light zones become soluble in a particular solvent, while other zones remain insoluble.
- Negative resist: the light zones become insoluble in a particular solvent, while the other zones can be dissolved in that same solvent.

Physically speaking, the resist must be sufficiently transparent to allow the illumination of the whole thickness of the deposited layer, and sufficiently sensitive to the light to induce chemical reactions. This delicate equilibrium limits the thickness of a large number of photosensitive resists. In this respect, the invention of SU8 by IBM several years constituted a small revolution in the field, as SU8 is a resist with high photosensitivity and can also be deposited in thick (tens of micrometers) layers.
An important point is that at the level of the resist, the size of the zone δ in which diffraction phenomena are developed is not on the order of the wavelength of the light (as a single reasoning would conclude), but is much higher. The estimation of such a region is given by the following formula:

$$\delta \approx 3\sqrt{\lambda s}$$

where λ is the wavelength of the luminous flux (assumed to be monochromatic), and s is the thickness of the polymer film.
Once the master is fabricated, the micro-channels are formed in PDMS by replica molding. Replica molding is simply the casting of pre-polymer against a master and generating a negative replica of the master in the PDMS. The polymer is provided in an uncured form. Users have to mix the polymer base with a part of curing agent, the usual ratio is 10:1, in order to activate the cross-linking process and to get the material to solidify. Silicon hydride groups present in the curing agent react with vinyl groups present in the base and form a cross-linked, elastomeric solid [7].
Access holes for channels and reservoirs for buffer can be added in the replication step by appropriate placement of posts on the master or punched out the cured layer by using a borer.
Molding provides a PDMS replica that contains three of the walls necessary for enclosed channels. Sealing the replica to a flat surface provides the fourth wall. The flat material could be PDMS, or other materials; often a glass slide is used.
Sealing occurs in two ways : (i) reversible, conformal sealing with a flat surface, and (ii) irreversible sealing upon exposure of both surfaces to a gas plasma.
A permanent sealing between PDMS and glass, is obtained by an exposure to an oxygen plasma of the surfaces of both PDMS and flat material. After the two materials are exposed to the plasma, -OH groups are activated. By putting one surface on the other, siloxane bonds (Si–O–Si) are formed. These covalent bonds forms the basis of a tight, irreversible seal, and attempting to break the seal results in failure in the PDMS bulk.

This approach makes the channels more hydrophilic, allowing for easier fluid filling for a period of time after the oxygen plasma treatment. However, the surfaces can quickly revert to their hydrophobic tendency if exposed to atmosphere [9].

Surface chemistry is of great importance in microfluidic systems, this is another reason for what silicon is not a preferred material for lab-o-chip application, since it does not generally lend itself to chemical modification.

Otherwise, PDMS has the highly desirable property of being biocompatible[10], impermeable to water and gas permeable. These characteristics make the polymer a suitable material for cells culturing and manipulation.

Therefore, PDMS based micro-systems can be fabricate quickly and easily, and they can be used as a useful step to test new designs, or as a final product, as shown by a number of functional devices developed in academic institutions and private companies.

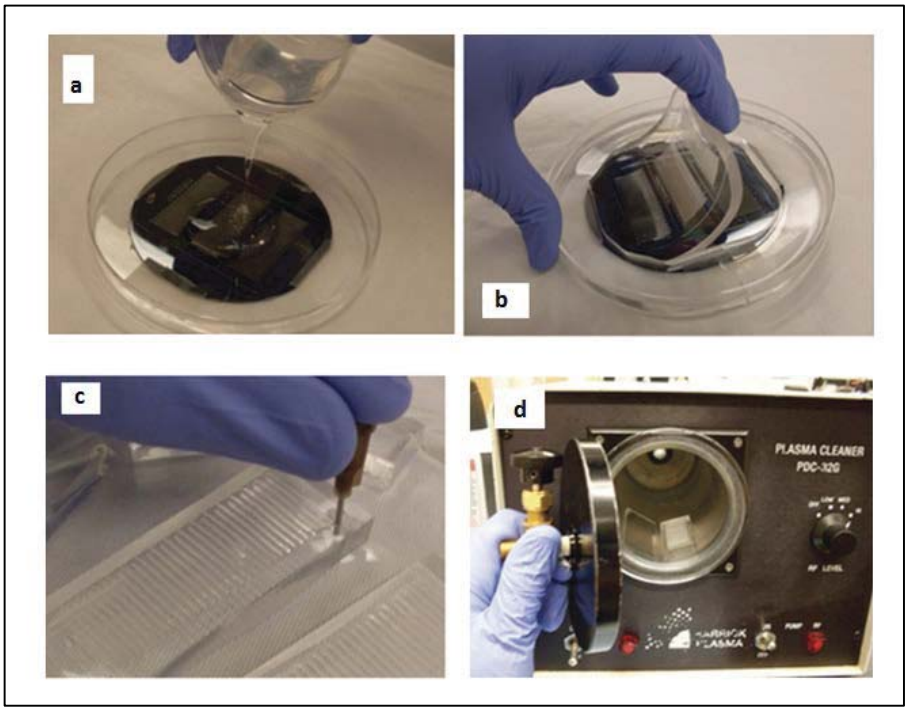

Figure 5: Fabrication of a micro-chip in PDMS. (a) The mixture of the uncured polymer and curing agent is poured on the master. (b) After the polymer is solidified, it is peeled off from the master. (c) Punching of the holes for the fluid inlet and the outlet. (d) Permanent sealing of the polymer with a glass slide through a oxygen plasma process. (images from Xona Microfluidics LLC).

2.4 An overview on Microfluidic Applications

The rapid development of the microfluidic technologies is revolutionizing the biochemical analysis field and biomedicine. Devices, that are millimeters-centimeters in size, are capable of making complex analysis and procedures usually requiring a well-equipped laboratory. These novel micro-systems have found applications in different fields, such as analysis of potable water, pollution monitoring, clinical diagnostics, drug discovery, and so on. About ten years ago, the sentence ''microfluidics has the potential to significantly change the way modern biology is performed'' [11], gave an idea of what was and would be the impact of the micro-devices in the biomedical research. Most of the groups involved in the biology and medical research have recognized the high contribution introducing by microfluidic technology. One of the fields in which microfluidic devices have found a large use is cell culturing. Indeed, mammalian cell cultures play a crucial role in biotechnology, related to a wide range of applications, such as testing novel drugs effects on different biological samples.

The limit in the use of the traditional cell cultures methods is primarily related to high cost of samples and reagents. The miniaturization of the standard cell cultures could allow to considerably reduce the costs for that systems, and therefore make these cell experiments accessible in laboratory, clinical, and field settings. Microfluidic technology allows realizing systems that are perfectly suitable for reproducing a biological environment. Actually cells form a microsystems, and therefore it is easier to control their micro-environment at the micro-scale. Among the application in this field, a microfluidic cell culture system that reproduces all the processes, performed in the traditional eukaryotic culture techniques, has been realized [12]. The device provides the environment needed for cell growth and manipulation without requiring an incubator. The temperature can be controlled with a transparent ITO (Indium Tin Oxide) heater.

In another work, a micro-bioreactor array was designed [13] demonstrating for the first time an 8x8 addressable cell micro-bioreactor. The device allows also to control the fluid transport through the system, and at the same time to maintain a favorable environment for cells. This is achieved by realizing a two levels structure, in order to separate the cellular compartment from the fluid flow. The operation of the culture-on-chip has been demonstrated by observing the serum response of HeLa human cancer cells in 64 parallel cultures.

An important research field that can significantly take advantages from the microfluidic technology is the one focused on the stem cells. The interest of the medical world in stem cells is due to the capability of these cells in genetically differentiate into a specific cell type. This ability has given high promises in fields such as the tissue engineering or cell therapy. Stem cells are classified in different types: totipotent, the ones that can differentiate into any cell type; pluripotent, that have the ability to differentiate into nearly all cell types; and multipotent, that can only differentiate into a closely related family of cells [14]. By using microfluidic technology, stem cells studies can give better results than conventional tissue culture dish, primarily due to the possibility to well control the culture micro-environment.

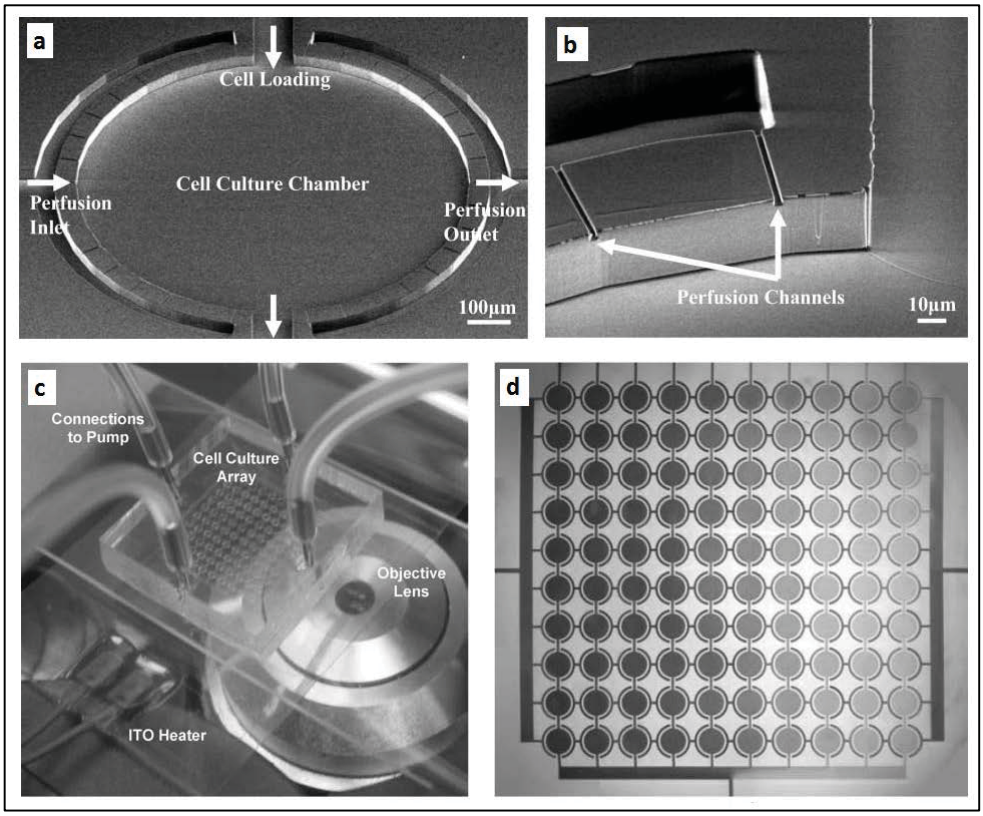

Figure 6: Hung et al. 2005 [12] (a) The single unit of the cell culture chamber. (b) Detail of the perfusion channels size. (c) Picture of the proposed device. (d) A 10 x 10 microfluidic cell culture array .

A microfluidic device that allows to optimize the proliferation and differentiation conditions for neural stem cells NSCs [15], is another example of lab-on-chip technology applied to the research on stem cells. In the device, the human NSCs are in a continuous concentration gradient of known growth factors. The device consists of two types of chambers, a gradient chamber and two control chambers. The gradient chamber consists of two parts: the gradient-generating microchannel network and the cell culture area near the bottom of the device across which the gradient is applied. Two control cell culture chambers are also fabricated next to the main gradient chamber for positive and negative controls. The stem cells have exhibited proliferation and differentiation responses that were concentration-dependent and quantitatively similar to those seen in parallel control cultures.

It has also been demonstrated the possibility to control proliferation and stimulate differentiation of human mesenchymal cells (MSCs), by using a microfluidics based cell culture system [16]. A cell culture platform was made in PDMS. The microfluidic chip consists of 96 individually addressable culture chambers. The individual addressability allows to re-create distinct culture environments from chamber to chamber.

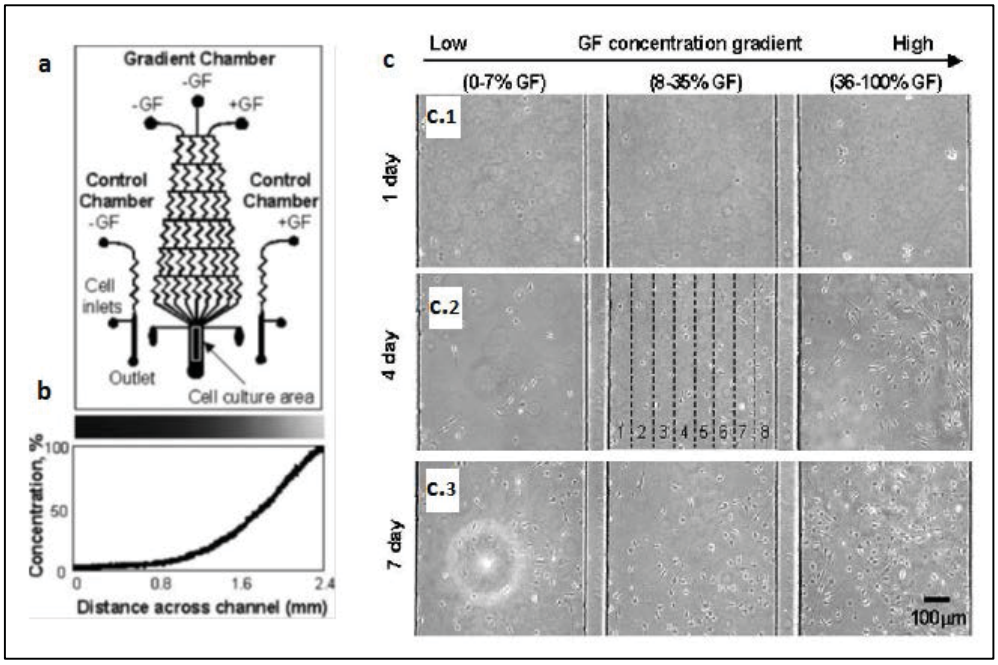

Figure 7: Chung et al. 2005 [15] (a) Schematic design of the microfluidic device showing the gradient chamber and two control chambers. (b) The gradient profile generated within the gradient chamber. (c) Proliferation of human NSCs in the gradient chamber.

So, the proposed device provides stimulation of the cells using complex time-varying schedules, and in situ mixing of media and reagents, while allowing time-lapse microscopic imaging.

In the recent years, polymer based microfluidic devices have also given an important contribution in the developments of the assisted reproductive technologies (ART) [17]. ART refers to in vitro handling of cattle or human oocytes, sperm, or embryos to induce pregnancy. Ejaculated motile sperm is selected for successful fertilization in the oviduct. In ART, selection and sorting of motile sperm are routine processes. Microfluidic devices give the possibility to sort spermatozoa, by reducing the time needing for these procedures and the stress on the cells, that characterize the standard methods.

Among the sorting methods, sperm chemotaxis is the one that has more widely exploited. Chemotaxis is defined as the movement of cells toward a concentration gradient of chemoattractant. Referring to spermatozoa, the study of the motion of these cells, in correlation with the presence of a particular chemical substance, allows to verify sperm motility. In the evaluation of the sperm quality for the in-vitro fecundation, motility is one of the most important parameter.

Therefore, there is an important needing of reliable procedures motile sperm identification and selection. This is traditionally achieved by using the swim-up and the density-gradient centrifugal method are used for this purpose[18]. In 2010, a microfluidic device to monitor both sperm motility and chemotaxis [19-20] during sperm screening [21], has been proposed. The micro-chip consists of a straight channel connected with a bi-branch channel that mimics the mammalian female reproductive tract (Figure 8). The device was tested by using murine sperms, ant the results showed that it effectively allows to get simultaneously motility screening and chemotaxis testing.

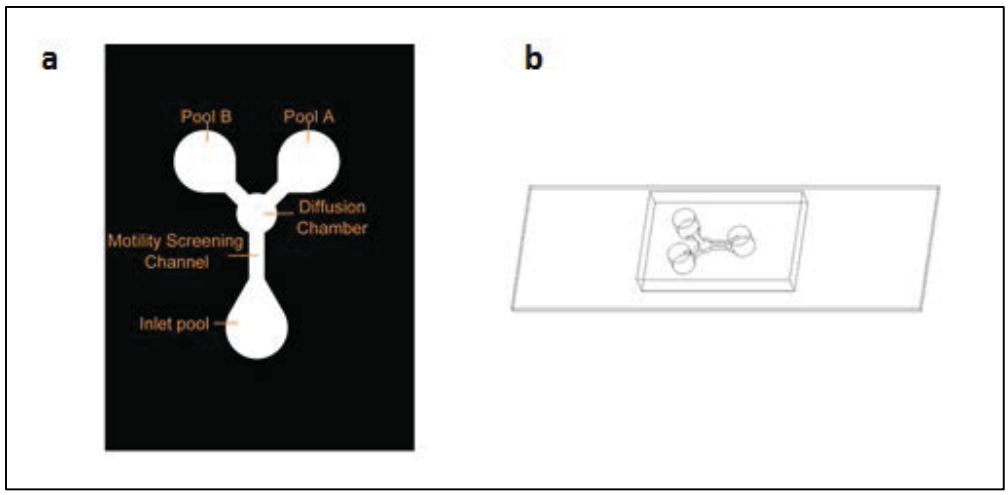

Figure 8: Xie et al. 2010 [21] (a) Schematic top view of the PDMS-glass structure. It mimics the in vivo structure with a screening channel (vagina), diffusion chamber (uterus), and bi-branch channel (oviduct). (b) Schematic of the sperm chemotaxis testing channel.

In a more recent work the microfluidic device that has been realized, allows to test the response of sperm to different chemoattractant concentrations [22].

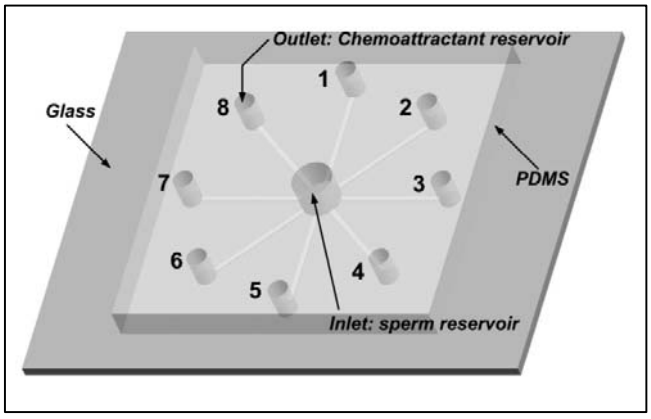

Figure 9: Ko et al. 2012 [22]. Design of microchip for sperm chemotaxis assay.

The designed device has a radial shape with eight micro-channels (Figure 9). The geometry allows determining the optimal chemical gradient of chemoattractant, by putting various concentrations of attractants at each outlet and obtain results for each concentration at once. The device has been tested by using mouse semen and acetylcholine as chemoattractant. The authors were able to show that the microchip provides a simple, convenient, and disposable platform for separation of motile sperm. They underlined that the reproducing of female oviduct environment in the device could do a strong improvement.
Another research group has realized a microfluidic device for sperm chemotaxis assay, which has been tested using mouse sperm and ovarian extract as chemoattractant [23]. The micro-chip design has three input channels and three output channels (Figure 10). Sperm cells were introduced into the chamber through the top center channel. Viable sperm swam randomly in the chamber and were dispersed across the chamber. Non-viable sperm were flushed directly through to the waste channel. If a chemoattractant was present in the extract channel, the sperm preferentially swam toward the attractant.

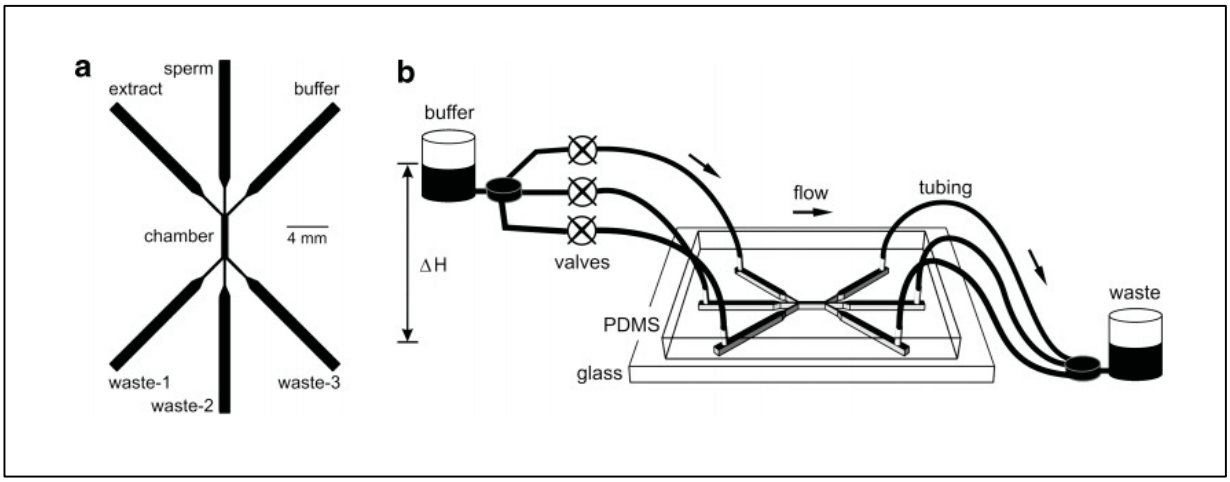

Figure 10: Koyama et al. 2006 [23]. (a) Schematic of the microfluidic device for chemotaxis assays. (b) Schematic of the microfluidic device with fluid control. Flow rates in the micro-channels were controlled hydrostatically by adjusting the height of the fluid in the buffer reservoir relative to the height of the fluid in the waste reservoir.

The applications that have just been showed in the field of ART, have showed that microfluidic chips could be established as an useful alternative to the traditional method for sperm sorting. Other works have been demonstrated the applicability of microfluidic technology also for fecundation and embryo development [24-25].
Starting from these results, some researchers have imagined to realize the total uterine function on a microfluidic chip. In one of these studies, a microfluidic uterus that implemented the procedures of ovulation, insemination and embryo development has been developed [26].

The microfluidic chip is made of three layers, in which a porous polycarbonate membrane is interposed between a top and a bottom PDMS layer (Figure 11). The top PDMS layer contained a zigzag shaped channel, whilst in the bottom one there is a series of micro-seviers on the bed of the channel, which are designed to capture and locate oocytes. Oocytes and endometrium cells are introduced by the top layer, and thanks to the porous membrane, they are captured in the micro-seviers in the bottom layer. The sperm and the nutrition media are flashed through the channel on the top layer. The authors have showed that steps related to embryo development, including ovulation, fertilization, implantation and embryo formation, can be implemented on the microfluidic chip.

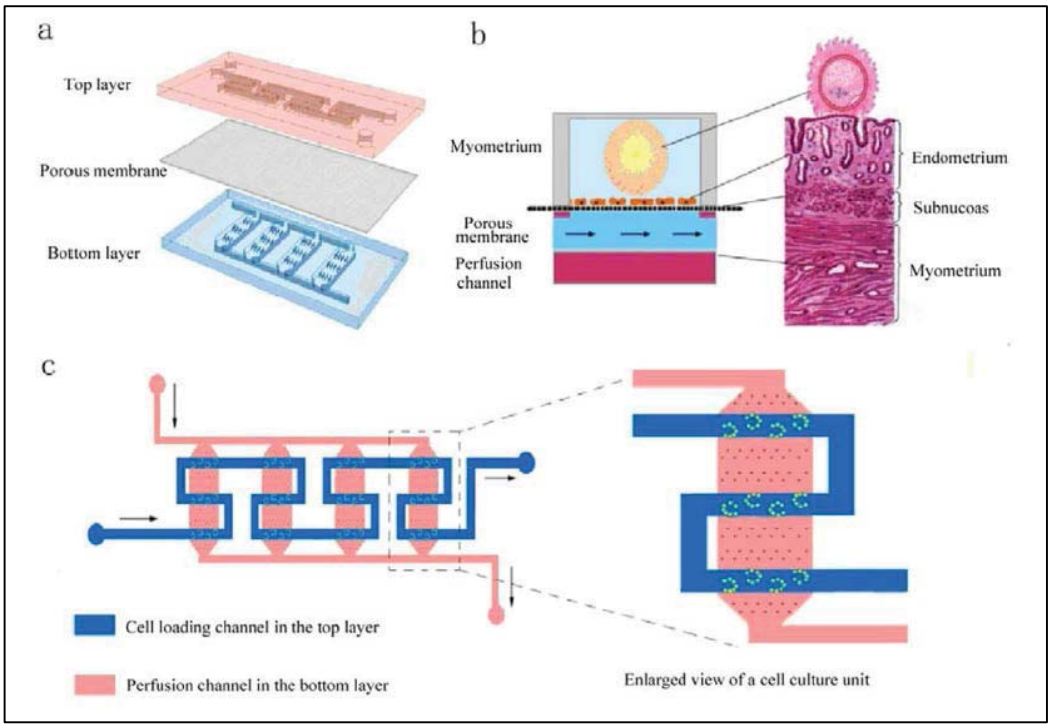

Figure 11: Li et al 2013 [26]. (a) Schematic illustration of the structure of the microchip. (b) A section-view picture illustrating the microchip that mimics the uterus. (c) Top-view picture showing the pattern of the microfluidic channels (left) and an enlarged view of a single perfusion culture unit.

This last example can be considered as part of a novel research field that has been named as Organs on a Chip. The groups that are working in this research area are focused on the development of microfluidic devices that can mimic the physiological activities of human organs.

Indeed, organs-on-chips have been defined as "*microfluidic devices for culturing living cells in continuously perfused, micrometer-sized chambers in order to model physiological functions of tissues and organs* [27]".

One of the main motivations for the high interest that has been showed in for this novel application of microfluidic technology, is related to the drug testing. Nowadays, scientists can only perform their experiments in-vivo, on animals, or in-vitro, in small cells culture. In the first case, the research activity is really expensive and it is the center of a continuous heated discussion on its ethnicity. Moreover, in both in-vivo and in-vitro models, the results could not be perfectly a reflection of the effects on human beings. Therefore, the possibility to have micro-devices, that are easy to fabricate and that can be used as model of the single human part, would bring a lot advantages in the actual way in which drug tests are performed [28].

The first step to the organs-on-chips developments has been done by the use of microfluidic technologies for realizing 3D culture-models [29]. These new micro-engineering approaches give the possibility to reconstitute more complex 3D organ-level structures. Organs-on-chips promised to the scientists all over the world, the possibility of having in-vitro model that are closer to the effective organs [30-31].

In Figure 12, a lung-on-chip [32] micro-device that has been designed in order to mimic the human breathing on a chip.

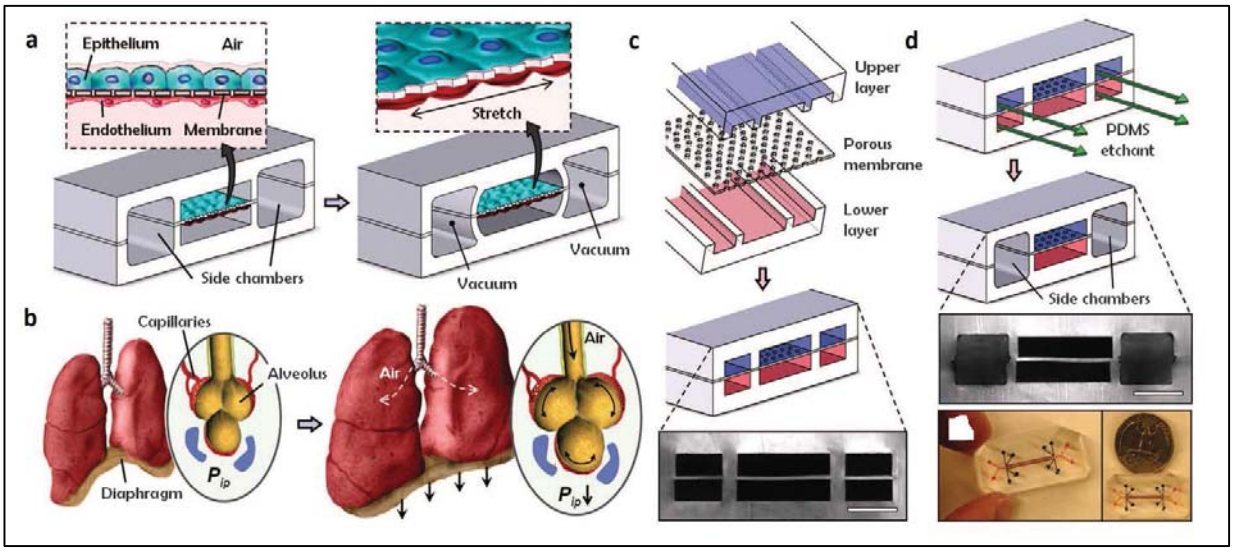

Figure 12: Huh et al. 2010 [32]. (a) The micro-fabricated lung mimic device uses compartmentalized PDMS microchannels to form an alveolar-capillary barrier on a thin, porous, flexible PDMS membrane coated with ECM. The device recreates physiological breathing movements. (B) During inhalation in the living lung leading to distension of the alveoli and physical stretching of the alveolar-capillary interface. (C) Three PDMS layers are aligned and irreversibly bonded to form two sets of three parallel micro-channels separated by a 10-mm-thick PDMS membrane containing an array of through-holes with an effective diameter of 10 mm. (D) After permanent bonding, PDMS etchant is flowed through the side channels. Selective etching of the membrane layers in these channels produces two large side chambers to which vacuum is applied to cause mechanical stretching.

Beside the already mentioned applications, it has been underlined, that microfluidics has the potentiality to analyze cells, molecules or particles while they are flowing. Among the examples that fall in this area, the possibility to realize a microflow cytometer has been widely investigated[33-35].

Flow cytometry is a powerful, high-throughput tool that can perform both quantitative and qualitative multi-parametric analyses of individual cells. In a typical flow cytometer, the cell sample is injected through the inner tube of a coaxial channel, while sheath flows from the outer tube compress the sample flow to form a single-file stream of cells, a process known as *hydrodynamic focusing*. The focused cells pass through a laser beam, generating three types of output optical signals: forward scatter (FSC), side scatter (SSC), and fluorescence (FL). FSC is the light deflected by a cell at a small angle (2°–20°) relative to the input laser beam. The intensity of the FSC signal is indicative of the size and refractive index of the cells. SSC is the light diffused in all directions due to cellular granularity. FL is normally collected using the same optics as SSC and is later split to different detectors based on the light frequency. Each of these detection signals (FSC, SSC, and FL) is eventually processed to identify individual cells in a mixed cell population based on cell size, granularity, and various fluorescence markers.

Flow cytometry offers high potentiality as clinical diagnostic tool, but its cost, bulky size, mechanical complexity, and need for highly trained personnel can limit the utility of this technique.

In order to overcome the limitations of conventional flow cytometry systems, researchers are doing significant efforts to developing microfluidics-based flow cytometry devices [36-37] that could be more accessible and affordable for research laboratories and clinics.

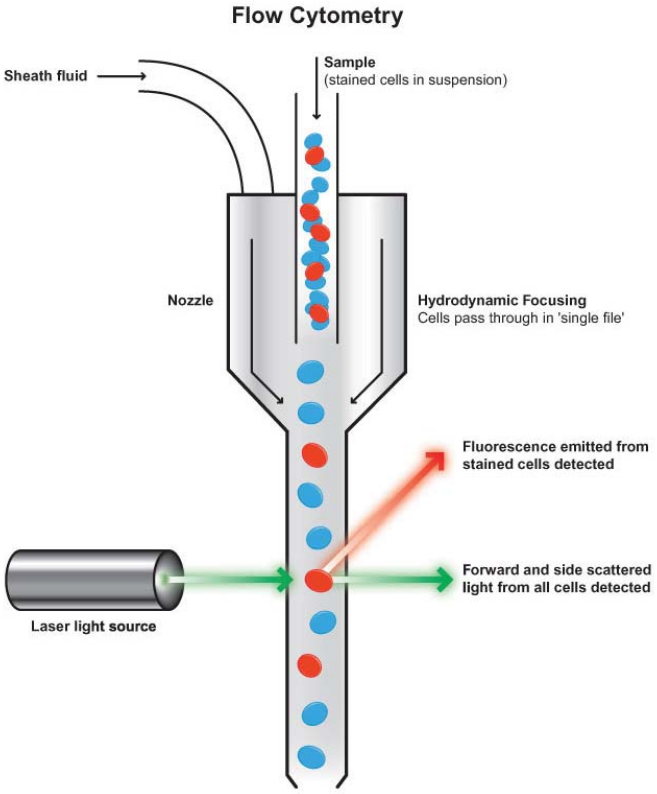

Figure 13: Schematic of a flow cytometer.

Since cells focusing is the key point for the correct operation of a flow-cytometry, a significant attention has been given to the achievement of flow focusing in a micro-flow cytometers. Various particle focusing methods have been developed in microfluidic devices, which may be conveniently classified as sheath flow focusing and sheath-less focusing. Sheath flow focusers use one or more sheath fluids to pinch the particle suspension flow and thus focuses the suspended particles. Sheath-less focusers achieve particle focusing in a pressure-driven or electrokinetic suspension flow by the use of either an externally applied or an internally induced force field.
Sheath-less particle focusers typically rely on a force to manipulate the suspended particles laterally to their equilibrium positions. This force can be either externally applied such as acoustic [38], dielectrophoretic[39], magnetic[40] and optical [41] forces, or internally induced by channel topology including hydrophoretic [42-43] and inertial [44-47].

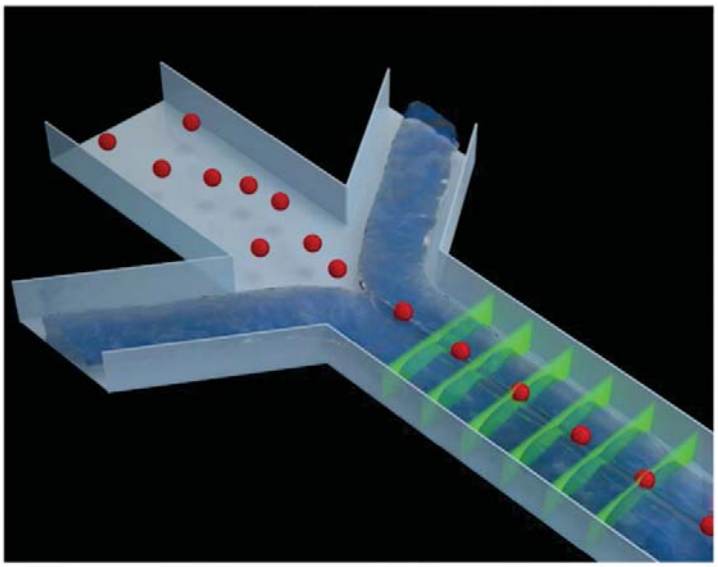

Figure 14: Schematic of two-dimensional hydrodynamic focusing in a microfluidic device. Particles coming from the central channel are put in one single line, due to the outer sheath fluid injected at an higher flow rate.

Among the diverse particle focusing methods, sheath flow focusing may be the most common one that has been adopted in microfluidic devices. In this approach, the outer sheath flow is injected at a much higher flow rate than the inner sample flow to create hydrodynamic focusing to position cells in the core of the flow.
The alignment of the hydro-dynamically focused cell stream with the laser ensures identical interrogation conditions for each individual cell, to improve the fidelity and accuracy of the detection.
The fluidic system will also require a fluid-pumping mechanism that transports a sample of cells through the channel. Traditionally, flow cytometers uses peristaltic, syringe pumps and pressure-based pumps.
In general, one or more sheath fluids should be used in order to obtain a two-dimensional (2D) or three-dimensional (3D) particle focusing. A 2D focusing normally indicates the horizontal focusing of particles to the center plane of a microchannel, where particles still scatter over the channel depth.

However, for the application to flow cytometers, 2D focusing frequently suffers from some problems such as the probability of coincident events due to the fact two or more particles could pass through the detection region at the same time, at different heights.
These problems are not encountered in 3D focusing, where particles are focused in both the horizontal and the vertical directions.
In most of the 3D hydrodynamic focusing devices that have been reported, 3D focusing is achieved by delivering sheath flows from both vertical and horizontal directions using multi-layer 3D microfluidic devices [48-49]. Multi-step photolithography and assembly protocols have been developed for fabricating the 3D microfluidic structures needed for 3D hydrodynamic focusing. However, such methods require either tedious assembly of individual components or multiple alignments and exposures during mold fabrication. These limitations inevitably increase the cost and complexity of the device and ultimately hinder their applicability.
Recently, a method for inducing 3D hydrodynamic focusing technique named microfluidic drifting. The uniqueness of this technique lies in its ability to achieve 3D hydrodynamic focusing in a single-layer planar (2D) microfluidic structure. As a result, the device can be readily fabricated via standard soft lithography involving only one device layer and one photolithography mask, which makes it ideal for mass-producible flow cytometry devices.
The applications that have been reported here are only a small part of the many microfluidic works on which the scientific community is working on.
Relaying on these examples, we can assert that microfluidics has the potential to allow the realization of a fluidic subsystem that could help in bio-particles and cells manipulation.
It has to be underlined that lab on chip technology has the prospective to miniaturize complete analysis systems on a single device.
Micro-devices that could substitute a macro-system for cells or particles analysis, has to integrate the fluidic subsystem with additional sub-systems, i.e. optical or electrical, in order to have a chip hand-handling , cheap, easy to transport and to use.

2.5 Parallelization: a great advantages of microfluidic technology

As already discussed at the starting of this chapter, microfluidic systems consist in channels networks which characteristic length is typically in a range from ten to hundred micrometers.
This lead to the possibility to manipulate quantities of sample and reagents that are in the nano or pico scale.
Furthermore, as it has been showed in many works, miniaturization enables to realize devices in which it is allowed to make highly parallelized [50-52] experiments, thus drastically increasing the throughput.
The positive effect of miniaturization and parallelization, using microfluidic systems, has been seen clearly with next-generation of sequencing systems that have drastically reduced time and cost compared to traditional technologies [53]. Moreover, it has been demonstrated the great advantages of using parallelized micro-chip for cell culturing [54-55].
Actually, advantages of parallelization have been exploited in many other scientific fields, such as synthesis of nanoparticles [56] and droplet generation [57].
Single channels [58-60] microfluidic devices for focusing, sorting and analysis of biological samples have been widely exploited. However, referring to some applications, such as microflow-cytometry, the architecture with a single-channel is a limit. In order to overcome it, scientists have started working on parallelized devices.

Among these works, a research group developed a 384-channel parallel microfluidic cytometer (PMC) [61] . The multichannel architecture allows 384 unique samples for a cell-based screen to be read out in approximately 6–10 min, about 30-times the speed of a conventional fluorescence-activated cytometer system (FACS). The advantages of the device have been confirmed by using the system to count rare clonal osteocytes in the most difficult early stages of an expression-cloning screen for the carboxy-terminal parathyroid hormone receptor (CPTHR).
What the authors have demonstrated, and what has been clearly showed from all the others related works, it is the high improvement achieved in systems for analysis of flowing cells by introducing parallelization.
In particular, we could summarize the main advantages of using parallelized devices in the characterization of flowing objects, as follows:

- Throughput increasing;
- Possibility to slow down the flow velocity by maintaining the same throughput of a single channel device;
- In relation to the previous point, flowing objects can be imaged without the needing of really high performance acquisition systems ;
- Increasing in the operation time of any device, by limiting the chip failure due to the clogging phenomena.

2.6 Conclusions

At the end of this chapter we can have a more clear idea about what microfluidics is and what it can be used for.
In the same way in which integrated circuits have revolutionized computation, microfluidics seeks to integrate high levels of wet laboratory functionality on a microfabricated fluidic chip. Microfluidic systems hold similar promise for the large-scale automation of chemistry and biology, suggesting the possibility of numerous experiments performed rapidly and in parallel, while consuming little reagent.
Rapid and low cost prototyping of microfluidic devices has been made possible by the introduction of the soft lithography technique. Indeed, when considering cost, time and labor, polymers and elastomers become more and more attractive. Among the various polymers, PDMS is by far the dominant polymeric material utilized for microfluidics. This can be attributed to its numerous salient features including its elastomeric properties, biocompatibility, gas permeability, optical transparency, ease of bonding to itself and glass, and relatively high chemical inertia.
Microfluidics is revolutionizing the way we handle fluids in almost any field one can imagine including biotechnology, biomedicine, chemical synthesis, environmental monitoring, advanced materials, and so on. Application of microfluidic devices is growing explosively due to their inherent advantages associated with miniaturization, integration, parallelization, as well as portability and automation, including low consumption of reagents and samples, rapid analysis, cost-effectiveness, high efficiency and less human interference during operation.
In relation to bio-applications, several research groups have demonstrated the integration and miniaturization of many key functions for different purposes. For the future this holds the promise of truly portable and

compact systems that can bring the biochemistry lab to the user. It will enable the delivery of healthcare to the masses.

The aging population will have many health kits to provide preventive medicine (personalized medicine or assistive medicine). Medical checkups can be performed daily. Healthcare costs will be reduced due to the availability of microfluidics instruments. Chronic disease patients can have home diagnostics systems and high risk patients (e.g. post-surgical) can also enjoy the comfort of being at home knowing that lab-on-a-chip devices will be monitoring and pre-warning patients with high risks of infection, blood clots. Personalized medicine with genetic information to assist in the prescription and administration of drugs and treatments will greatly increase the efficacy and safety of the future of medicine enabled by microfluidic home test machines [62].

Microfluidics offers great potential in addressing those challenges in biomedical applications. Countless microfluidic systems have been developed for high-throughput genetic analysis, single-cell analysis, proteomics, low-cost diagnosis, pathogen detection, controlled- drug release, and tissue engineering.

The analogy between the microfluidic integrated circuit and the microelectronic integrated circuit is still, however, quite insightful and is especially useful for contextualizing the potential of microfluidic technology. As electronic components have become smaller and smaller, consumer electronics have become smaller, cheaper, and more useful. Twenty years ago not every household had a personal computer but now it seems just about everyone has a smart phone. Equally, as smaller and more efficient microfluidic elements are successfully integrated into hand held devices, there is no doubt that we will see the impact all over the world, from home medical diagnostics to point-of-care diagnostics in the developing world**.**

References

1 G. M. Whitesides, The origins and the future of microfluidics, 2006, Nature 442, 368-373
2 Henrik Bruus, Theoretical microfluidics, Oxford, 2008
3 Xia, Y. and Whitesides, G.M. (1998) Soft Lithography. Ann. Rev. Mater. Sci. 28,153–184.
4 N.-T. Nguyen, S. T. Wereley, Fundamentals and Applications of Microfluidics, 2006, Artech House
5 A. del Campo and C. Greiner, SU-8: a photoresist for high-aspect-ratio and 3D submicron lithography, J. Micromech. Microeng. 17 (2007) R81–R95
6 R. Daunton, A. J. Gallant and D. Wood, Manipulation of exposure dose parameters to improve production of high
aspect ratio structures using SU-8, J. Micromech. Microeng. 22 (2012) 075016 (8pp)
7 J.C. McDonald, G.M. Whitesides, Poly(dimethylsiloxane) as a material for fabricating microfluidic devices, Acc. Chem. Res., 35 (2002), pp. 491–499
8 J. Cooper McDonald, David C. Duffy, Janelle R. Anderson, Daniel T. Chiu, Hongkai Wu, Olivier J. A. Schueller and George M. Whitesides, Fabrication of microfluidic systems in poly(dimethylsiloxane), Electrophoresis 2000, 21, 27–40
9 Mark A. Eddings, Michael A. Johnson and Bruce K. Gale, Determining the optimal PDMS–PDMS bonding technique for microfluidic devices, J. Micromech. Microeng. 18 (2008) 067001
10 Voskerician, G., Shive, M.S., Shawgo, R.S., von Recum, H., Anderson, J.M., Cima, M.J.and Langer, R., Biocompatibility and biofouling of MEMS drug delivery device, 2003, Biomaterials 24, 1959–1967.
11 Beebe, D. J., Mensing, G. A. & Walker, G. M. Physics and application of microfluidics in biology. Annu. Rev. Biomed. Eng. 4, 261–286 (2002).
12 Paul J. Hung, Philip J. Lee, Poorya Sabounchi, Nima Aghdam, Robert Lin and Luke P. Lee, A novel high aspect ratio microfluidic design to provide a stable and uniform microenvironment for cell growth in a high throughput mammalian cell culture array, Lab Chip, 2005,5, 44-48.
13 Lee, P.J., Hung, P.J., Rao, V.M. and Lee, L.P. (2005) Nanoliter scale microbioreactor array for quantitative cell biology. Biotechnol. Bioeng. 94(1), 5–14.
14 Huei-Wen Wu, Chun-Che Lin, and Gwo-Bin Leea, Stem cells in microfluidics, 2011, Biomicrofluidics 5, 013401
15 Chung BG, Flanagan LA, Rhee SW, Schwartz PH, Lee AP, Monuki ES, Jeon NL, Human neural stem cell growth and differentiation in a gradient-generating microfluidic device, 2005, Lab Chip, 5(4):401-6
16 Gómez-Sjöberg R1, Leyrat AA, Pirone DM, Chen CS, Quake SR., Versatile, fully automated, microfluidic cell culture system, Anal. Chem. 2007, 79, 8557-8563
17 Matsuura, K, and Naruse, K. : Use of Silicone Elastomer-Based Microfluidic Devices and Systems in Reproductive Technologies. In "Advanced Elastomers: Technology, properties and applications" , ed. A. Boczkowowska, pp.243-262, InTech, Rijeka, Croatia, 2012
18 Xu L, Lu RK, Chen L, Zheng YL. Comparative study on efficacy of three sperm-separation techniques. Asian J Androl 2000;2:131– 4.
19 M. Eisenbach, Sperm Chemotaxis, 1999, Reviews of Reproduction, 4, 56–66
20 Jiandong Wu,ab Xun Wuad and Francis Lin, Recent developments in microfluidics-based chemotaxis studies, Lab Chip, 2013, 13, 2484
21 Xie L, Ma R, Han C, Su K, Zhang Q, Qiu T, Wang L, Huang G, Qiao J, Wang J, Cheng J., Integration of sperm motility and chemotaxis screening with a microchannel-based device, Clin Chem. 2010 Aug;56(8):1270-8
22 Ko YJ, Maeng JH, Lee BC, Lee S, Hwang SY, Ahn Y, Separation of Progressive Motile Sperm from Mouse Semen Using On-chip Chemotaxis, Analytical Sciences Vol. 28 (2012) No. 1 P 27

23 Koyama S, Amarie D, Soini HA, Novotny MV, Jacobson SC, Chemotaxis assays of mouse sperm on microfluidic devices, Anal Chem. 2006 , 15;78(10):3354-9.
24 Chao Han, Qiufang Zhang, Rui Ma, Lan Xie, Tian Qiu, Lei Wang Keith Mitchelson, Jundong Wang, Guoliang Huang, Jie Qiao and Jing Cheng, Integration of single oocyte trapping, in vitrofertilization and embryo culture in a microwell-structured microfluidic device, Lab Chip, 2010, 10, 2848-2854
25 Y.S. Heo,1,6, L.M. Cabrera, C.L. Bormann, C.T. Shah, S. Takayama, and G.D. Smith, Dynamic microfunnel culture enhances mouse embryo development and pregnancy rates, Hum Reprod. Mar 2010; 25(3): 613–622.
26 Wei-Xuan LI, Guang-Tie LIANG, Wei YAN, Qiong ZHANG, Wei WANG, Xiao-Mian ZHOU, Da-Yu LIU, Artificial Uterus on a Microfluidic Chip, Chin J Anal Chem, 2013, 41(4), 467–472.
27 S. N Bhatia & D. E. Ingber, Microfluidic Organs-on-chips, Nature Biotechnology 32, 760–772 (2014)
28 M.B. Esch, T.L. King, and M.L. Shuler, The Role of Body-on-a-Chip Devices in Drug and Toxicity Studies, Annu. Rev. Biomed. Eng. 2011. 13:55–72
29 Huh D, Hamilton GA, Ingber DE., From 3D cell culture to organs-on-chips, Trends Cell Biol. 2011, 21(12):745-54
30 Moraes C, Mehta G, Lesher-Perez SC, Takayama S., Organs-on-a-Chip: A Focus on Compartmentalized Microdevices, Ann Biomed Eng. 2012 Jun;40(6):1211-27
31 Huh D, Torisawa YS, Hamilton GA, Kim HJ, Ingber DE, Microengineered physiological biomimicry: organs-on-chips, Lab Chip. 2012 Jun 21;12(12):2156-64
32 D Huh, B. D. Matthews, A. Mammoto, M. Montoya-Zavala, H. Y. Hsin, D. E. Ingber, 2010, Reconstituting organ-level lung functions on a chip, Science 328 (5986):1662–1668.
33 Huh D, Gu W, Kamotani Y, Grotberg JB, Takayama S., Microfluidics for flow cytometric analysis of cells and particles, Physiol Meas. 2005 Jun;26(3):R73-98
34 Chung TD, Kim HC., Recent advances in miniaturized microfluidic flow cytometry for clinical use, Electrophoresis. 2007 Dec;28(24):4511-20
35 Ateya DA, Erickson JS, Howell PB Jr, Hilliard LR, Golden JP, Ligler FS, The good, the bad, and the tiny: a review of microflow cytometry, Anal Bioanal Chem. 2008 Jul;391(5):1485-98
36 N. Demierre, T. Braschler, R. Muller, P. Renaud, Focusing and continuous separation of cells in microfluidic devices of cells in a microfluidic device using lateral dielectrophoresis
37 C. Simonnet and A. Groisman, Two-dimensional hydrodynamic focusing in a simple microfluidic device, Applied Physics Letters, 2005, 87:114104.
38 Jinjie Shi, Xiaole Mao, Daniel Ahmed, Ashley Colletti and Tony Jun Huang, Focusing microparticles in a microfluidic channel with standing surface acoustic waves (SSAW), Lab Chip, 2008, 8, 221-223
39 I-Fang Cheng, Hsien-Chang Chang, Diana Hou, and Hsueh-Chia Chang, An integrated dielectrophoretic chip for continuous bioparticle filtering, focusing, sorting, trapping, and detecting, Biomicrofluidics 1, 021503 (2007)
40 N. Pamme, Magnetism and microfluidics, Lab Chip, 2006, 6, 24-38
41 Zhao Y, Fujimoto BS, Jeffries GDM, Schiro PG, Chiu DT (2007), Optical gradient flow focusing. Opt Express 15:6167–6176
42 Choi S, Song S, Choi C, Park JK, Sheathless Focusing of Microbeads and Blood Cells Based on Hydrophoresis, Small. 2008 May;4(5):634-41
43 Choi S and Park JK, Sheathless Hydrophoretic Particle Focusing in a Microchannel with Exponentially Increasing Obstacle Arrays, Anal. Chem. 2008, 80, 3035-3039
44 Di Carlo D, Inertial microfluidics, Lab Chip, 2009, 9, 3038–3046
45 Bhagat AA, Kuntaegowdanahalli SS, Kaval N, Seliskar CJ, Papautsky I., Inertial microfluidics for sheath-less high-throughput flow cytometry, Biomed Microdevices (2010) 12:187–195
46 Daniel R. Gossett and Dino Di Carlo, Particle Focusing Mechanisms in Curving Confined Flows, Anal. Chem. 2009, 81, 8459–8465

47 Dino Di Carlo, Daniel Irimia, Ronald G. Tompkins, and Mehmet Toner, Continuous inertial focusing, ordering, and separation of particles in microchannels, Proc. Natl. Acad. Sci. USA, 104, 18892-18897 (2007)
48 Chih-Chang Chang, Zhi-Xiong Huang and Ruey-Jen Yang, Three-dimensional hydrodynamic focusing in two-layer polydimethylsiloxane (PDMS) microchannels, J. Micromech. Microeng. 17 (2007) 1479–1486
49 Yu-Jui Chiu, Sung Hwan Cho,d Zhe Mei, Victor Lien, Tsung-Feng Wu, and Yu-Hwa Lo, Universally applicable three-dimensional hydrodynamic microfluidic flow focusing, Lab Chip. 2013 May 7; 13(9): 1803–1809
50 Vyawahare S, Griffiths AD, Merten CA, Miniaturization and parallelization of biological and chemical assays in microfluidic devices, Chem Biol. 2010 Oct 29;17(10):1052-65
51 E. Schonbrun, S. S. Gorthi, and D. Schaak, Microfabricated multiple field of view imaging flow cytometry, Lab Chip, 2011, 12 , 268-273.
52 Shin-Hyun Kim, Jin Woong Kim, Do-Hoon Kim, Sang-Hoon Han, David A. Weitz, Enhanced-throughput production of polymersomes using a parallelized capillary microfluidic device, Microfluidics and Nanofluidics March 2013, Volume 14, Issue 3-4, pp 509-514
53 Metzker, M.L. (2010). Applications of next-generation sequencing technologies— the next generation. Nat. Rev. Genet. 11, 31–46
54 Régis Baudoin, Giulia Alberto, Patrick Paullier, Cécile Legallais, Eric Leclerc, Parallelized microfluidic biochips in multi well plate applied to liver tissue engineering, Sens. Actuat. B: Chem., 173 (2012), pp. 919–926
55 P. Chao, T. Maguire, E. Novik, K.C. Cheng, M.L. Yarmush, Evaluation of a microfluidic based cell culture platform with primary human hepatocytes for the prediction of hepatic clearance in human, Biochemical Pharmacology 78 (2009) 625–632
56 Lim, J.-M., Bertrand, N., Valencia, P.M., Rhee, M., Langer, R., Jon, S., Farokhzad, O.C., (...), Karnik, R., Parallel microfluidic synthesis of size-tunable polymeric nanoparticles using 3D flow focusing towards in vivo study (2014) Nanomedicine: Nanotechnology, Biology, and Medicine, 10 (2), pp. 401-409.
57 D. Conchouso, D. Castro, S. A. Khanb and I. G. Fouldsac, Three-dimensional parallelization of microfluidic droplet generators for a litre per hour volume production of single emulsions, Lab Chip, 2014,14, 3011-3020
58 P. S. Dittrich and P. Schwille, An integrated microfluidic system for reaction, high-sensitivity detection, and sorting of fluorescent cells and particles, Anal. Chem., 2003, 75, 5767–5774.
59 M. M. Wang, E. Tu, D. E. Raymond, J. M. Yang, H. Zhang, N. Hagen, B. Dees, E. M. Mercer, A. H. Forester, I. Kariv,
P. J. Marchand and W. F. Butler, Microfluidic sorting of mammalian cells by optical force switching, Nature Biotech, 2005, 23, 83–87.
60 M. McClain, C. Culbertson, S. Jacobson and M. Ramsey, Flow Cytometry of Escherichia coli on Microfluidic Devices, Anal. Chem., 2001, 73, 5334–5338.
61 McKenna BK, Salim H, Bringhurst FR, Ehrlich DJ., 384-channel parallel microfluidic cytometer for rare-cell screening, Lab on a Chip. 2009;9:305–310.
62 J Berthier, P SIlberzan, Microfluidics for Biotechnology, Artech House, 2nd Edition, 2010

3. Numerical simulation for the fluid dynamic design of microfluidic devices

Microfluidic technology allows realizing devices suitable for each particular application. In the design phase, it is useful to have the possibility to predict the fluid behavior inside the designed pattern, without the need of practically realizing and testing the device.
In this Chapter, after a brief introduction to the numerical methods, the software COMSOL Multiphysics is introduced, in particular referring to the Microfluidics Module. Results of numerical simulations for characterization of hydrodynamic focusing in microchannels are reported in the next chapters.

3.1 Introduction to Numerical Simulation and Finite Element Method (FEM)

Numerical simulation method is based on the theoretical description of the physical systems. Initially, the mathematical equations are derived for a continuous domain. Then, the equations are discretized, applied and solved only in a finite number of points of the domain. Discretization of the analyzed system is the bases for numerical simulation. The discretization of the domain in finite elements, generates the so called *mesh*.
Various methods of discretization have been proposed.
The Finite Element Method (FEM) is considered as a general discretization procedure of continuum problems [2]. The method was originally developed to study the stresses in complex air-frame structures [3] and was later extended to the general field of continuum mechanics [4].
The finite element considers that the solution region comprises many small, interconnected, sub-regions or elements and gives a piece-wise approximation to the governing equations, that is, the complex partial differential equations are reduced to either linear or nonlinear simultaneous equations. Since the finite element method allows us to form the elements, or sub-regions, in an arbitrary sense, a close representation of the boundaries of complicated domains is possible. The solution of a continuum problem by the finite element method is approximated by the following step-by-step process [5]:

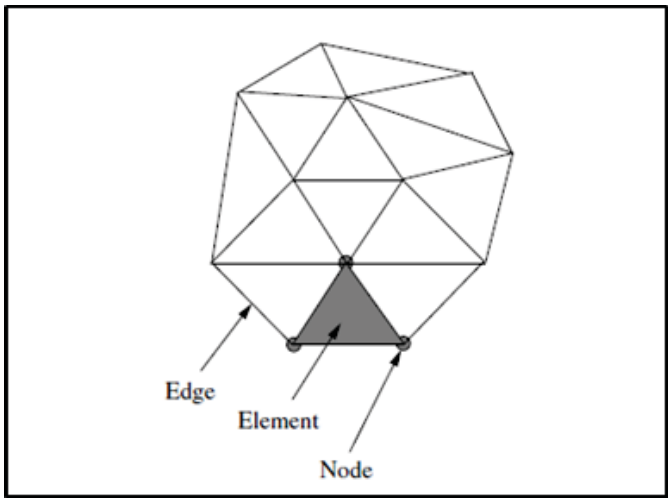

Figure 1: Typical finite element mesh. Elements, node and mesh [5]

- Discretize the continuum: divide the solution region into non-overlapping elements or sub-regions. The finite element discretization allows a variety of element shapes, for example, triangles, quadrilaterals. Each element is formed by the connection of a certain number of nodes (Figure 1).
- Select interpolation or shape functions: the next step is to choose the type of interpolation function that represents the variation of the field variable over an element.
- Form element equations (Formulation)
- Assemble the element equations to obtain a system of simultaneous equations
- Solve the system of equations.

In this thesis k attention is kept on the application of numerical simulation is the investigation of the behavior of fluid flow.

3.2 COMSOL Multiphysics

COMSOL Multiphysics software is a powerful finite element (FEM), partial differential equation (PDE) solution engine. The basic COMSOL Multiphysics software has eight add-on modules that expand the capabilities of the basic software into the following application areas: AC/DC, Acoustics, Chemical Engineering, Earth Science, Heat Transfer, MEMS, RF, and Structural Mechanics [6].
Multiphysics is a recent conceptualization to categorize modeling where different physicochemical mechanisms are prevalent in a given application, but to be multiphysics, the field equations must couple [7].
So, "multiphysics" refers to simulations that involve multiple physical models or multiple simultaneous physical phenomena.

3.2.1 The COMSOL Microfluidics Module [8]

The COMSOL Microfluidics Module is used by engineers and scientists to understand, predict, and design microfluidic systems.
The Microfluidics physics interfaces are used to set up a simulation problem. Each physics interface expresses the relevant physical phenomena in the form of sets of partial or ordinary differential equations, together with appropriate boundary and initial conditions. Each feature added to the interface represents a term or condition in the underlying equation set. The Microfluidics Module includes a number of physics interfaces for modeling different types of microfluidic device.

3.2.2 The COMSOL Laminar Flow Interface

The Laminar Flow interface, found under the Single-Phase Flow branch when adding a physics interface, is used to compute the velocity and pressure fields for the flow of a single-phase fluid in the laminar flow regime. A flow will remain laminar as long as the Reynolds number is below a certain critical value. At higher Reynolds numbers, disturbances have a tendency to grow and cause transition to turbulence.
The Reynolds number is given by [9]:

$$Re = \frac{\rho\, u\, L}{\mu}$$

where ρ is the fluid density, u the velocity of the flow, L the characteristic length scale of the system, and μ the dynamic viscosity. The physical significance of the Reynolds number is that it is a measure of the ratio between inertial forces and viscous forces in a particular flow. The different regimes of behavior are:

- Re << 1viscous effects dominate inertial effects (completely laminar flows);
- Re ≈ 1 viscous effect comparable to inertial effects (vortices begin to appear);
- Re >> 1 inertial effects dominate viscous effects (turbulence occurs).

In Microfluidics due to the small length of the system, we are in Laminar Flow condition. Inertial Forces are negligible.
The equations solved by the Laminar Flow interface are the Navier-Stokes equations for conservation of momentum (1) and the continuity equation (2) for conservation of mass [10]:

$$\frac{d\vec{u}}{dt} + (\vec{u} \cdot \nabla)\vec{u} = -\frac{1}{\rho}\nabla p + u\nabla^2\vec{u} + \vec{g} \quad (1)$$

$$\nabla \cdot \vec{u} = 0 \quad (2)$$

The equation (1) is a balance of the forces acting on a single fluid element:

$$\vec{f}_{net\ inertial} = -\vec{f}_{net\ pressure} + \vec{f}_{net\ viscous} + \vec{f}_{net\ body} \quad (3)$$

3.2.3 The COMSOL Transport of Diluted Species Interface

The Transport of Diluted Species interface is used to compute the concentration field of a dilute solute in a solvent. The driving forces for transport can be diffusion by Fick's law or convection, when coupled to fluid flow.
The default node attributed to The Transport of Diluted Species Interface assumes chemical species transport through diffusion and convection and implements the mass balance equation:

$$\frac{dc}{dt} + u \cdot \nabla c = \nabla \cdot (D\nabla c) + R \quad (4)$$

With c the concentration of the species, D denotes the diffusion coefficient, R is a reaction rate expression for the species, and u is the velocity vector.
The diffusion constant D thus determines how fast a concentration diffuses a certain distance. Values of D are listed typically are [13]:

- D ≈ 2×10^{-9} m^2/s, small ions in water
- D ≈ 5×10^{-10} m^2/s, sugar molecules in water
- D ≈ 4×10^{-11} m^2/s, 30-base-pair DNA molecules in water
- D ≈ 1×10^{-12} m^2/s, 5000-base-pair DNA molecules in water

which for diffusion across the typical microfluidic distance L_0 = 100 µm give the times

- T_0(100 µm) ≈ 5 s, small ions in water
- T_0 (100 µm) ≈ 20 s, sugar molecules in water
- T_0 (100 µm) ≈ 250 s ≈ 4 min, 30-base-pair DNA molecules in water
- T_0(100 µm) ≈ 104 s ≈ 3 h, 5000-base-pair DNA molecules in water.

The Péclet number is the dimensionless number relevant in the study of transport phenomena in fluid flows. It is defined to be the ratio of the rate of convection of a physical quantity by the flow to the rate of

diffusion of the same quantity driven by an appropriate gradient. For high Péclet number we are in a convection dominate regime: the molecules transport due to convection happens faster than the one due to diffusion. For low Péclet number we are in a diffusion dominate regime: diffusion happens much faster than convection. The latter one is the typical condition that rules in microfluidics.

3.2.4 The COMSOL Particle Tracing Module [11]

Since one of the main goal of microfluidic technology is the analysis of cells while they are flowing, it becomes useful to have a support that helps to predict the behavior of objects diluted in the fluid.
The Particle Tracing Module is a general purpose, flexible tool that allows tracing the trajectories of particles in the presence of an external field. There is also a dedicated interface for tracing particle trajectories in a fluid system (Particle Tracing for Fluid Flow Module). The Particle Tracing for Fluid Flow Interface is designed for modeling microscopic and macroscopic particles in a background fluid. In order for the particle tracing approach to be valid, the fluid system should be a dilute or dispersed flow. This means that the volume fraction of the particles is much smaller than the volume fraction of the continuous phase, generally less than 1%. When the volume fraction of the particles is not small, the fluid system is categorized as a dense flow and a different modeling approach is required.

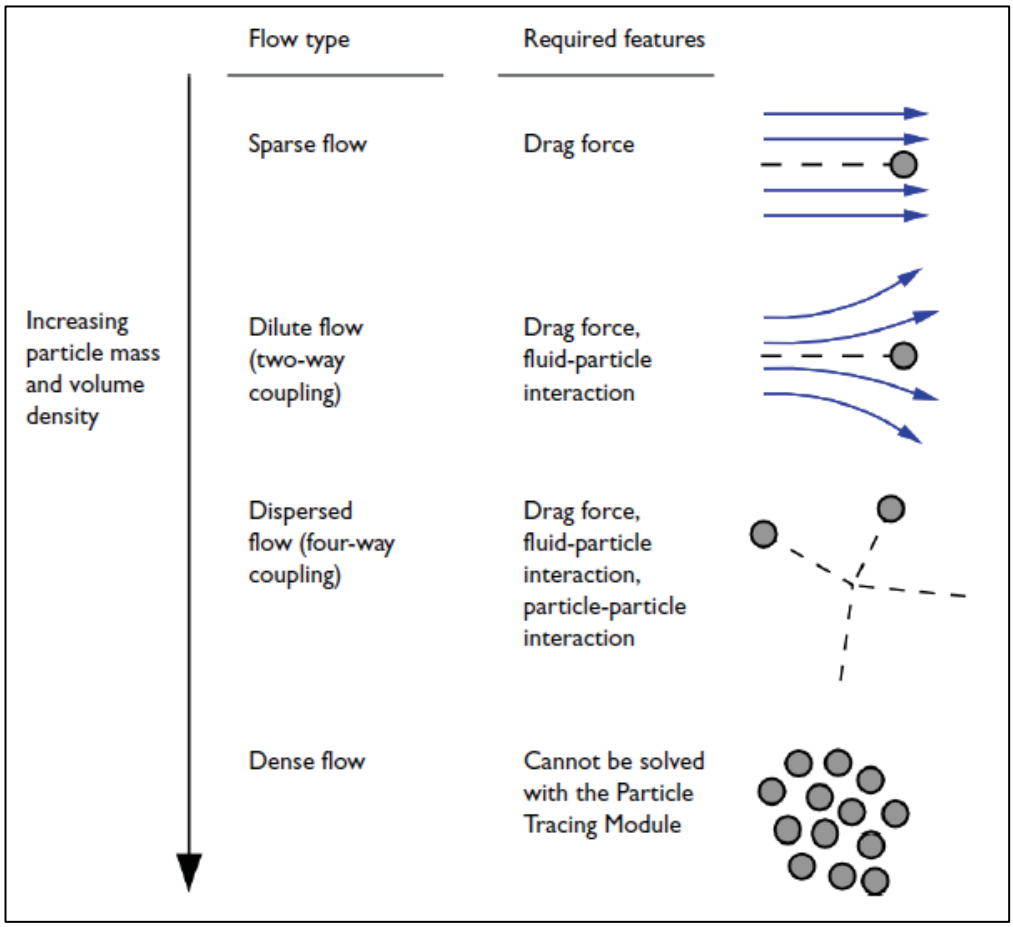

Figure 2: The physics features required to model sparse, dilute, and disperse flow in the COMSOL Particle Tracing

Particle tracing provides a Lagrangian description of a problem by solving ordinary differential equations using Newton's second law of motion:

$$m\,\frac{dx^2}{dt^2} = F\left(t, x, \frac{dx}{dt}\right) \quad (5)$$

where x is the position of the particle, m the particle mass, and F is the sum of all forces acting on the particle. Examples of forces acting on a particle in a fluid are the drag force, the buoyancy force, and the gravity force. The drag force represents the force that a fluid exerts on a particle due to a difference in velocity between the fluid and the particle.
The drag coefficient depends upon the particle characteristics and so, upon the Reynolds particle number Re_p:

$$Re_p = \frac{|u - u_p|2a\rho}{\mu} \quad (6)$$

where u is the velocity of the fluid, u_p the particle velocity, a the particle radius, ρ the fluid density, and μ the fluid dynamic viscosity.
The empirical expression for the drag force F is the following one [12]:

$$F = \pi a^2 \rho\, |u - u_p|(u - u_p)\left[1.84\, Re_p^{-0.31} + 0.293 Re_p^{0.06}\right]^{3.45} \quad (7)$$

3.3 COMSOL tools for the hydrodynamic characterization of microfluidic devices

As explained in the Chapter 1, the first major step to reproduce a flow cytometry on a chip is to substitute the traditional glass capillary chamber with a microfluidic channel. In the traditional technology, particles are focused in order that only once per time can pass to the interrogation/detection region. This particles focusing is achieved by adding an additional sheath fluid, that surrounding the sample fluid, allows aligning the particles in the middle of the stream.
The described focusing effect is called hydrodynamic focusing. Since microfluidic technology has been developed, various examples of lab on chip device for particles focusing have been designed and realized.
These micro-devices allow also to exploit different method to induce particles focusing: hydrodynamic[16], electro-osmotic[18] focusing, dielectrophoretic[19-20] (DEP), hydrophoretic[21], and inertial focusing[22-23].
In many of these works it has been showed as numerical simulations give an important support in the design phase of a new device. Actually, a complete numerical analysis must follow the following steps:

- Design of the micro-channel geometry;
- Definition of the values for the fundamental physical parameters;
- Visualization of the results in the post-processing analysis.

So, the first step consists in the design of the channel geometry. In order to tracing the trajectories of particles flowing in a fluid, at the starting phase of the numerical simulation, it is necessary to define the values for the parameters fundamental for solving the physical equations. The list of these parameters is summarized in Table 1. It can be seen that there is the needing to define the fluid (Laminar Flow Physics) and the particles (Particle Tracing Physics) characteristics.

PARAMETER	DESCRIPTION
T	Ambient Temperature
Sample Flow Rate	Sample Flow Rate
In-Plane Sheath Flow Rate	Horizontal Focusing Sheath flow rate
Out-of-Plane Sheath Flow Rate	Vertical Focusing Sheath Flow Rate
Particles Density	Latex Density
Particles Diameter	Diameter of latex particles

Table 1: List of the parameters that have to be defined in order to tracing particles flowing in a fluidic channel.

Once the equations are solved, the post-processing analysis will allow to visualize the obtained results. ***2D and 3D plots*** on a selected data set can be used to understand the behavior of a physical quantity on the analyzed domain, i.e. the *velocity map* (Figure 3) or *concentration of diluted species (*Figure 4).

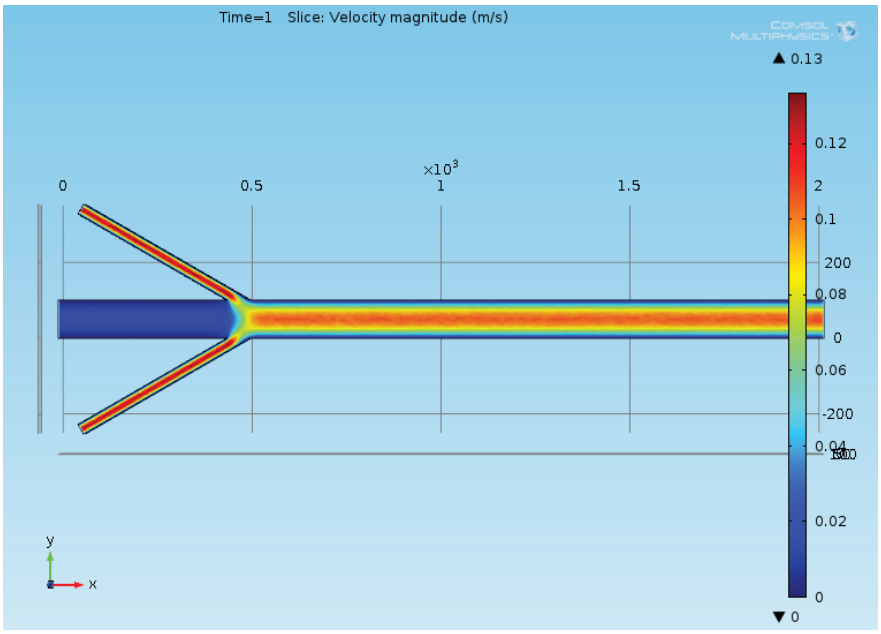

Figure 3: Velocity Magnitude (m/s) of the fluid flow in the microchannel reported on a 2D plot.

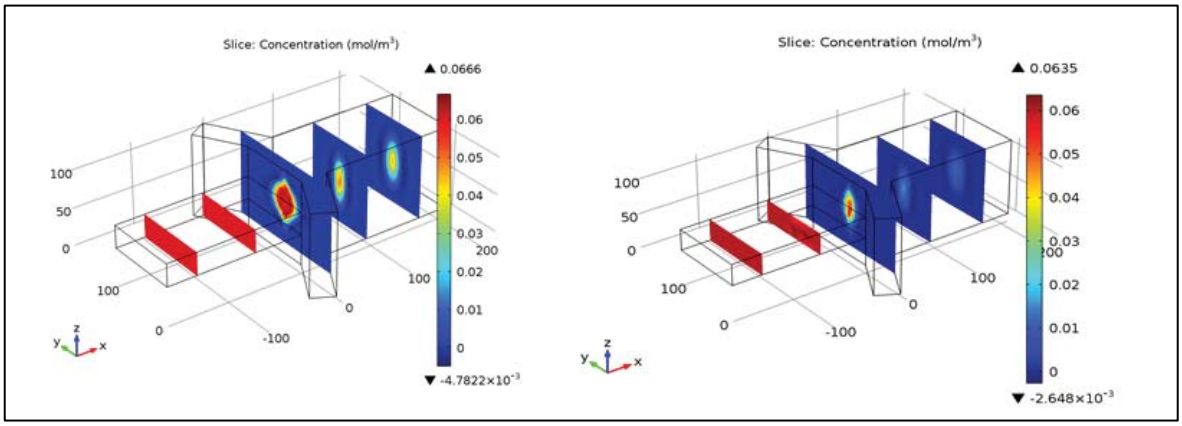

Figure 4: Slices defined on 3D plots allow to visualize the concentration of diluted species at different positions.

Moreover, from the particle tracing study, the ***particles trajectories*** (Figure 5.a) can be plotted. In addition, an useful way of plotting particles position is to use a ***Poincaré Map***. This plot type is useful to visualize the particle trajectories in a plot that represents the position of the particles in a section that is usually transversal to the particle trajectories. The resulting plot places a dot on the cut plane at the location where a particle crossed the plane (Figure 5.b).

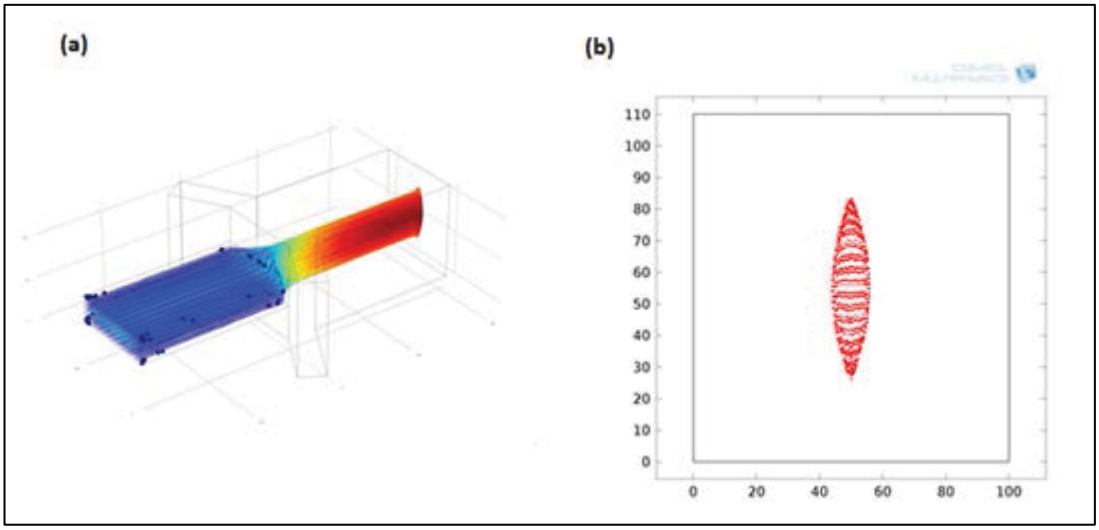

Figure 5: (a) Particle Trajectories (b) The Poincaré map shows the particles position in a section transversal to the particle trajectories.

3.4 Conclusions

Numerical simulations give the possibility to characterize the behavior of physical systems in different fields.

In recent years, a considerable progress has been made in the field of miniaturization. It is now effectively possible to miniaturize all kinds of systems—e.g. mechanical, fluidic, electromechanical, or thermal—down to sub-micrometric sizes [24]. In particular, there is a diffuse interest in the realization of micro-chips that allow to reproduce processes and reactions that are usually performed on a bench.

Among the proposed applications, miniaturization of traditional instrumentation for cells analysis has promised to realize systems that cheaper, easily transportable, and therefore suitable for the Point-of-Care (POR) diagnostics.

In this chapter, it has been showed how numerical simulations can be useful for the characterization of a novel microfluidic structure.

Using the commercial software Comsol Multiphysics, the behavior for both the fluid flow and particles can be predict. In addition, the available tools for the post-processing analysis allow to well visualize the results (i.e. fluid velocity and particles position).

References

1 Griebel M., T. Dornseifer, and T. Neunhoeffer, Numerical Simulation in Fluid Dynamics: A Practical Introduction, Society for Industrial and Applied Mathematics (SIAM), 1998

2 Zienkiewicz O.C., Taylor R. L., The Finite Element Method. Volume 1: The Basis, Fifth Edition, Butterworth-Heinemann, 2000

3 Clough RW, The finite element analysis in plane stress analysis, Proc. 2nf ASCE Conf. on Electronic Computation, Pittsburgh, PA, September 1960

4 Zienkiewicz OC and Cheung K, Finite elements in the solution of field problems, Engineer, 200, 507–510, 1965

5 R.W. Lewis, P. Nithiarasu, K.N. Seetharamu, Fundamental of the Finite Element Method for Heath and Fluid Flow, John Wiley & Sons, Ltd, 2004

6 Pryor R. W., Multiphysic Modeling using COMSOL. A First Principles Approach, Jones and Bartlett Publishers, 2000.

7 W. B. J. Zimmerman, COMSOL Process modeling and simulation with finite element methods, World Scientific Publishing Co. Pte. Ltd., 2004

8 COMSOL Multiphysics Documentation: The Microfluidics Module

9 Nam-Trung Nguyen and Steven T. Wereley, Fundamentals and Applications in Microfluidics, 2006 ARTECH HOUSE, INC.

10 Kleinstreuer C., Modern Fluid Dynamics. Basic Theory and Applications in Macro- and Micro-Fluidics, Springer, 2010

11 COMSOL Multiphysics Documentation: The Particle Tracing Module

12 J.M. Coulson and J.F. Richardson, Particle Technology and Separation Processes, Chemical Engineering, Volume 2, Butterworth-Heinemann, 2002.

13 H. Bruus, Theoretical Microfluidics, Oxford Master Series in Condensed Matter Physics, 2007

14 H. M. Shapiro, Practical Flow Cytometry, 4th edition, Wiley Liss, 2003

15 C. D. Chin, V. Linder and S. Sia, Lab-on-a-chip devices for global health: Past studies and future opportunities, Lab on Chip, 7, 41-57, 2007

16 Simonnet, C., Groisman, High-throughput and high-Resolution flow cytometry in molded microfluidic devices, A. Anal. Chem. 2006, 78, 5653−5663.

17 J. G. Santiago, Electroosmotic Flows in Microchannels with Finite Inertial and Pressure Forces, Anal. Chem. 2001, 73, 2353-2365.

18 L. Wang, L. A. Flanagan, N. Li Jeon, E. Monuki and A. P. Lee, Dielectrophoresis switching with vertical sidewall electrodes for microfluidic flow cytometry, Lab Chip, 2007, 7, 1114–1120.

19 J. Gao, R. Riahi, M. L. Y. Sin, S. Zhang and P. K. Wong, Analyst, Electrokinetic Focusing and Separation of Mammalian Cells in Conductive Biological Fluids, 2012, 137, 5215–5221.

20 Choi, S., Park, J.-K., Sheathless hydrophoretic particle focusing in a microchannel with exponentially increasing obstacle arrays, Anal. Chem. 2008, 80, 3035–3039.

21 D. Di Carlo, D. Irimia, R. G. Tompkins and M. Toner, Continuous inertial focusing, ordering, and separation of particles in microchannels, Proc. Natl. Acad. Sci. USA, 2007, 104, 18892–18897

22 D. Di Carlo, Inertial Microfluidics, Lab Chip, 2009, 9, 3038–3046

23 N. Watkins, B. M. Venkatesan, M. Toner, W. Rodriguez and R. Bashir, A robust electrical microcytometer with 3-dimensional hydrofocusing, Lab Chip, 2009, 9, 3177–3184.

24 P. Tabeling, Introduction to Microfluidics, Oxford, 2005

4. Hydrodynamic self-focusing in a parallel microfluidic device through cross-filtration

In this chapter we present a novel parallelized microfluidic device that allows to achieve hydrodynamic focusing by needing of only one inlet. This is achieved by introducing a cross-filter region at each one of the parallel channels. The great advantage in the proposed device is that, since only one inlet is needed, multiple parallel micro-channels can be easily introduced into the design. Numerical simulations were performed in order to test and define the optimal design. The operation of the realized devices was tested by using both polystyrene beads and Acute Lymphoid Leukemia (ALL) cells.

4.1 Introduction

Focusing is a fundamental prior step in order to sort, analyze and detect particles flowing in a fluidic system. For instance, in cytofluorimeters it allows to align the target cells in a single line, as they pass through the detection region.

In lab-on-a-chip development, cell focusing is still an open problem. Since microfluidic technology has been introduced, different methods to get cells focused have been exploited: hydrodynamic [1-3], electro-osmotic [4] (EOF), dielectrophoretic [5-6] (DEP), hydrophoretic [7], and inertial focusing [8-10].

Among these proposed methods a simplest approach to achieve particle focusing is driving the particle solution through a converging microchannel whose small passage ensures particles to travel in a single line. This method is, however, only applicable to dilute particle solutions, and so the particle throughput is very limited. The other particle focusing methods may be conveniently classified as *sheath flow focusing* and *sheathless focusing* [11].

Sheathless focusers achieve particle focusing in a pressure-driven or electrokinetic suspension flow by the use of either an externally applied or an internally induced force field. EOF, DEP, hydrophoretic and inertial focusing methods are included in this group.

DEP is the translational motion of particles due to either the induced (i.e., in polymer beads, cells, viruses, etc.) or native (i.e., in proteins) electrical dipoles in an electric field gradient.

Therefore, if in the electric field non-uniformities normal to streamlines exists, particles can be deflected across the streamlines by DEP and focused to tight stream in the region of balanced forces. Traditional dielectrophoretic particle focusing methods are based on the non-uniform AC electric field between pairs of patterned microelectrodes inside microchannels. The main drawback of using this approach is that there is the needing of suppressing Joule heating effects and electrochemical reactions (e.g., generating bubbles and other deleterious chemicals), which may cause adverse effects to bioparticles especially severe to mammalian cells. In addition, the focusing efficiency is very sensitive to the particle location as the dielectrophoretic force decays rapidly away from the electrode surfaces.

About hydrophoretic focusing, it is based on hydrophoresis effect, that indicates the movement of suspended particles in response to a microstructure-induced pressure field. Research groups have demonstrated he possibility to exploit this motion for microspheres and cells separation when obstacles are introduced in a microchannel. Hydrophoretic particle focusing it seems simple to control. However, the patterning of micro-obstacles on channel walls requires a non-trivial fabrication. Moreover, as the obstacle height needs to be comparable to the particle size for efficient focusing, particle throughput may be limited due to the potentially large probability of clogging.

Inertial focusing utilizes the cross-stream particle motion to focus particles into one or multiple streams through a microchannel. The first related experiment was done by Segre and Silberberg (1961), where particles were observed to migrate toward a narrow annulus in a centimeter-scale circular pipe. This effect is a result of

competition of inertial lift forces acting on particles, of which the two dominant ones are the walls lift and the shear-gradient induced lift. This condition is achievable for particle motion in laminar microfluidic devices.
Inertial focusing has been investigated in both straight and curved microchannels. In particular, in curved channels, when inertia is important, a secondary transverse flow is formed. This double recirculation, exerts a position-dependent Dean drag force on particles, which biases the particle equilibrium positions. By engineering the microchannel symmetry, researchers observed the possibility to focus micro-particles in a single point by using an asymmetric sinusoidal channel. Inertia-based particle focusing method is simple and able to offer a very high particle throughput, which, on one hand, makes this method suitable for high-speed applications such as flow cytometry, while on the other hand, poses difficulty on the treatment of rare or precious particles as the particle suspension must flow very fast to induce a decent inertial motion in microchannels. Moreover, as both the number and the equilibrium positions of the focused particle stream are sensitive to the particle Reynolds number, the operation of such inertial particle focusers becomes difficult and complicated.
Sheath flow focusers use one or more sheath fluids to pinch the particle suspension flow and thus focuses the suspended particles. Hydrodynamic focusing, the standard method used in flow cytometry, is the focusing method that traditionally is classified as sheath based. In microfluidics, it's the easiest method to realize, from a design and fabrication point of view, and the most diffused [12]. Its applications have been employed in a wide variety of biological analyses, including on-chip flow cytometry, single molecule detection, and laminar mixers for the study of rapid chemical and enzymatic kinetics.
The principle of hydrodynamic focusing is simple: a central sample solution with a low flow rate flows within an outer fluid sheath traveling at a higher flow rate, thus enabling the compression of the inner sample flow.
Anyway, the micro-channel configurations till now adopted, have the main drawback of requiring of multiple inlets. This induces an undesired complication, strongly limiting the actual exploitation of parallelization, that is one of the main advantages introduced by microfluidic technology. Indeed, the possibility of having more channels working simultaneously helps with the clogging problems and, at the same time, increases the throughput [13].
In this chapter it has been developed a device that realize an hydrodynamic flow focusing by only needing of one inlet.
This is achieved by adopting a cross-filter configuration. In a cross-filter, the fluid flows parallel to the pores membrane. This allows having a better filter efficiency than a traditional dead-end filter and well fit the requirement of disposable microfluidic devices.
The cross-filter is realized through two arrays of pillars, and the gap size between two consecutive pillars determines the size of the pores of the membrane. The device has to be designed according to the diameter of the target particles. In this way only the fluid can cross the membrane, whilst particles or cells are forced to stay confined at the center. At the end of the filter region, the "sample fluid" from the center, and the "sheath fluid" from the lateral channels, are recombined in what we call "focusing region".
The operation of the device was tested first by numerical simulation, and the results were adopted to define the geometrical parameters.
Microfluidic applications of the cross-filtration method are generally devoted to the realization of sorting devices. Among these works, some try to realize devices for red blood cells (RBC) and white blood cells [14] separation, and for separation of cells from blood plasma [15].
We have found out that, once the pores and the pillars size is defined, the diameter of the focused stream, and therefore the sheath to sample ratio, is mainly a function of three geometrical parameters:

- L, the length of the filter region;
- W_L, the width of the lateral channels;
- φ, the inclination angle of the pillars arrays.

The novel designed device has the advantage to generate hydrodynamic focusing and also to have multiple parallel channels.

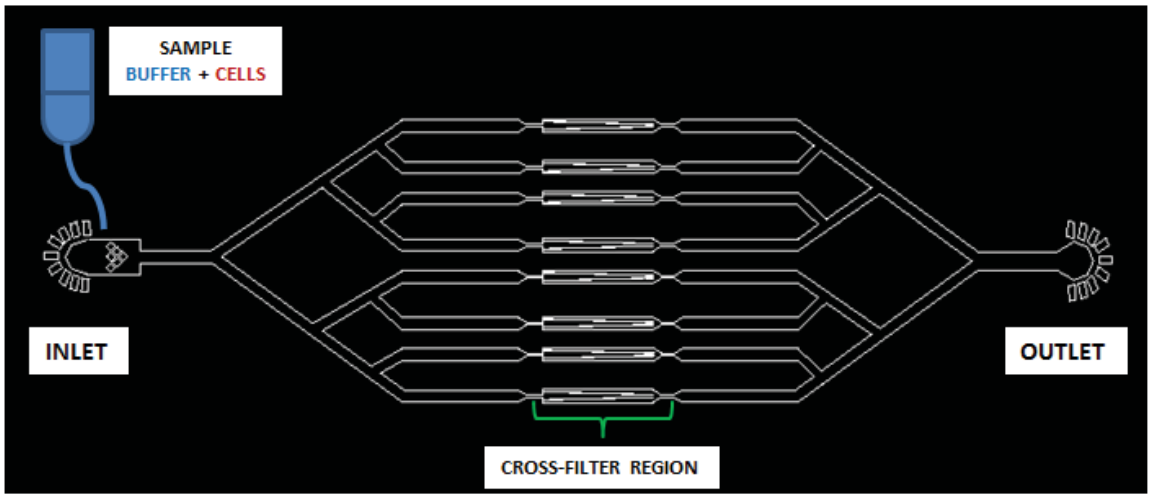

Figure 1: CAD design of the realized parallel microfluidic device.

Moreover, by adjusting the geometrical parameters of the filter region, it is possible to customize the device for each specific application. This kind of approach well fits the needing of the market interested into the production of cheap and disposable microfluidic devices for the point-of-care diagnostics.

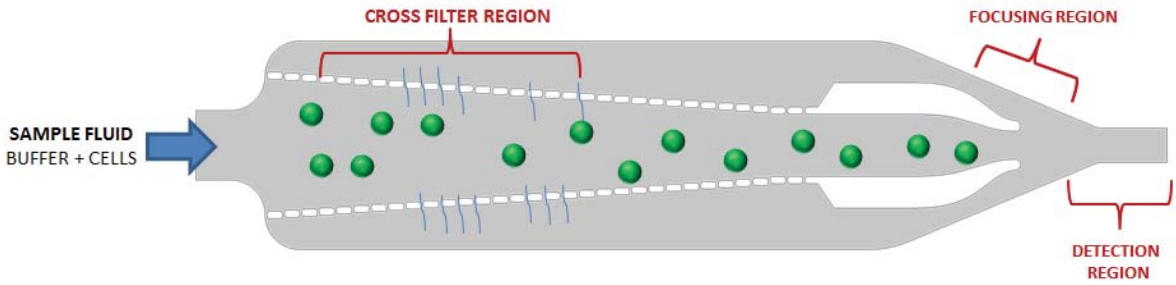

Figure 2: The designed parallel microfluidic device. The design has eight channels, working at the same time. The figure shows the detail of the cross-filter region. Two arrays of pillars separate that area in three regions. The gaps between the pillars act as pores of a membrane. The gaps size determine the selection of the particles/cells that can pass through the membrane.

4.2 Micro-chip design

In this section the theoretical assumption for the design of the device are presented. Moreover, here we report the numerical simulations results, performed by COMSOL Multiphysics, in order to define the optimal parameters for the final chip configuration.

4.2.1 Operating Principle

The developed device has only one inlet and one outlet. The sample fluid coming from the single inlet is then split into eight parallel micro-channels.
Each channel has a separation region that works on the cross-filtration principle. In a cross-filter [16] the fluid flows parallel to the filter pores, in contrast to what happens in a traditional dead-end filter [17], in which the fluid direction is perpendicular to the filter surface.
The filter is obtained by introducing two pillars arrays into the device. The gaps between the pillars operate as pores of a filter membrane.
The size of the filtering pores was chosen in order to allow only particles with a specific size to cross the filter. The length and pillars positioning were chosen in order to reduce the filter clogging problem. The gaps size have been chosen according to the target cells size. In particular, pores must be smaller than the mean cells diameter. In this way, when the sample fluid comes in the filtration region, only to the buffer solution is allowed to laterally moves, whilst cells are forced to stay confined into the central region.
Then, in what we call focusing region, the "sheath" fluid coming from the lateral channels, and the "sample" fluid coming from the center are recombined in one single channel. Cells will result to be focused in the interrogation region (Figure 2).

4.2.2 Theoretical assumptions for the design

In cross-flow filtration the fluid flows tangentially to the filter surface. The portion of fluid that can cross the filter pores is really small, compared to a dead-end filter configuration.

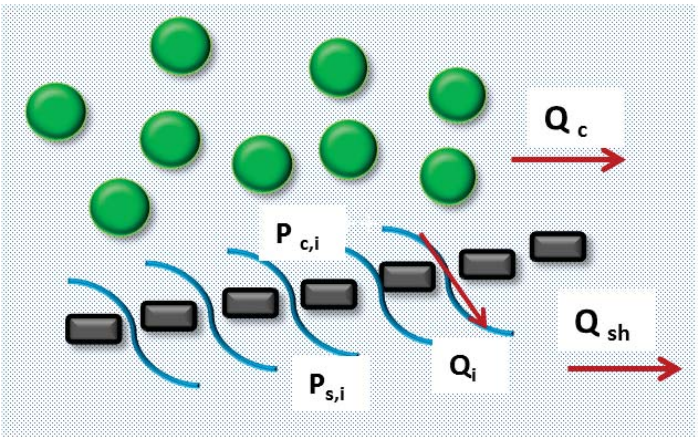

Figure 3: Schematic of a cross-filter separation region.

The equation that relates the pressure and the flow rate is

$$\Delta P = R_h \, Q$$

with R_h the hydraulic resistance of the channel. For a rectangular channel R_h is

$$R_h = \frac{12\mu L}{w\,h^3}\left[1 - \frac{h}{w}\left(\frac{192}{\pi^5}\sum_{n=1,3,5}^{\infty}\frac{1}{h^5}\tanh\frac{n\pi w}{2h}\right)\right]$$

where *h* is the channel depth and *w* is the channel width. If *w* << *h* or *h* << *w*, the previous expression can be simplified as follows

$$R_h = \frac{12\,\mu\,L}{w\,h^3}$$

Our filter was designed by considering that the flow rate through the i-th pore is mainly a function of two parameters:

$$\Delta Q_i \propto f(\Delta P_i, s\,)$$

where *s* is the gap size and $\Delta P_i = \left|P_{c,i} - P_{s,i}\right|$ is the pressure drop at the *i*-th gap, given by the difference between the pressure at the center and the side of the channel at the i-th gap.
At each side the total sheath flow rate is given by

$$Q_{sh} = \sum_{i}^{N}\Delta Q_i$$

with *N* the total number of pores in the device.
The sheath flow rate Q_{sh} determines the diameter *d* of the focused sample stream. In the proposed device, the total flow rate Q_{IN} is given by the value set at the inlet. Then the flow is split between the center, Q_{sa}, and the side, Q_{sh}. The following relation exists:

$$d = K\frac{Q_{sh}}{Q_{sa}}$$

Where *K* is a factor that has the dimension of a length.
For a channel with an arbitrary cross-sectional shape [18], the flow rate can be expressed by the following form of the Hegen-Poiseuille equation:

$$Q = \frac{1}{\gamma}\frac{\Delta P}{2\mu L}\frac{A^3}{P^2}$$

where γ is a dimensionless factor depending on the channel geometry, and P is the perimeter and A the area of the of the channel cross-section.
Using the previous equation, in the hypothesis that the pressure difference Δp, between the begin and the end of the filter region, is the same for the lateral and the central channel:

$$d = K\,\frac{\frac{1}{\gamma_L}\frac{A_L^3}{P_L^2}}{\frac{1}{\gamma_C}\frac{A_C^3}{P_C^2}}$$

Where the subscripts *L* and *C* denotes the geometrical parameters which refer to the lateral and the central channel. Therefore, the diameter of the focused stream is a function of the geometry of the filter region.

4.2.3 Numerical simulations to define the device geometry

Numerical simulations have been performed using COMSOL Multiphysics in order to define the right parameters for the final chip configuration. In this way, the desired value for the sheath to sample ratio has been achieved.
The numerical simulations results showed that the fluid fraction that cross the filter barrier, that contribute to the formation of the sheath flow rate Q_{sh}, depends upon the geometry of the cross-filter region.
Since, the diameter of the focused stream is a function of the Q_{sa} /$Q_{sh,}$ its value also depends upon the filter geometrical parameters. In particular we found out that:

$$d = f(W_L, L, \varphi)$$

where

- L, the length of the filter region;
- W_L, the width of the lateral channels;
- and φ, the inclination angle of the pillars arrays.

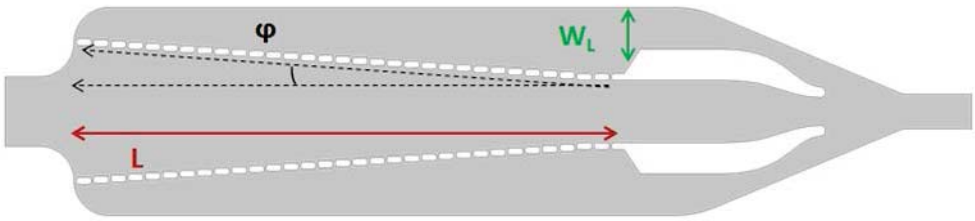

Figure 4: Critical parameters of the cross-filter geometry for the determination of the sheath to sample ratio

The inclination of the pillars arrays plays a significant role in controlling the pressure drop across the filter region. We studied the pressure profile along the filter region for a configuration with φ=0° and for one with φ= 1.5°. The results showed that for the first case, almost at the end of the filter, the pressure at the central channel gets lower than the pressure at the lateral channels. The fluid across the pores start to flow from the lateral channels to the center (figure 5). By adding a slope the pillars arrays this undesired effect is removed.
Figure 6.a and 6.b show the pressure profile at the central and lateral channel, respectively for the configuration with straight and inclined posts, are presented. It's clearly seen that in the second case the pressure at the center is higher than the pressure at the side for all the filter length. Figure 6.c shows the module of the pressure drop across the filter region, for the two filter configurations. For the design with straight posts the pressure difference changes in sign, this means by the physic point of view that the fluid change the flowing direction. This effect is not observed for the design with inclined posts.
A first numerical analysis was performed in order to demonstrate that, at a fixed channel thickness, the sheath flow rate increases by increasing the width of the lateral channels.

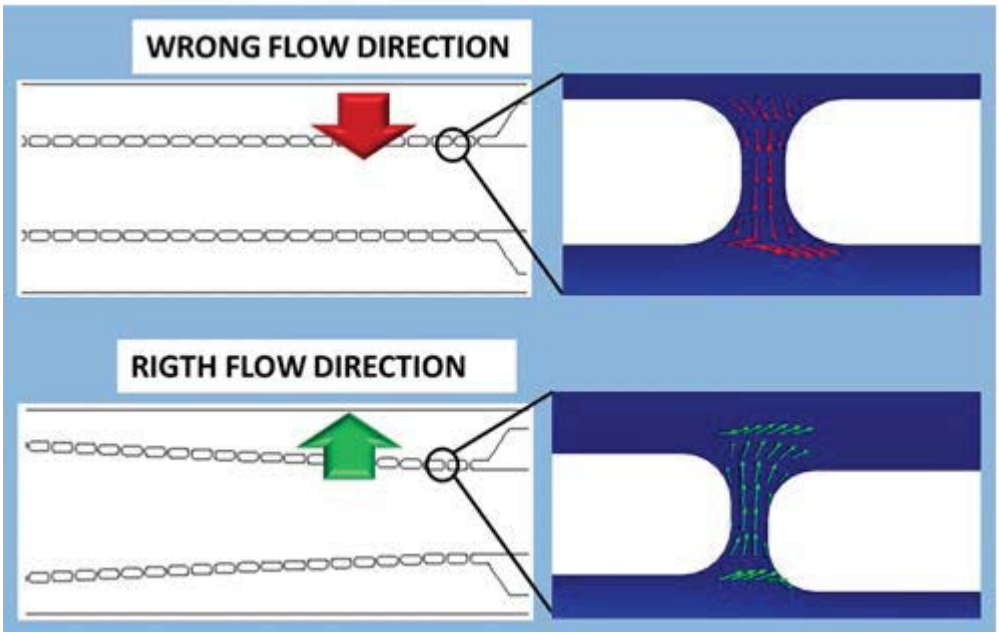

Figure 5: COMSOL Multiphysics results. The two filters are characterized by the same geometrical parameters. Only the inclination of the pillars arrays change. In the first case (up in the figure), in a condition with phi = 0°, almost at the end of the filtering region, the flow goes from the lateral channels to the center. This effect contribuite to weaken the focusing power. By adding a slight inclination, phi ≈ 1.5°, the previous effect is avoided.

In the performed analysis the width of the central channel was kept at constant value WC= 50 µm, and the lateral width has been varied W L = 35, 45, 55, 65, 75 and 85 µm.
The thickness of the channel was set at 10 µm, and the inlet flow rate was set at 100 µl/h.
The velocity profile at the end of the filtering region, where the sample and the sheath fluids recombine, was analyzed in order to calculate the sheath to sample ratio for the six different configurations.
The results show that the sheath to sample ratio linearly increase by increasing W_L (Figure 7). Then, the focusing power was studied as function of the length of the filtering region. The width of the central channel and the width of the lateral channel were fixed, WC= 50 µm and WL = 85 µm respectively.
Six different values of the length of the filtering region were considered, L = 420, 520, 620, 720, 820 and 920 µm. The analysis results (Figure 8) show that passing from L = 420 µm to 520 µm an increasing of $\Delta r \approx 0.5$ in the sheath to sample ratio is obtained. Instead, a less substantial change in the focusing power is observed for the subsequent filter length ($\Delta r \approx 0.1$).
Furthermore, the diameter d of the focused stream in the interrogation region was evaluate as function of the sheath to sample ratio r (Figure 9). The analysis says which is the sheath to sample ratio that we need to achieve in the designed geometry, according to the size of the target cells or particles.
As explained above in this chapter, the value of sheath to sample ratio, and hence the focusing power, depends upon the amount of fluid that moves across each pore to the lateral part of the filter. In particular, by adding an inclination to the pillars array it's possible to control the pressure drop along the filter region, and so Qsh.
Parametric numerical simulations have been performed using the COMSOL live-link for Matlab. Different cross-filter geometries have been studied and for each of them the sheath to sample ratio has been evaluated. From the results, we were able to build some contour maps that can be an useful support in the design phase of a device suitable for the desired target cell size.

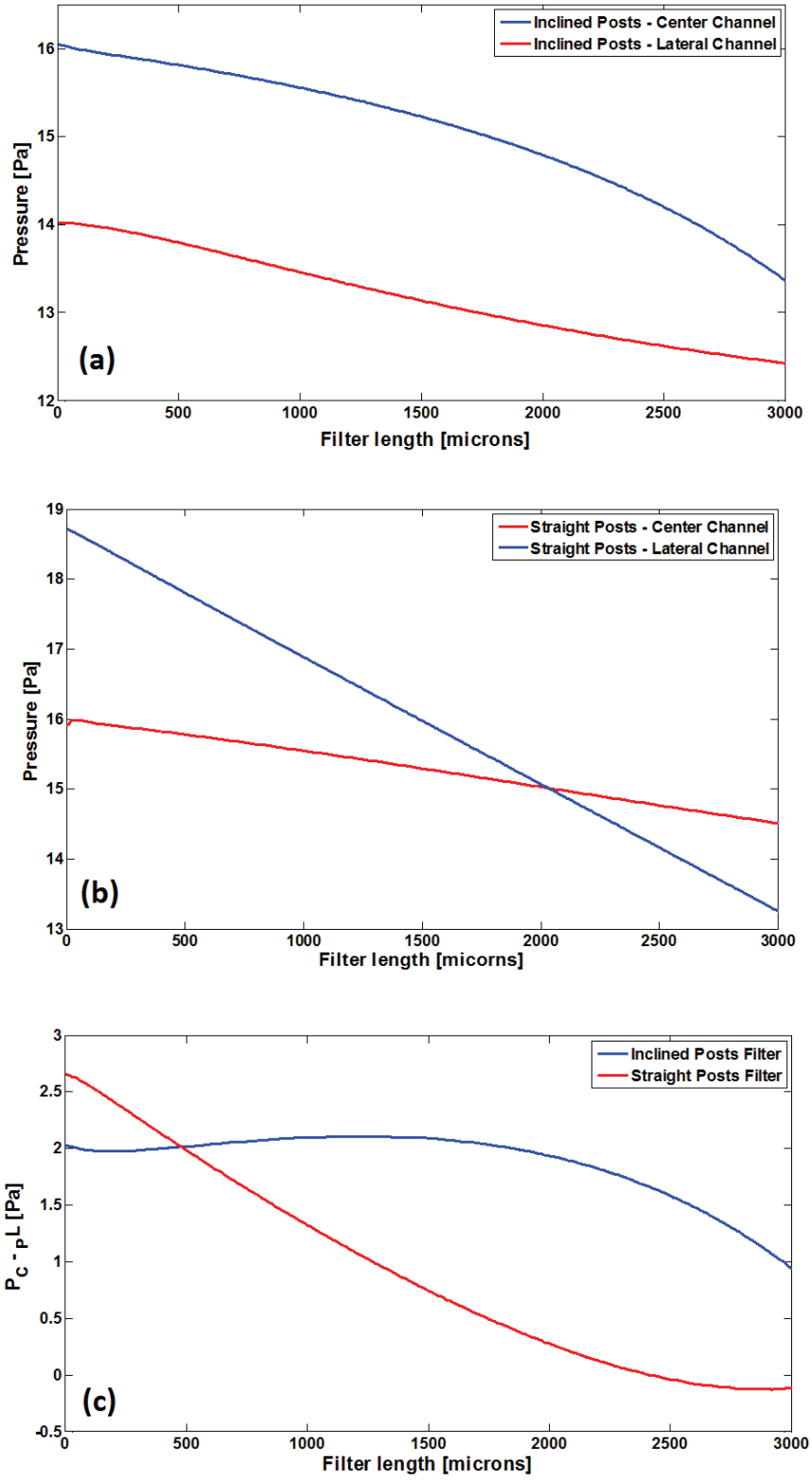

Figure 6: COMSOL simulation results at the filter region. (a) Pressure profile at the central and lateral channel for a configuration with the pillars array slightly inclined. (b) Pressure profile at the central and lateral channel for a configuration with the pillars array without any inclination. (c) Module of the pressure drop across the filter region for both the two configurations with pillars array inclined and not.

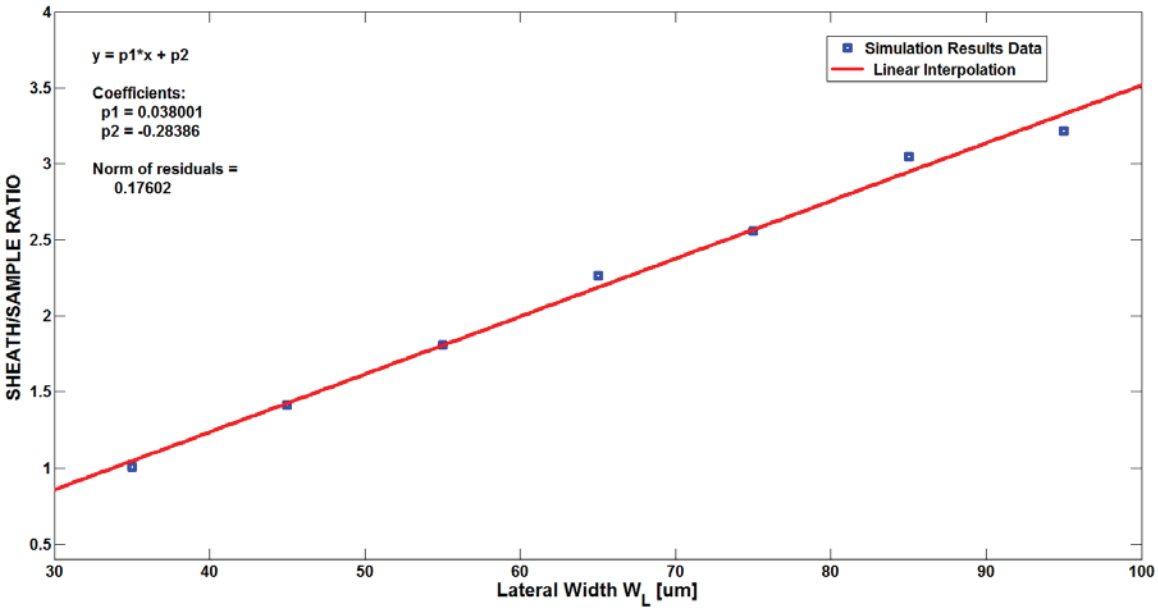

Figure 7: COMSOL Multiphysics simulation results. The graph shows that the sheath to sample ratio at the end of the filter region, linearly increases with the width of the lateral channels.

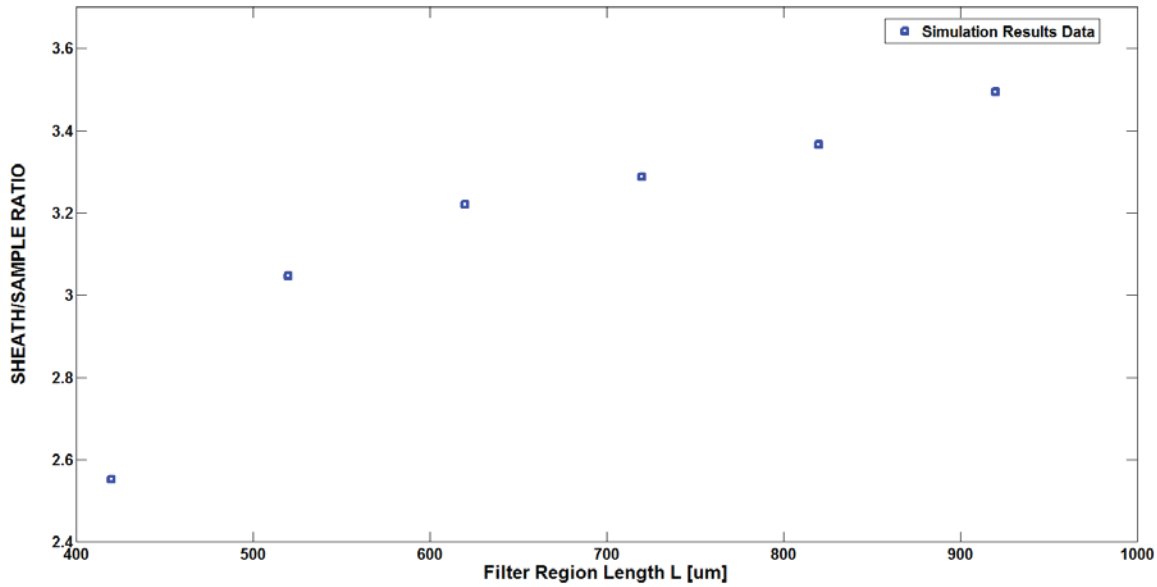

Figure 8: COMSOL Multiphysics simulation results. The graph shows the behavior of the sheath to sample ratio at the end of the filter region, when the length of the filter region varies in a range of 500 µm.

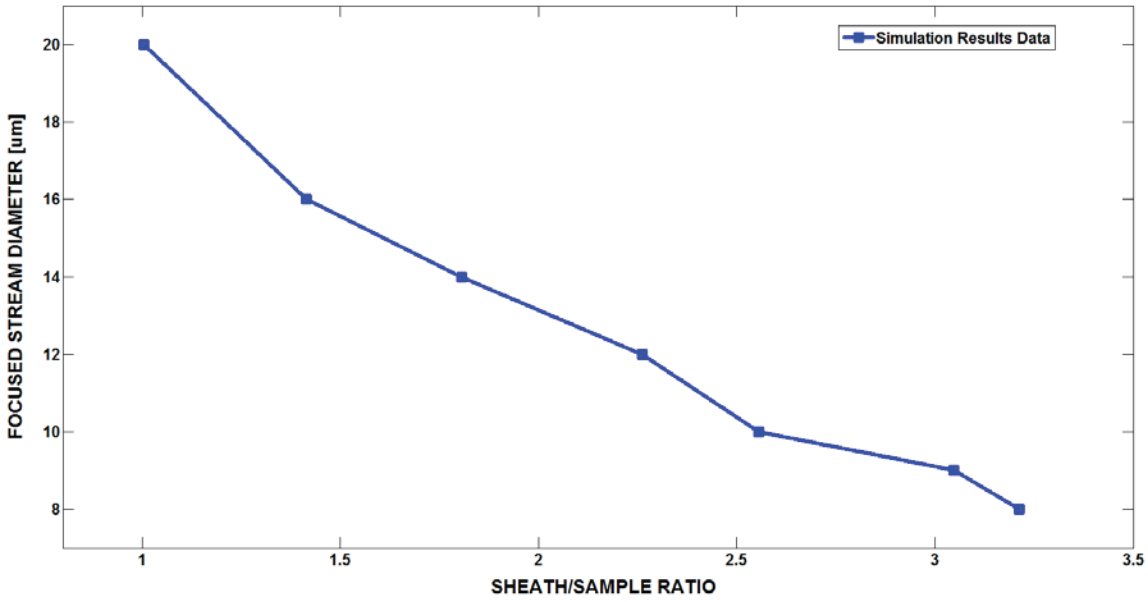

Figure 9: COMSOL Multiphysics simulation results. The graph shows the decreasing low for the diameter of the focused stream, when the sheath to sample ratio increase.

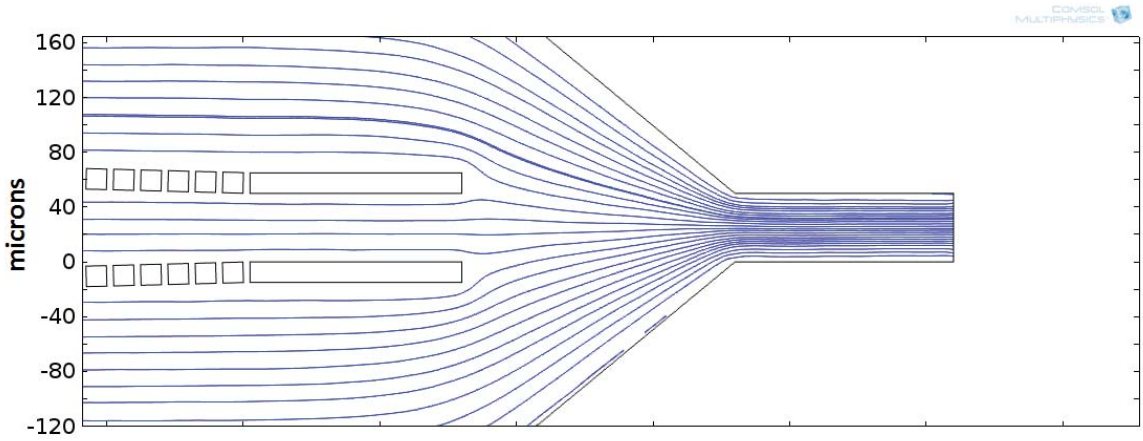

Figure 10: COMSOL Multiphysics post-processing plot. The velocity streamlines show the sample fluid after the cross-filter region get focused for effect of the sheath coming from the lateral channels.

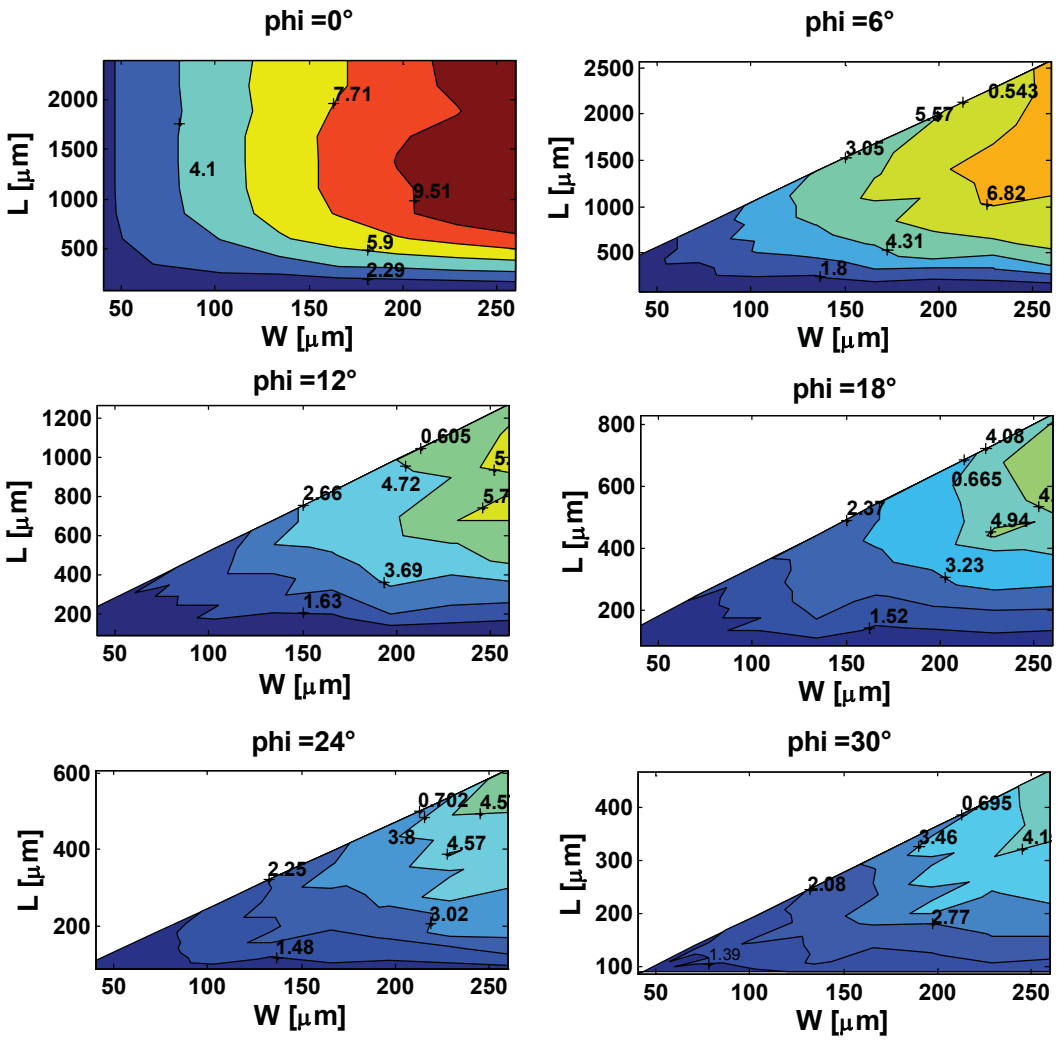

Figure 11: COMSOL – Matlab simulation results. In the contour maps, the sheath to sample ratio is a function of the length of the filter region, and the width of the lateral channel. Each map is parametrized for a particular value of the inclination angle of the pillars arrays.

The contour maps allow to have in advance an estimation of the sheath to sample ratio, for each one of the analyzed different combinations of the three critical parameters. The sheath to sample ratio has been calculated by considering the flow rate at a cut plane at the end of the filter region.

In Figure 11 , eight generated contour maps are reported. In each plot the sheath to sample ratio is a function of the length of the filter region and the width of the lateral channels. Each one of the eight plots refers to different values of the inclination angle of the pillars arrays.

It is important to notice, that when an inclination to the pillars arrays is introduced, for the considered range, not all the combinations length-width, are allowed. This is way there are blank regions in some of the reported plots.

In conclusion, we have showed that the optimal geometry for a target particle size can be find by choosing the right three parameters which value is critical for the definition of the focusing power in each designed device.

4.3 Materials and methods

4.3.1 Device Design

Different devices geometries have been realized and tested in order to find the one that induces the optimal flow focusing for our target application.
Our goal was the focusing of Acute Lymphoid Leukemia (ALL) cells. In particular, we would like to align cells from the M60 cell line. These are characterized by a diameter that is in the range of 5-8 µm.
We choose for the testing three devices characterized by a sheath to sample ratio: (1) *low*, r<1; (2) *medium*, r ≈2.5; and *high* r ≈6.
In the first device, the low focusing power is related to the fact that the central region became narrower just before the beginning of the focusing region. Indeed, with this shape, the fluid coming from the center, as observed both from experiments and numerical simulations, tends to laterally expands as it pass to the focusing region. This has the effect to weaken the focusing power.
The shape of the terminal part of the cross-filter region has been changed in the *medium* and the *high* designs.
The tested devices have been chosen according to the contour maps obtained by Comsol-Matlab numerical simulations. The value for the inclination of the pillars arrays φ was set to 1.5°, for the *low* and *high* configuration, and to 10° for the *medium* one. The number of pillars for each one of the three device is: N = 30, 22 and 120, for the *low*, the *medium* and the *high* respectively. The pillars gap size was set to 3 µm for all the three devices.

4.3.2 Device Fabrication

The microfluidic device was realized using the standard PDMS (polydimethylsiloxane) soft-lithography technique. First, a photolithography process was performed in order to obtain a negative master mold of the designed patterns. A chromium on quartz mask (JD Photo-Tools) was used for this step. The SU8-3010 negative photoresist was spinned at 3000 rpm, in order to get a resist thickness of about 10-11 µm. The thickness of the obtained structure was measured by using a profilometer.
A 10:1 mixture of PDMS oligomer and crosslinking agent (Sylgard 184), was poured onto master mold. The polymer was cured on a hot plate at 95°C for 1 h. Then, a special attention has been paid to unmould each PDMS chip after curing in order to avoid the possible collapse of the PDMS pillars.
After the cured PDMS was unmolded, the holes for the inlet and the outlet were performed. The permanent sealing with a thin glass substrate (166 µm) and the PDMS sample was obtained through an oxygen plasma treatment of both surfaces (Rie Chamber, Oxford Instruments).

4.3.3 Experimental **Set-up**

Two different types of experiments were performed in order to complete characterize the three devices.
In a first experiment, a sample solution was prepared by mixing polystyrene beads of different sizes: 2 µm and 10 µm.
In this way, since the pillars gap size was set to 3 µm, the 2 µm beads could pass through the filter pores, whilst, the 10 µm ones were forced to stay confined in the central region. So, we have been able to study the fluid-dynamics in all-over the device.
A total of 300 µl of sample fluid was prepared. 140 µl of DI water were added to 150 µl of BSA (bovine serum albumin) 40% concentrated. Then 6 µl of the 10 µm beads and 4 µl of the 2 µm beads were added to the buffer solution.
Then, the focusing power of each configuration was tested using B-cell Acute Lymphoid Leukemia (B-ALL) cells.

B-cell acute lymphoblastic leukemia (B-ALL) is a clonal malignant disease that originates in a single cell and is characterized by an accumulation of blast B-cells resulting in the suppression of normal hematopoiesis and infiltration of various extra-medullary sites. The abnormal cells are arrested in the lymphoblast stage of the normal maturation pathway [19]. ALL is one of the four main categories of human leukemia and the majority of ALLs are of the B-cell type [20].

Traditionally, the correlation between the different types of normal B-cell developmental stages and the types of B-ALL has been determined by the combined evaluation of microscopic appearance and immunophenotype. By these criteria, B-cell malignancies can be related in most cases to the different stages of normal B-cell differentiation. The maturation of bone marrow progenitor cells to mature B-cells proceeds through stages that can be identified by the status of the immunoglobulin gene rearrangements, the pattern of expression of cellular immunoglobulin proteins and the expression of cell surface antigens.

In our experiment we used B-cells precursor lymphoblastic cells from the M60 cell line. In comparison to the others ALL cell lines, cells from the M60 are bigger (5-8 µm), they are characterized by a more irregular shape and they have a bi-lobed nucleus. Moreover, they present surface markers that are not found on the other cell lines (CD80, CD37 and CD20). But the most important point is that on the cytoplasm they express the IgM antibody, this means that contrary to the other cell lines the immune system has started to change.

For this experiment a total of 300 µl of sample fluid was prepared. 150 µl of M60 cells in solution were added to 150 µl of blue food dye. In this way the contrast between cells and the background is increased.

Images of the working microfluidic devices were collected by using a CMOS camera (Teledyne DALSA Inc). As source light a 660 nm LED was used. Data were acquired at 1000 frame/s.

In all the experiments the flow rate was controlled using a syringe pump.

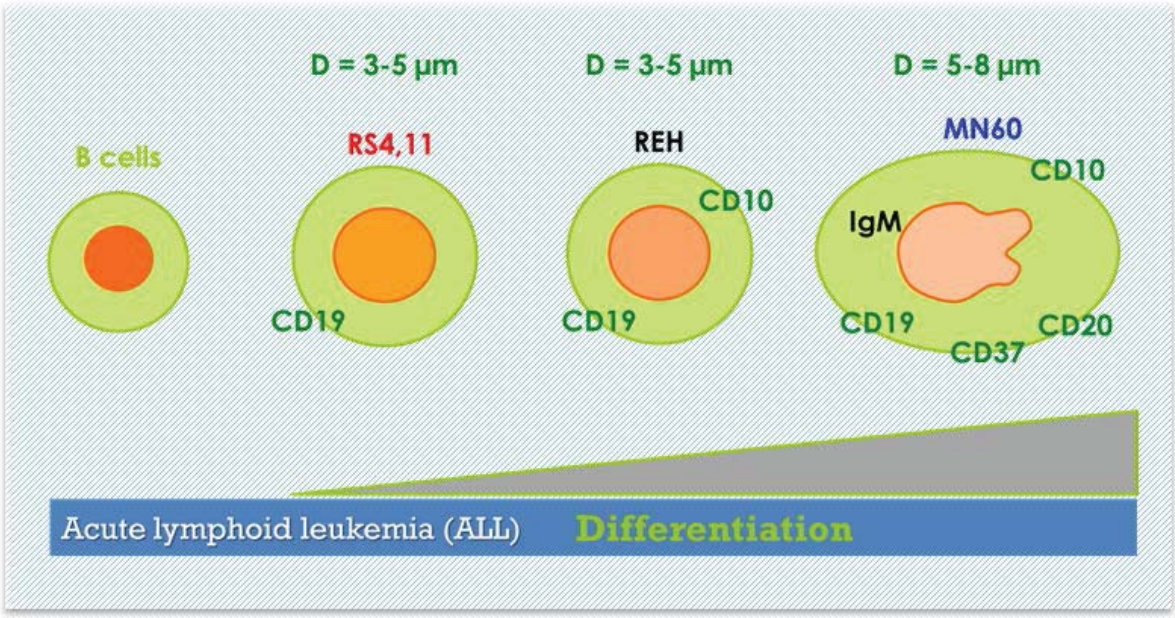

Figure 12: Three different cells line of B-cell Acute Lymphoid Leukemia (B-ALL). Cells from the RS4,11 and the REH lines are slight larger than a normal B cell. They are not morphologically distinguishable, but they are immunologically different, since they express different surface proteins (CD19 and CD10,CD19 for RS4,11 and REH respectively). Cells from the M60 are bigger (5-8 µm), they are characterized by a more irregular shape and they have a bi-lobed nucleus. They present surface markers that are not found on the other two cell lines (CD80, CD37 and CD20). In addition, they express the IgM antibody on the cytoplasm, that means that the immune system has started to change.

4.3.4 Particle Image Velocimetry (PIV) Analysis

The hydrodynamic behavior of the realized devices was tested by performing a Particle Image Velocimetry (PIV) [21-22] analysis.

As already underlined previous in this work, the development and analysis of the performance of microfluidic components for lab-on-a-chip devices are becoming increasingly important because microfluidic applications are continuing to expand in the fields of biology, nanotechnology, and manufacturing. Therefore, the characterization of fluid behavior at the scales of micro and nanometer levels is essential.

Microfluidic velocimetry techniques allow measuring fluid motion in a spatially resolved manner with length scales ranging from10^{-4} to 10^{-7} m. Fluid motion is observed through examination of tracer particles within the fluid. Indeed, PIV allows measuring instantaneous velocity fields using images of particles moving into the field. Considering two successive frames of a video. If particles are moving, they will occupy different positions (Figure 12). The cross-correlation (*cc*) between the two frames gives information on the object velocity.

$$cc = I(t) * I(t + \Delta t)$$

If the image has N x M pixels, the cross-correlation will be a matrix of (2N-1) x (2M-1) pixels. The difference between the position of the peak value and the center in the cross-correlation matrix, gives information about the average particles displacement between the two images.

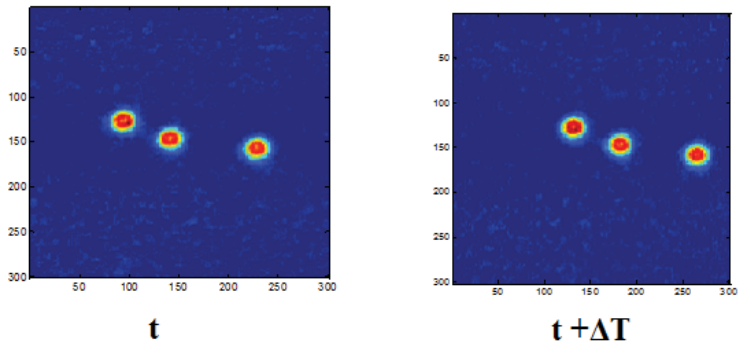

Figure 13: Experimental data of two different frames of a video of particle moving in a microfluidic channel.

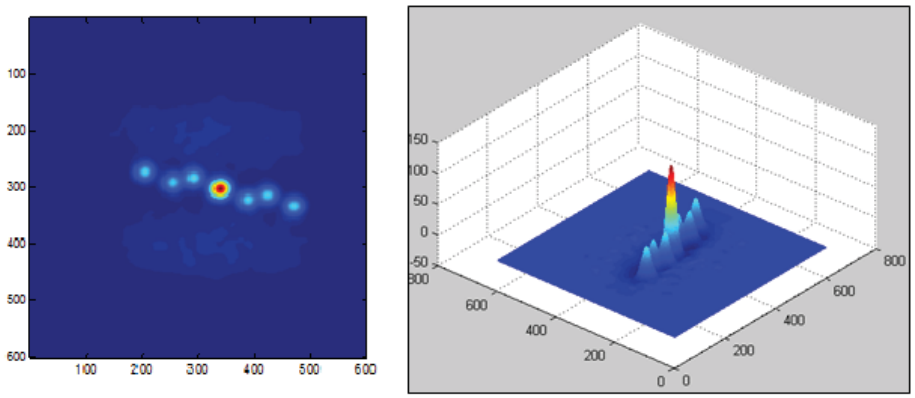

Figure 14: : Cross-correlation between the two images showed in Figure 13. The difference between the peak and the center of the matrix gives an estimation of the particles displacement.

4.4 Results and discussion

4.4.1 Master mold and PDMS samples characterization

The master mold and the PDMS samples have been characterized in order to verify that the channel thickness and the pillars size satisfied the desired values.
The main efforts that have been done during the fabrication of pillars [23] using the replica molding approach are:

[1] Making holes into the photoresist that reach the silicon substrate. This step is important, since the holes allow the pillars formation into the polymer replica.
[2] Avoid collapsing of the pillars when the PDMS is peeled from the mold.

The characterization of the Su-8 master mold was carried out by using as profilometer and an optical microscope.
The profilometer measurements allowed us to verify the thickness of the SU-8 structures on the mold. As we expected, the obtained thickness was in a range of 10-12 µm (according with the spin-rate used for the photolithography process). Figure 15 reports the profile for the device with a *low* sheath to sample ratio.
In order to verify the depth of the holes, several samples have been cut at the pillars area, in order to look at them from the cross-section. This kind of characterization allowed choosing the exposure time that allowed to obtain holes that reach the silicon substrate and wall profile as straight as possible. Figure 16 shows the cross-section of one hole for a sample that we found out to have the better profile, and therefore we found out the best recipe.
In Figure 17 the microscopy image of the master mold for the device with a *high* focusing power is reported. The images of fabricated PDMS samples for the device with a *medium* and *high* focusing power are reported in Figure 18 and Figure 19 respectively.

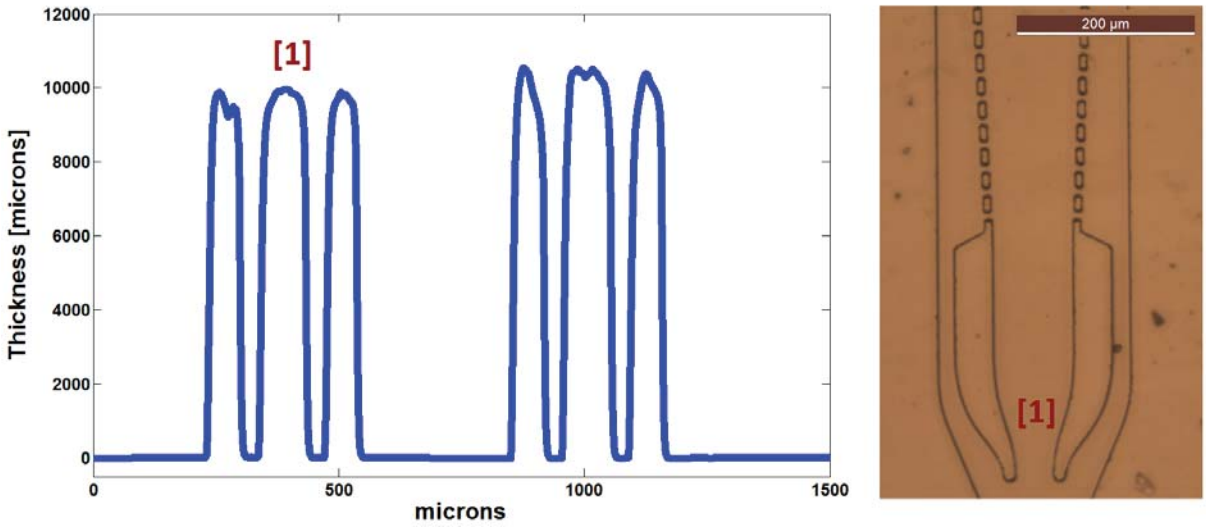

Figure 15: Profilometer measurements of one of the SU-8 master mold used for the PDMS chips fabrication.

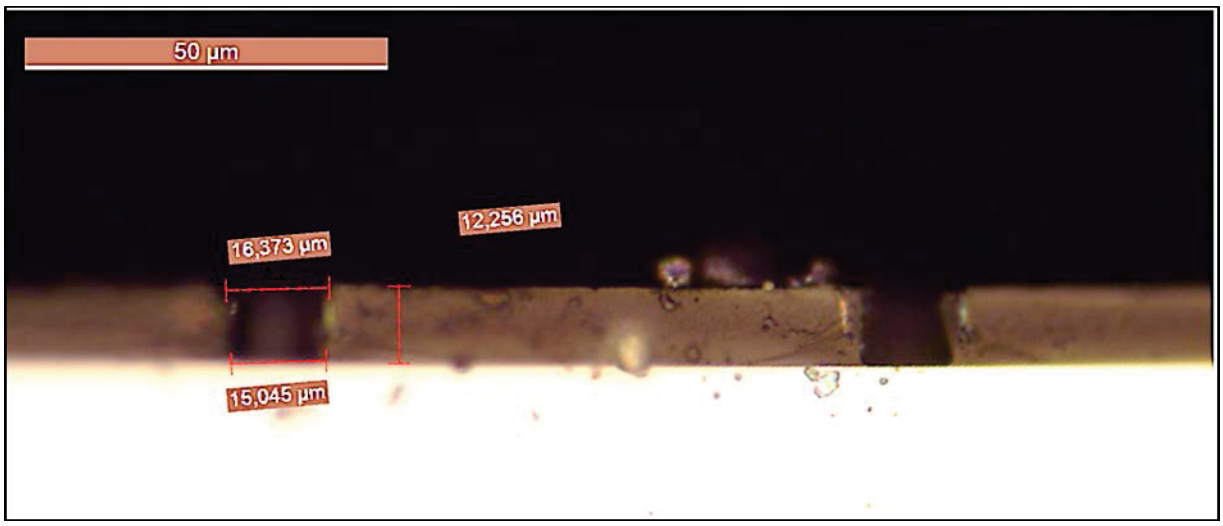

Figure 16: Cross-section image of one of the holes (pillars-negative) on a SU-8 master mold.

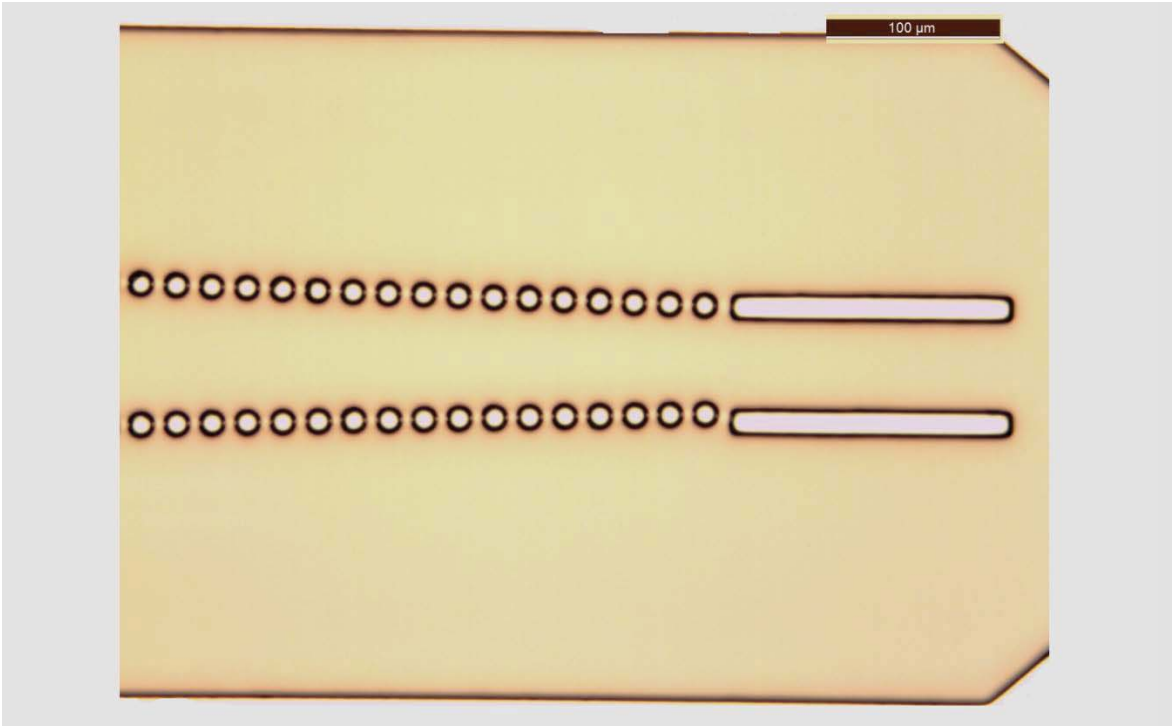

Figure 17: Microscopy image of the SU-8 master mold for the device characterized by a high sheath to sample ratio r = 6.

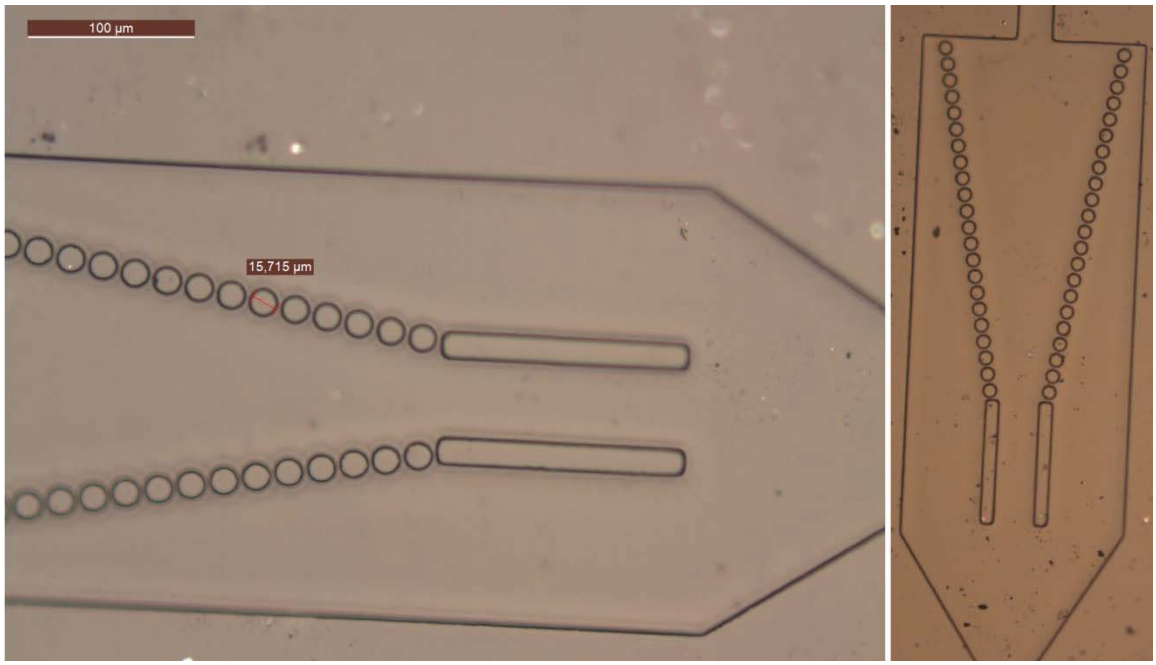

Figure 18: Microscopy images of a PDMS sample of the device characterized by a *medium* sheath to sample ratio.

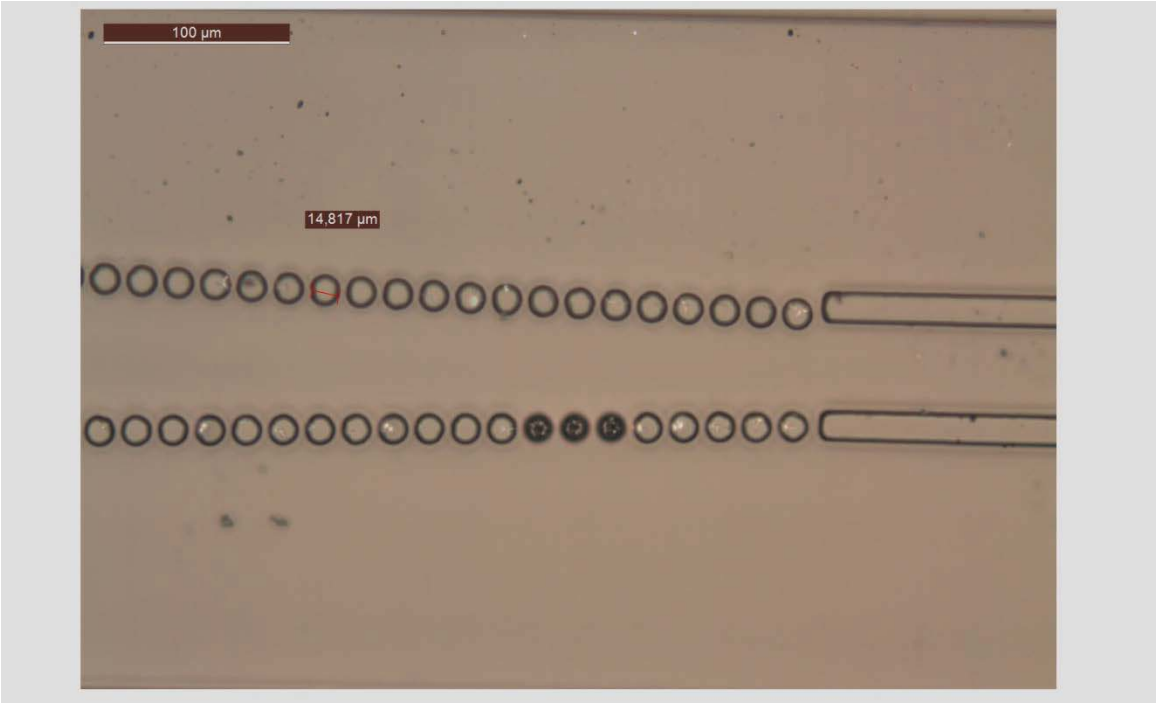

Figure 19: Microscopy images of a PDMS sample of the device characterized by a high sheath to sample ratio.

4.4.2 PIV and Image Processing Analysis

In order to estimate the flow velocity in the devices a Particle Image Velocimetry (PIV) analysis was performed on the data acquired during within the experiments performed using the mixing of the 2 µm and 10 µm polystyrene beads.

A ROI of 320x220 at end of the filter region was considered. A moving window of 16x11 pixels was used. The windows were overlapped at 50% in both vertical and horizontal direction.

The final velocity profile is obtained averaging the velocity matrixes obtained for 20 video, each of them consisting of 1500 frames.

In Figure 20 it is showed the velocity map obtained for the device with a low sheath to sample ratio. The velocity profiles at the region where the sheath and the sample fluid recombine are plotted in Figure 21. This profile allow us to estimate the sheath to sample ratio achieved for the device in the performed experiment.

Moreover, by image processing using Matlab, we were able to discriminate the position for the 2 µm and 10 µm beads. As we expected, the smallest one were distributed in all over the channel, whilst, the bigger ones were confined at the central channel (Figure 22).

For this device, the obtained diameter of the focused stream was ≈ 30 µm, value that is in agreement with the one expected from numerical analysis.

A total of 100 videos of 1500 frames were analyzed. The acquisition frame rate was set to 1000 frames/s.

The experiments performed with the M60 cells, allowed us to demonstrate the better focusing power of the devices with a *medium* and *high* sheath to sample ratio.

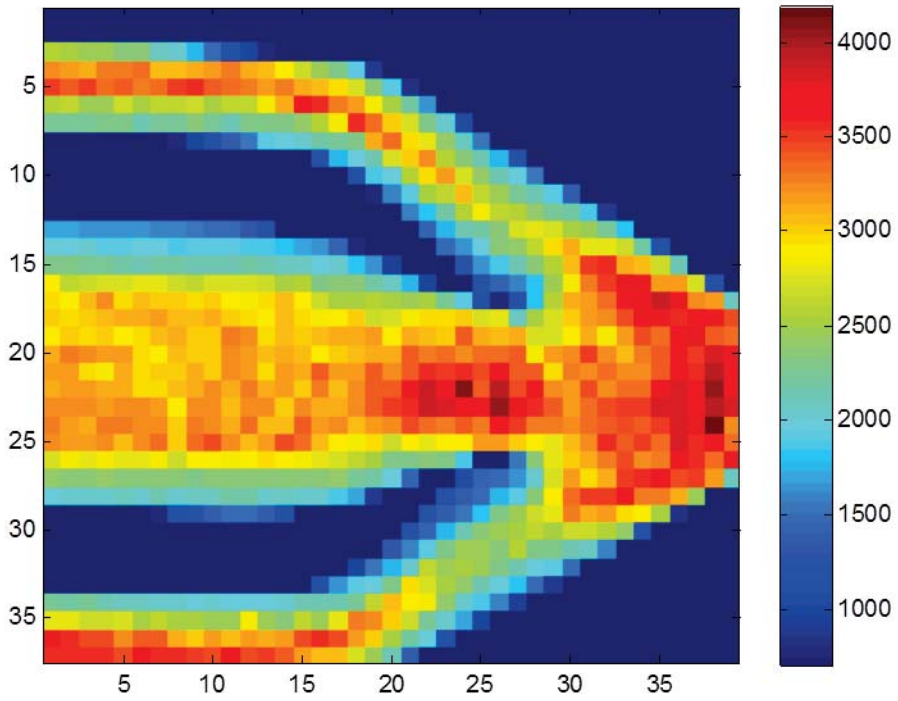

Figure 20: Velocity Map obtained by the Particle Image Velocimetry (PIV) analysis. The velocity values are in µm/s.

The distribution of the cells positions within the focused stream shows a Gaussian-like distribution (Figure 23), with a coefficient of variation CV = 1.8 % and CV = 3.7 % for the high and the medium channel configuration respectively.

The image analysis showed that for the chip characterized by a focusing ratio of ≈2.5, cells result to stay focused in a stream with a width of ≈ 10 pixels, corresponding to 25 µm (Figure 24).

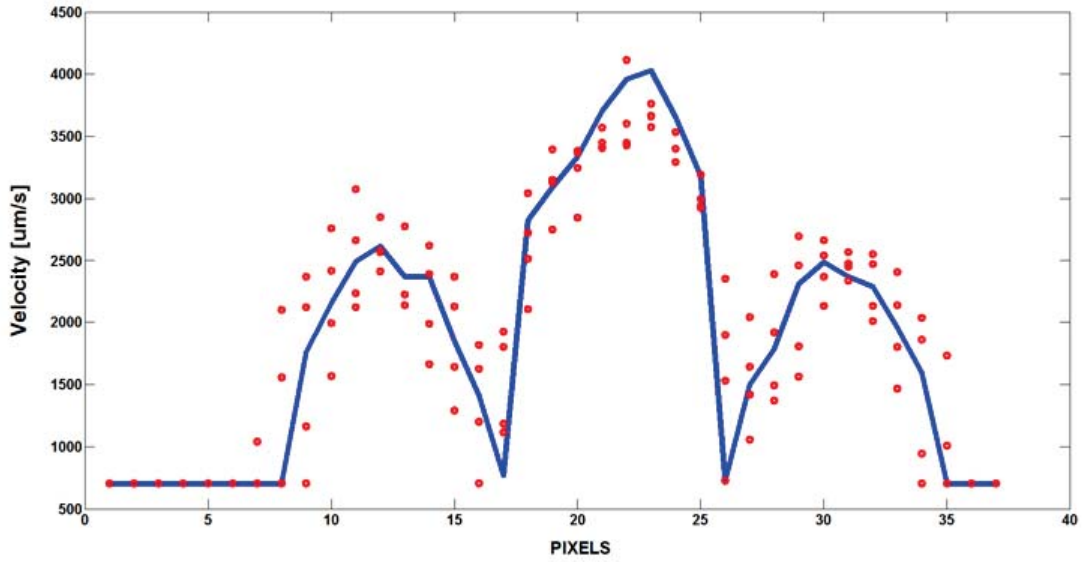

Figure 21: Velocity Profile at the end of the filter region, obtained from the PIV velocity map. The profile allows to have an estimation of the sheath to sample ratio *r* for the tested device. For this case, r ≈ 1, value in agreement with what expected from the numerical simulations

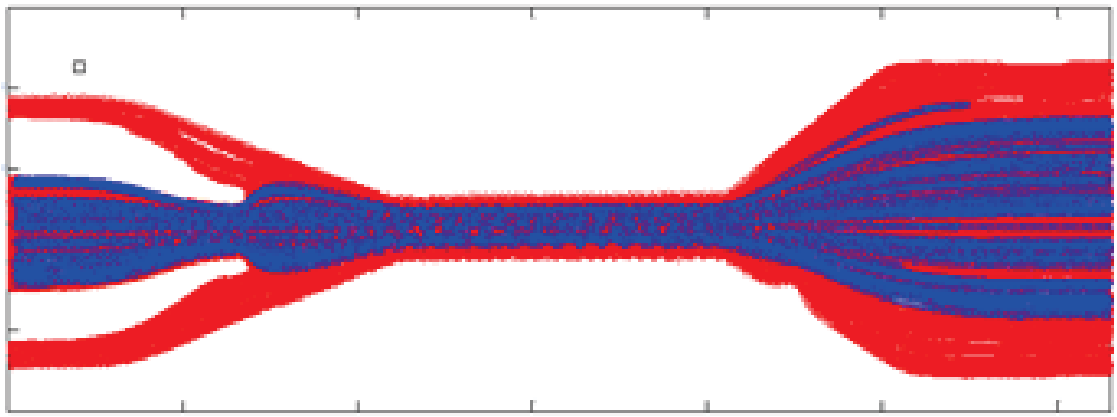

Figure 22: Matlab Image processing analysis. Position of the particles centroids. The 2 µm particles (RED) can move laterally though the filter, whilst the 10 µm ones (BLUE) stay confined at the center.

For the chip with the expected higher focusing power, the data analysis showed that the width of the focused stream stays confined in a range of ≈ 4 pixels, corresponding to 10 µm (Figure 25).
These values are in agreement with what with the Comsol simulations results, obtained using the Particle Tracing module. In Figure 27 the Poincaré maps show the particles positions for a cut plane at the detection region, respectively for the medium and high device. It can be easily seen that the simulation results are in agreement with what with obtained from the experimental data.

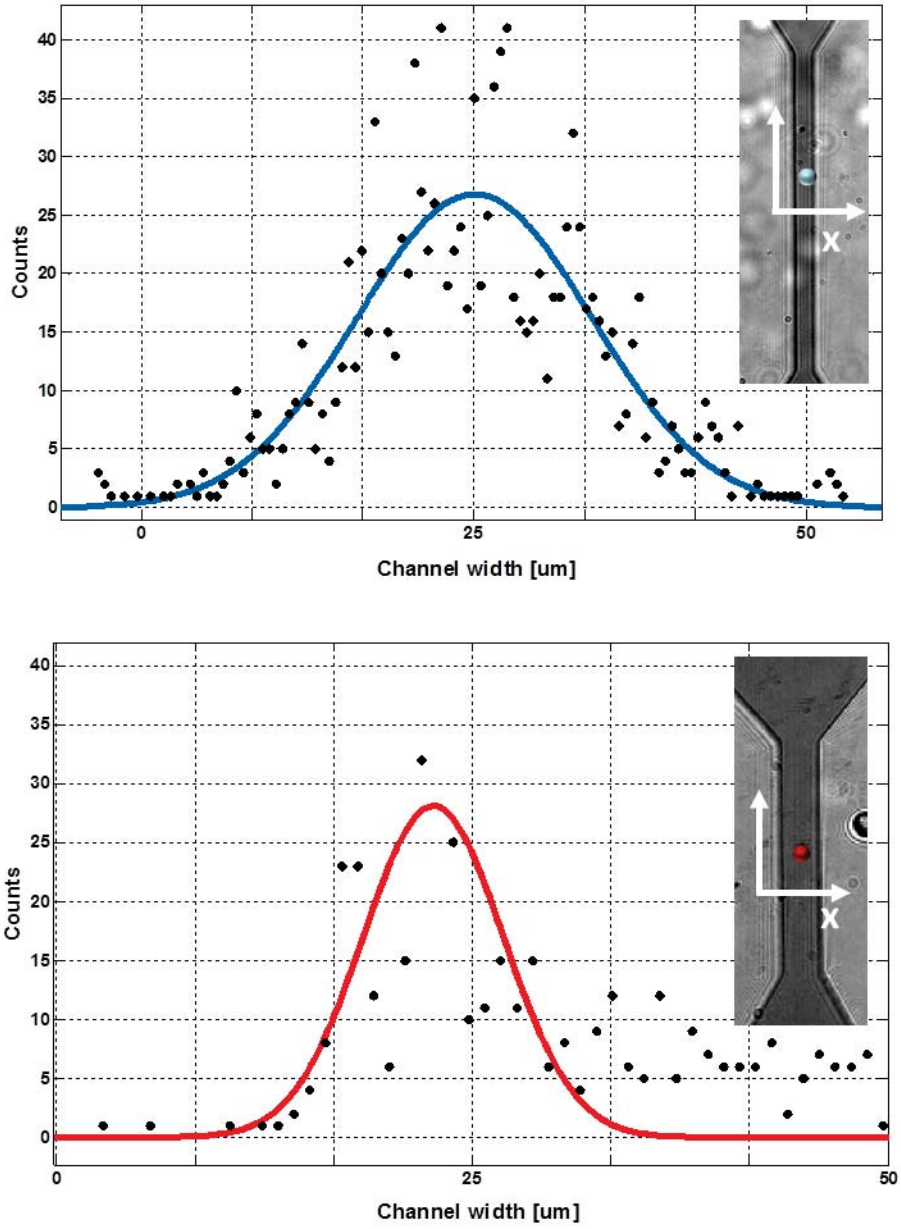

Figure 23: Distribution of the cells position across the channel for the medium (up) and high (down) device. Both the curves show a Gaussian profile. The positions are normalized to the mean value. The obtained coefficient of variation is CV = 3.7 % and CV = 1.8 % for the medium and the high respectively.

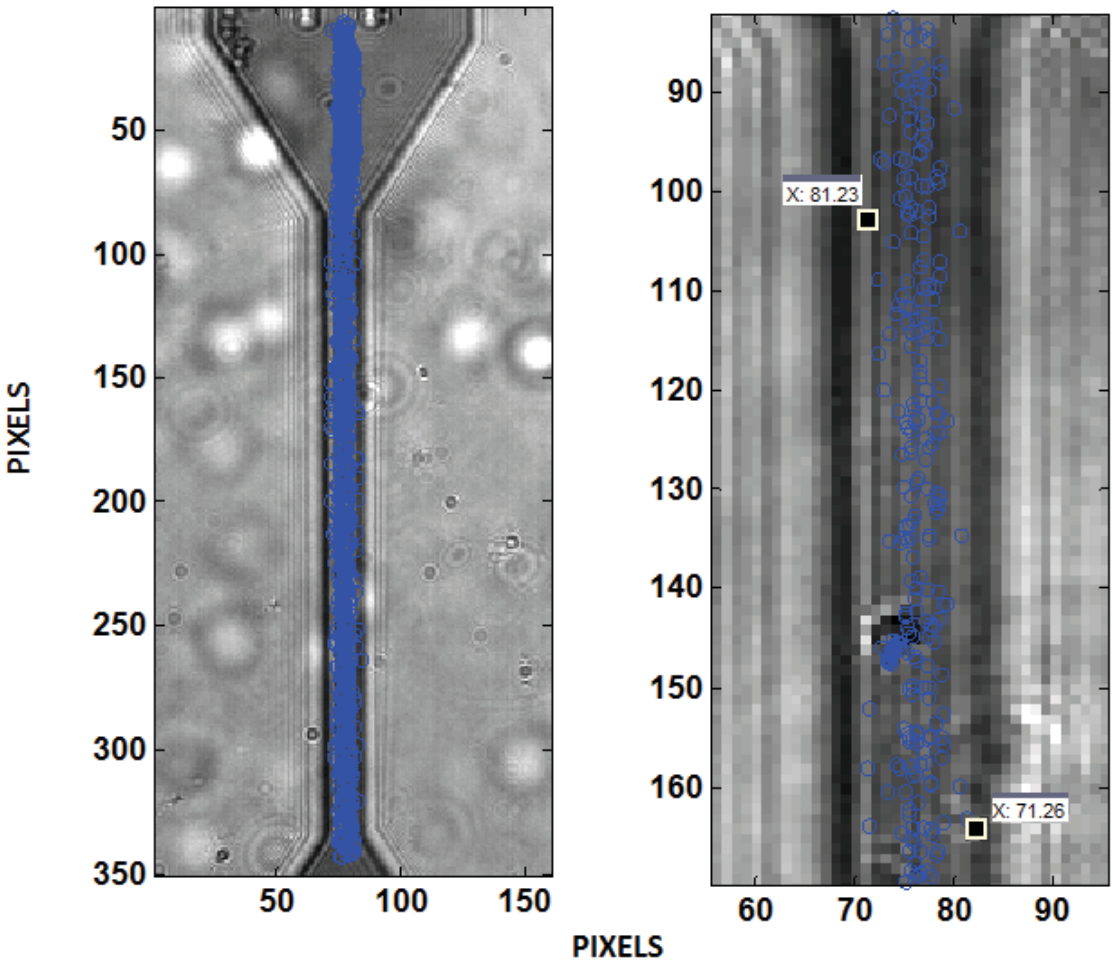

Figure 24: M60 cells focused at the detection region for the device with r=2.5. The blue dots refer to the cells centroids positions. Cells result to stay confined in a range of 10 pixels, corresponding to 25 µm, against a channel with a width of 50 µm.

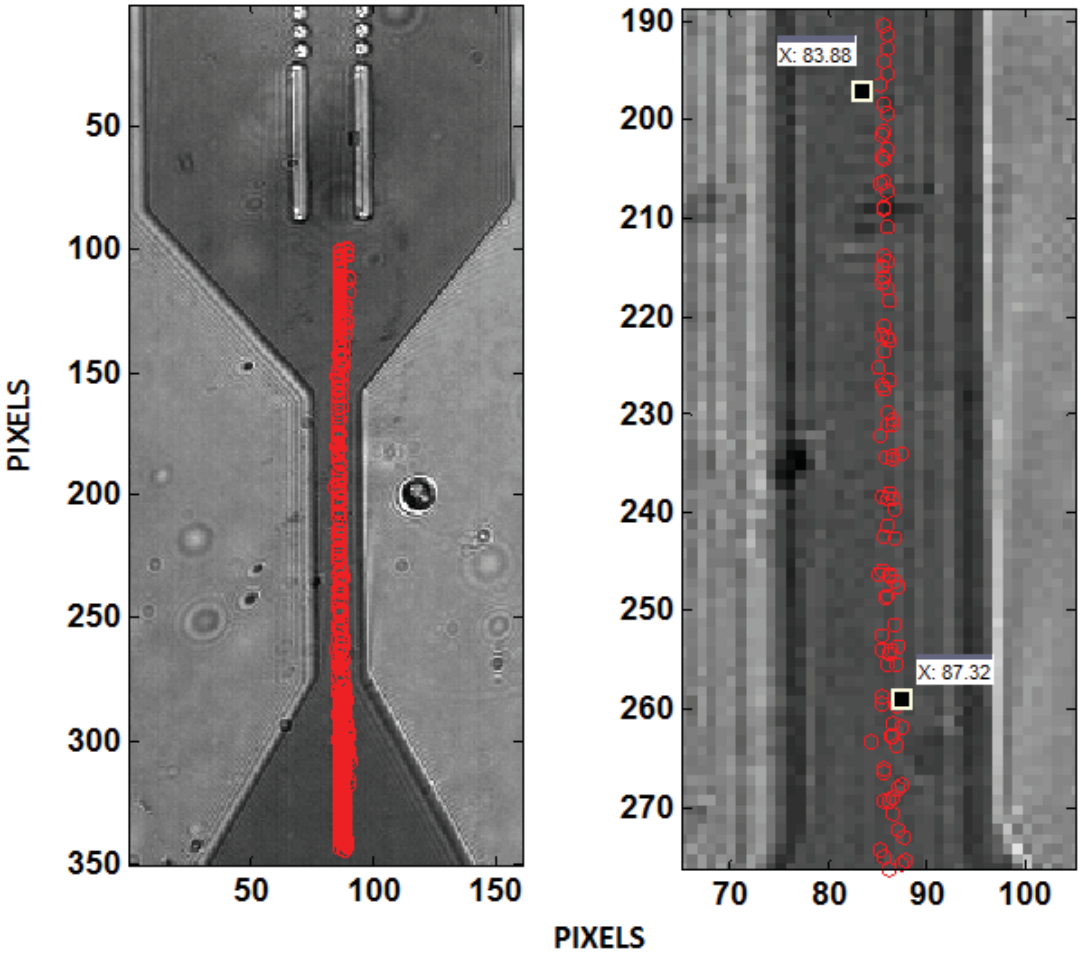

Figure 25: M60 cells focused at the detection region for the device with r=6. The red dots refer to the cells centroids positions. Cells result to stay confined in a range of ≈ 4 pixels, corresponding to 10 µm, against a channel with a width of 50 µm.

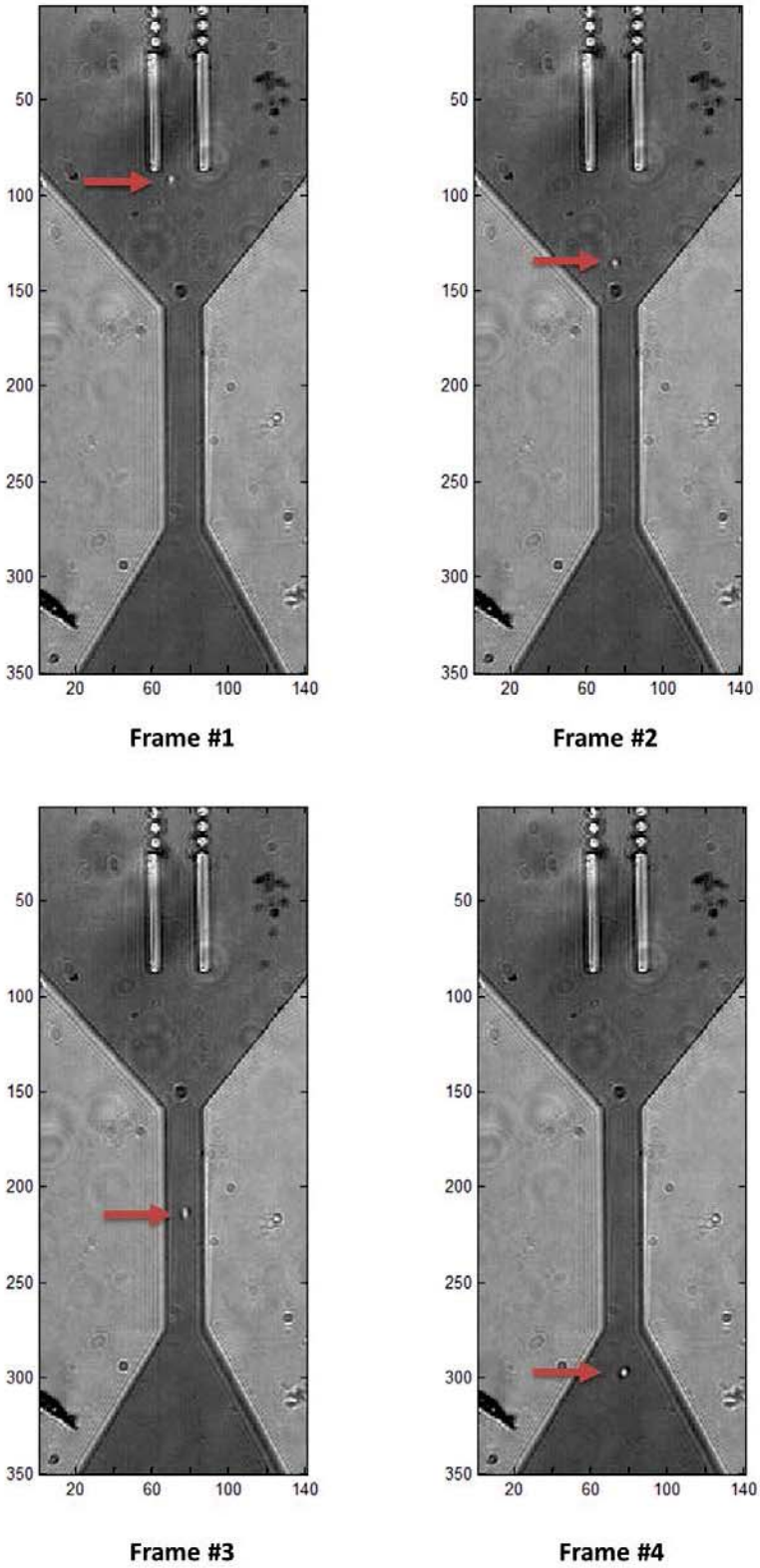

Figure 26: Four consecutive frames of a M60 cell travelling through the detection region in the device with an high sheath to sample ratio. It can be observed that even if at the recombination region the cell is slightly positioned on the left side, then the sheath fluid drives it at the center of the detection channel.

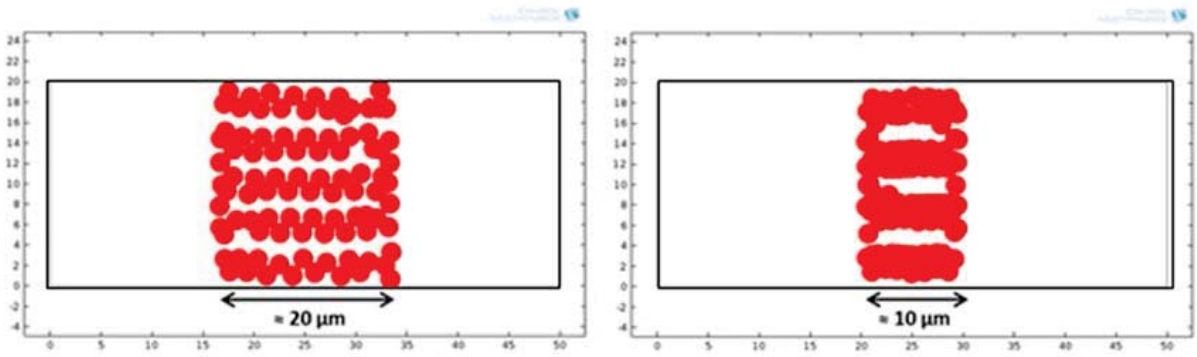

Figure 27: Comsol Multiphysics results. The Poincaré maps show the expected diameter of the focused stream for the medium (left) and the high (right) configuration. Notice that in the plot the particles size is not in scale.

4.4.3 Particle Counting

In addition to the previous characterizations, we also performed a counting of flowing particles into the realized device.

The schematic of the experimental set-up is reported in Figure 28. A green laser was used as light source. The size of the light spot on the channel was adjusted by using a 40x objective. The right sizing and positioning of the laser spot was achieved by imaging the device through a camera (Teledyne DALSA Inc). First the wider spot was positioned at one of the eight parallel channels, and then, by adjusting the focusing of the 40x objective, the spot diameter was reduced (Figure 29) until it reaches the desired size. The scattered light was collected by using a PMT (Hamamatsu H6780- 01), and the output of the PMT was sent and visualized on an oscilloscope.

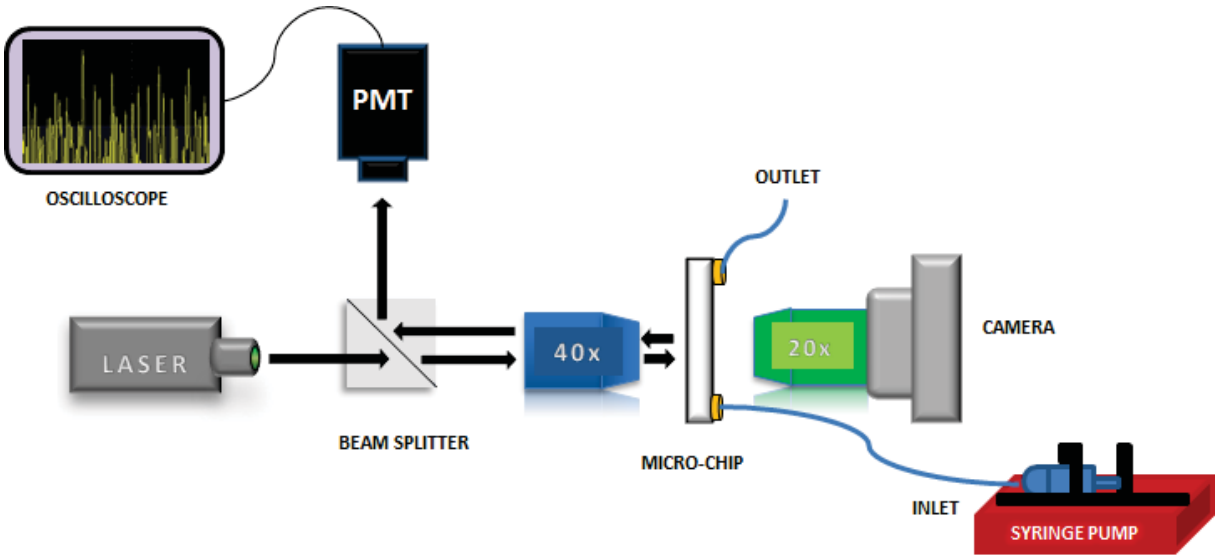

Figure 28: Schematic diagram of the experimental set-up for detection and counting.

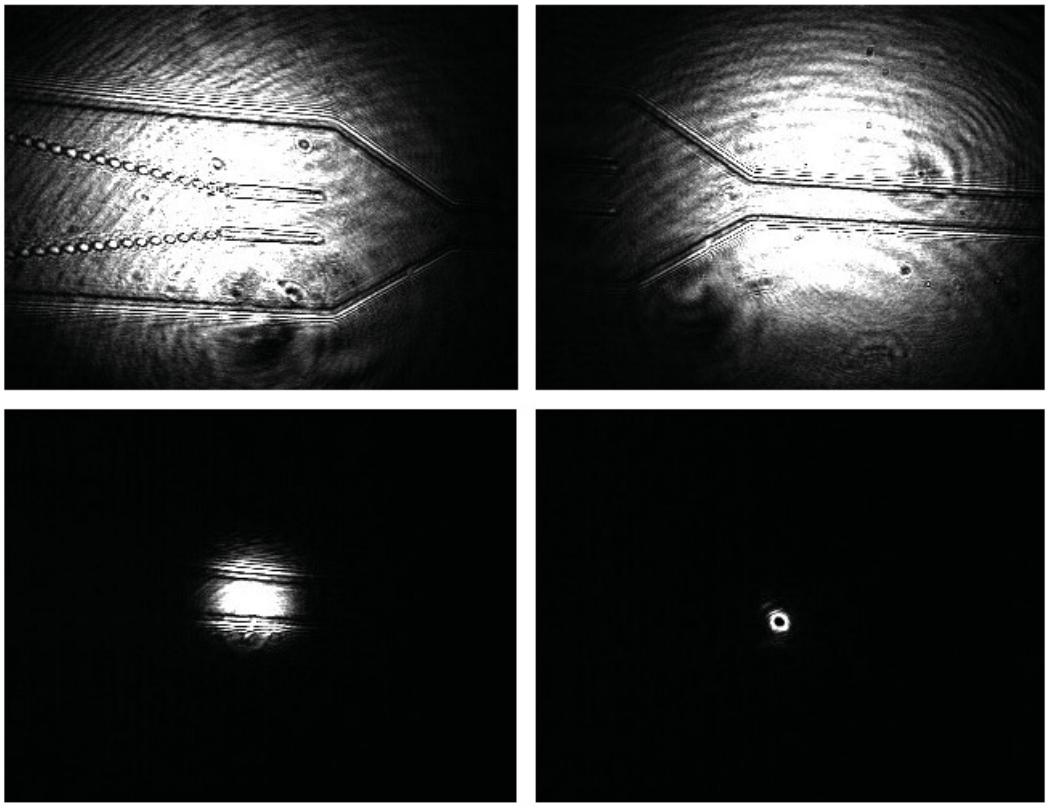

Figure 29: Images show the performed steps for the right sizing and positioning of the laser spot on the micro-channel.

For the experiment 150 µl of 7.5 µm diameter polystyrene particles (Bags Labs) were mixed to 800 µl of PBS (Phosphate Buffered Saline). The final concentration was of about 400 particles/µl. The flow rate during the experiment was varied from 100 µl/min to 50 µl/min. Considering that in the device there are eight parallel channels, we expected to have ≈ 65 particles/s and ≈ 35 particles /s for the two different flow-rates.
The graphs in Figure 30 and Figure 31 refer to two of the collected dataset for a flow rate of 100 and 50 µl/min respectively. We counted a total of 93 particles for the first case, and 59 particles in the second one. In both cases the referring time window was of 2 s. The obtained values are almost in agreement with what we expected form previous calculations. The low number of particles /s is mainly due to: (1) the low concentration of the starting solution; (2) the low flow-rate. By optimizing these two experimental settings, we expect to achieve an higher number of particles/s.

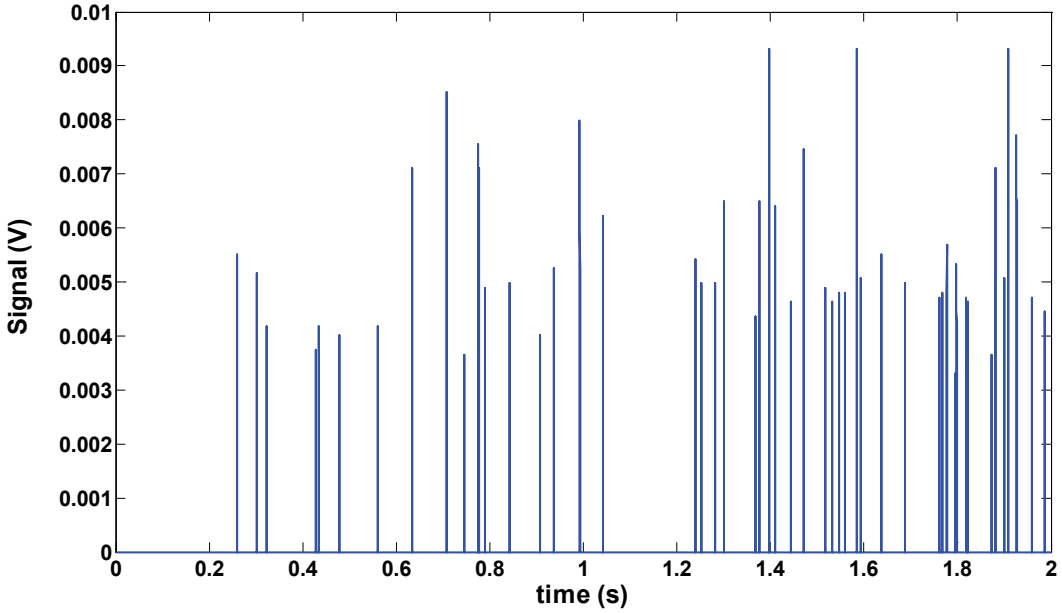

Figure 30: A 2 s region of the scattered signal collected for a flow-rate of 100 µl/min. Each peak refers to a single 7.5 µm particle passing through the detection region.

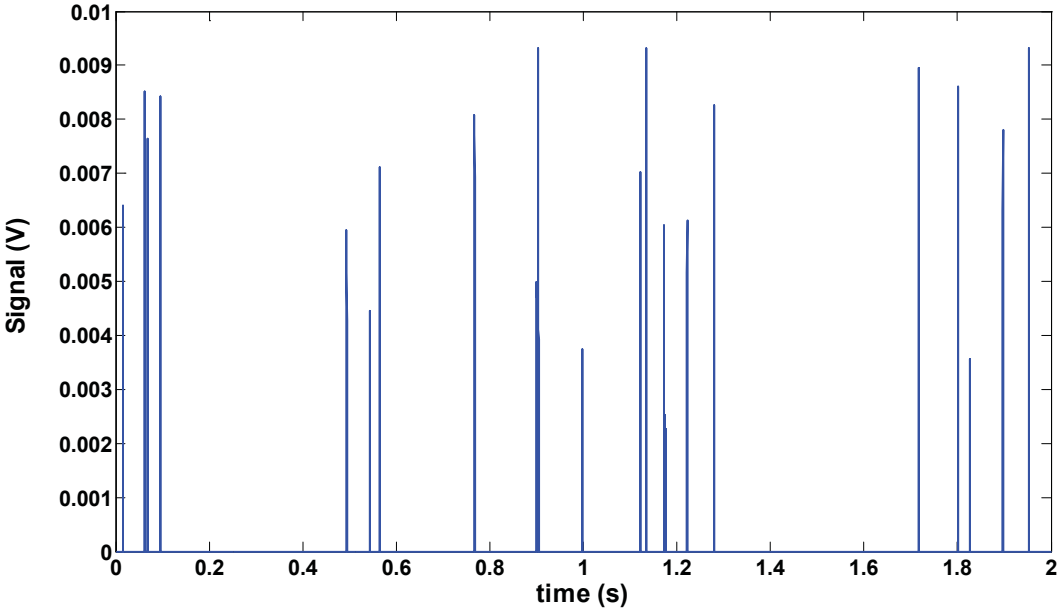

Figure 31: A 2 s region of the scattered signal collected for a flow-rate of 100 µl/min. Each peak refers to a single 7.5 µm particle passing through the detection region.

4.4.4 Filter membrane clogging

Cross-flow filtration is a diffuse approach in separation systems. In contrast to the classical dead-end configuration, it allows to reduce clogging problems and, at the same time, to increase the filter working time.
As well as in any filtration process, the clogging of the membrane is the main issue to overcome. PDMS micro-devices that reproduce filtration systems has been investigate in order to study the clogging phenomena [24].
From our results we are can say that the clogging phenomena has a dependence from the characteristics of the filter membrane.
This is way, the characteristics of the pillars arrays in each one of the realized devices have been optimized in order to achieve the focusing power and at the same time to reduce the clogging effects.
In particular, the operation time seems to be better in the designs with a high number of filter pores and a low inclination of the pillars arrays. Indeed, our experiments showed that, among the three tested devices, the clogging phenomena is less in the one with a *high* focusing ratio ($\varphi = 1.5°$ and $N_{pores} = 120$).
Figure 32 shows an image of the filter that has clogged after 1 hour that the experiment has been running.

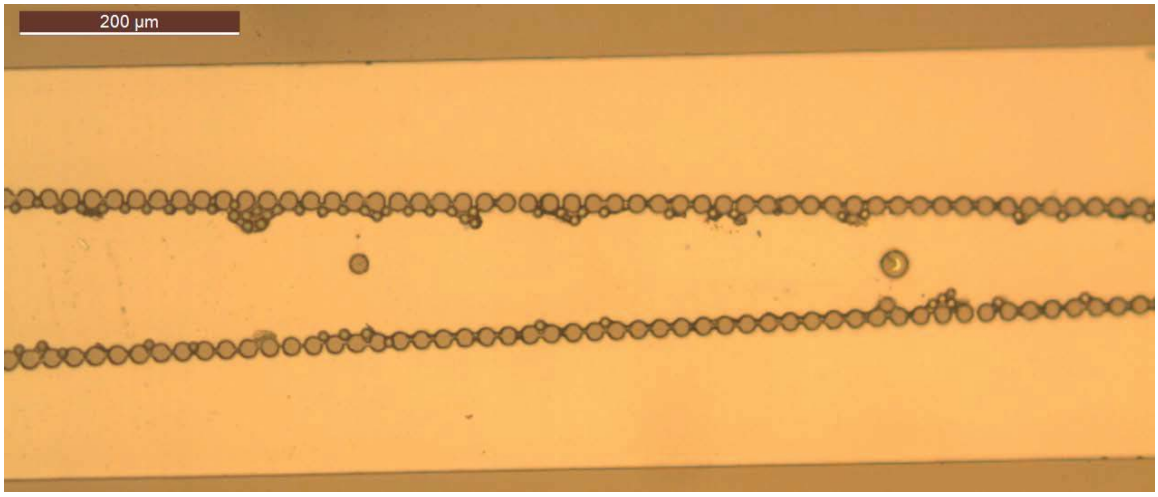

Figure 32: Clogging of the filter region for a PDMS device with a high sheath to sample ratio. The phenomena has been observed after about one hour of operating time.

4.5 Conclusions

Hydrodynamic focusing is the most used method for inducing cells alignment in microfluidic applications.
The main drawback in the conventional adopted micro-chip configurations is that multiple inlets are required.
In this chapter we have presented a microfluidic device that using a cross-filter approach, allows to generate hydrodynamic focusing, without the needing of an additional inlet for the sheath fluid.
This simplification in the geometry leads to the possibility to design a structure with multiple parallel micro-channels, without the needing of complicated geometries.
In the hydrodynamic focusing approach, the diameter *d* of the focused sample stream depends upon the sheath to sample ratio.
By numerical simulation, we have found out that the diameter of the focused stream $d = f(W_L, L, \varphi)$.
The optimal geometry suitable for each particular application, it is achieved by combining the right values for these three parameters.

In particular, we realized a cross-filter configuration, that allow to hydro-dynamically focus Acute Lymphoid Leukemia cells form the M60 cell line. The size of these target cells is in the range of 5-8 μm.
This kind of approach well fits the needing of the market interested into the production of cheap and disposable microfluidic devices for the point-of-care diagnostics.
No more expensive instrumentations dedicated to multiple applications, but cheaper devices ad hoc for a particular analysis.

References

1 Simonnet, C.; Groisman, High-throughput and high-Resolution flow cytometry in molded microfluidic devices, A. Anal. Chem. 2006, 78, 5653−5663.
2 N. Watkins, B. M. Venkatesan, M. Toner, W. Rodriguez and R. Bashir, A robust electrical microcytometer with 3-dimensional hydrofocusing , Lab Chip, 2009, 9, 3177–3184.
3 X. Mao, J. R. Waldeisena and T. J. Huang, "Microfluidic drifting"—implementing three-dimensional hydrodynamic focusing with a single-layer planar microfluidic device, Lab Chip, 2007, 7, 1260.
4 J. G. Santiago, Anal. Chem. 2001, Electroosmotic Flows in Microchannels with Finite Inertial and Pressure Forces, 73, 2353-2365.
5 L. Wang, L. A. Flanagan, N. Li Jeon, E. Monuki and A. P. Lee, Dielectrophoresis switching with vertical sidewall electrodes for microfluidic flow cytometry, Lab Chip, 2007, 7, 1114–1120.
6 J. Gao, R. Riahi, M. L. Y. Sin, S. Zhang and P. K. Wong, Electrokinetic focusing and separation of mammalian cells in conductive biological fluids, Analyst, 2012, 137, 5215–5221.
7 Choi, S.; Park, J.-K., Sheathless Hydrophoretic Particle Focusing in a Microchannel with Exponentially Increasing Obstacle Arrays, Anal. Chem. 2008, 80, 3035–3039.
8 Gossett, D. R.; Di Carlo, D., Particle Focusing Mechanisms in Curving Confined Flows, Anal. Chem. 2009, 81, 8459−8465.
9 D. Di Carlo, D. Irimia, R. G. Tompkins and M. Toner, Continuous inertial focusing, ordering, and separation of particles in microchannels, Proc. Natl. Acad. Sci. USA, 2007, 104, 18892–18897
10 D. Di Carlo, Inertial microfluidics, Lab Chip, 2009, 9, 3038–3046
11 X. Xuan, J. Zhu, C. Church, Particle focusing in microfluidic devices, Microfluid Nanofluid (2010) 9:1–16
12 X. Mao, A. A. Nawaz, Sz-Chin S. Lin, M. I. Lapsley, Y. Zhao, J. P. McCoy, W. S. El-Deiry and T. J. Huang, An integrated, multiparametric flow cytometry chip using "microfluidic drifting" based three-dimensional hydrodynamic focusing, Biomicrofluidics, 2012, 6, 024113.
13 E. Schonbrun, S. S. Gorthi, and D. Schaak, Microfabricated multiple field of view imaging flow cytometry, Lab Chip, 2011, 12 , 268-273.
14 X. Chen, D. F. Cui, C. C. Liu, H. Li, Microfluidic chip for blood cell separation and collection based on cross flow filtration, Sensors and Actuators B 130 (2008) 216–221
15 V. VanDelinder and A. Groisman, Separation of Plasma from Whole Human Blood in
a Continuous Cross-Flow in a Molded Microfluidic Device, Anal. Chem. 2006, 78, 3765-3771
16 S. C. Gifford, A. M. Spillane, S. M. Vignes and S. S. Shevkoplyas, Controlled incremental filtration: a simplified approach to design and fabrication of high-throughput microfluidic devices for selective enrichment of particles, Lab Chip, 2014,14, 4496-4505
17 G. Foley, A review of factors affecting filter cake properties in dead-end microfiltration of microbial suspensions, J. Membr. Sci. 274 (2006) 38–46.
18 Bruus H., Theoretical Microfluidics. Oxford: Oxford University Press, 2008.
19 S.H. Faderl, H.M. Kantarjian, E.H. Estey , Hematologic Malignancies: Acute Leukemias, Springer Berlin Heidelberg 2008
20 Cobaleda C, Sánchez-García, B-cell acute lymphoblastic leukaemia: towards understanding its cellular origin, Bioessays. 2009 Jun;31(6):600-9
21 R. J. Adrian, Twenty years of particle image Velocimetry, Exp. Fluids, 2005, 39, 159–69
22 J. G. Santiago, CD Meinhart, ST Wereley, DJ Beebe, RJ Adrian, A particle image velocimetry system for microfluidics, Exp Fluids, 1998, 25:316–319
23 Laurène Aoun, Pierre Weiss, Adrian Laborde, Bernard Ducommun, Valérie Lobjois and Christophe Vieu, Microdevice arrays of high aspect ratio poly(dimethylsiloxane) pillars for the investigation of multicellular tumour spheroid mechanical properties, Lab Chip, 2014, 14, 2344

24 G.C. Agbangla, E. Climent, P. Bacchin, Experimental investigation of pore clogging by microparticles: Evidence for a critical flux density of particle yielding arches and deposits, Sep Purif Technol 2012, 101,42–48.

5. Inducing cell rotation in a microfluidic device by hydrodynamic forces

One of the main goals of microfluidic technology is the realization of devices in which cells can be manipulated and then imaged in their 3D shape while they are flowing in a fluid, overcoming in this way a strong limit of traditional microscopy where cells are observed while compressed on a glass slide. In particular, translation and rotation of cells are two fundamental manipulation requirements in applied biotechnological research. For instance, the controlled rotation of a cell in a fluidic system would make easily possible its 3D structure reconstructions by tomographic methods without the need of moving the imaging set-up.
In this chapter, it is reported a study related to the development of a microfluidic device that induces cell rotation by only taking advantages of hydrodynamic forces.

5.1 Introduction

Microfluidic technology allows realizing devices which gets easier to analyze cells while they are flowing[1-4]. Moreover, thanks to microfluidic technology, cells can be imaged while they are into their 3D shape, since they are not compressed on a glass slide as happens in traditional microscopy.
If we think at blood cells, microfluidic technology gives the possibility of reproducing the circulatory system on a chip. WBCs and RBCs can be analyzed as they behave when they are in the physiological condition[5].
Imaging cells from different points of view, while they are flowing, allows reconstructing their three-dimensional structure. This could be a useful support also in the application focused on the reconstruction of the fluorescent distribution from the images of cells flowing at high speed.
If cell rotation is induced, images at different views of the same cell can be collected without moving the imaging set-up. In order to achieve this scope, researchers have investigated a wide range of physical phenomena and they have proposed corresponding methods for cell rotation. In general, the majority of microchips include electric torque induced by dielectrophoresis (DEP) [6-8], optoelectronic torque (ODEP) [9] and magnetic torque. DEP has been widely attempted for trapping, translating and rotating cells. Subjected to a non-uniform electric field, any polarizable entity, which includes cells, experiences locally concentrated induced electric dipoles, which in turn undergo electric forces or torques in the electric field. Collectively, a net DEP force or torque is generated on the cell, leading to translation or rotation respectively. More recently, a new method of using DEP, by coupling it with optical means, has been introduce. Scientists refer to it as ODEP. Compared to conventional DEP, ODEP differs in applying the potential to electrodes by light induced electric field instead of an external potential source.
All these methods have been demonstrated to be capable of rotating cells, whose size ranges around 10 µm in diameter. However, they lack mainly in two points: 1) the needs of integrate additional elements (such as electrodes) into the microfluidic device; 2) the applied physical forces could generate un-desired effects on the biological sample.
Considering the limitations of these approaches, in this work it has been studied the possibility to induce cell rotation by only taking advantage of hydrodynamic effects. It is well known that for a pressure driven flow, the velocity profile behave as a Poiseuille flow, and the velocity profile is parabolic. The flow velocity has its maximum value at the center of the channel, and reaches the lowest value close to the walls. Based on this assumption, we designed a microfluidic device that induces cells rotation, since they are focused at the channel walls. The two different sides of the cell, the one close to the wall and the other closer to the channel center, are affected by two different flow velocity values. Due to this, a rotation in the cell is induced.
The realized device was first tested by using yeast cells, that are characterized by an asymmetrical shape when they are in the division phase. Then, its operation was verified also using Acute Lymphoid Leukemia (ALL) cells.

5.2 Theoretical background

The Hagen-Poiseuille equation is the physical law that relates the pressure drop in a fluid flowing through a long pipe with its volumetric flow rate. The main assumptions of the equation are that the fluid is viscous and incompressible, and the flow is laminar. These conditions are completely satisfied in microfluidics. For a cylindrical channel the velocity equation is:

$$u = -\frac{\Delta P}{L}\frac{1}{4\mu}(R^2 - r^2)$$

where u is the velocity, ΔP is the pressure drop across the channel, L is the channel length, μ is the viscosity of the fluid, R is the radius of the channel, and r is the radial position at which the velocity is calculated.
The same equation is rewritten for a flow between two parallel infinite plates as follows [10]:

$$u_x(z) = -\frac{\Delta P}{2\mu}(z\,H - z^2)$$

with u_x the component of the velocity in the flow direction, ΔP is the pressure drop across the channel, μ is the viscosity of the fluid, z the position in the vertical direction, and H the vertical gap between the walls.
The equation for the velocity says that a Poiseuille flow is characterized by a parabolic velocity profile, in which the velocity of flow in the center of the channel is greater than that toward the outer walls (Figure 1).

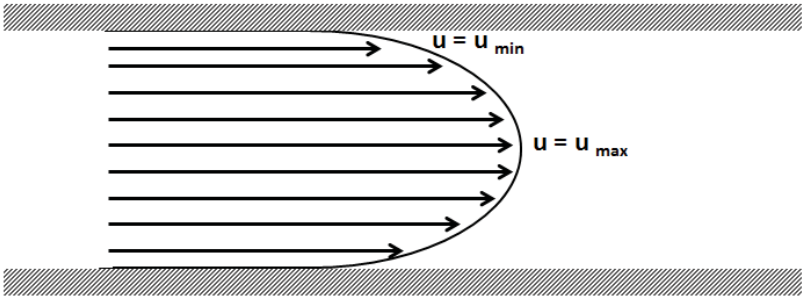

Figure 1: The cartoon shows the parabolic velocity profile in a microfluidic channel

The volumetric flow rate and the pressure drop are related by the following equation:

$$\Delta P = R_H Q$$

For a rectangular micro-channel, the expression for the hydraulic resistance is more complicated:

$$R_h = \frac{12\mu L}{w\,h^3}\left[1 - \frac{h}{w}\left(\frac{192}{\pi^5}\sum_{n=1,3,5}^{\infty}\frac{1}{h^5}\tanh\frac{n\pi w}{2h}\right)\right]$$

where h is the channel depth and w is the channel width. If w << h or h << w, the previous expression can be simplified as follows

$$R_h = \frac{12\,\mu\,L}{w\,h^3}$$

Combining the two previous expressions, the equation that describes the average velocity inside the channel is obtained:

$$U = \frac{Q}{wh}$$

that is the flow rate divided by the channel cross section.
Due to the parabolic velocity profile, if a cell is close to the wall, its surface will be affected by different velocity values. In particular, the side that is closer to the center of the channel will be affected by a higher velocity than the side closer to the wall. The couple of forces acting on the cell generates a torque, and so a rotation is induced.

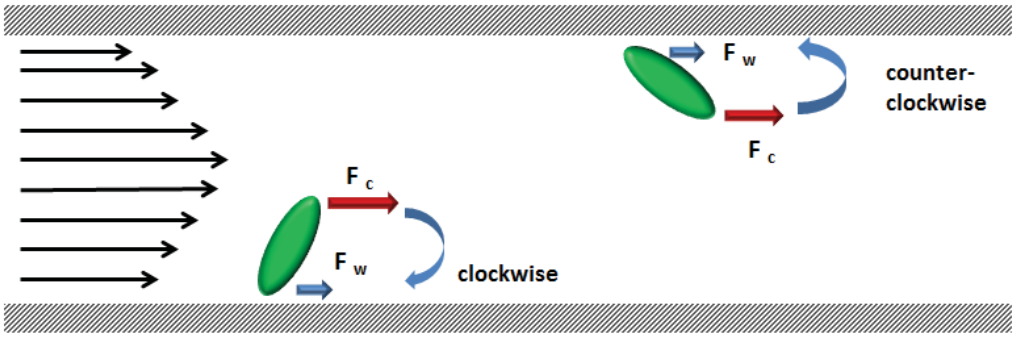

Figure 2: The cartoon explains the rotation effect, caused by the parabolic velocity profile, when objects are close to the channel walls.

Since in microfluidics the Reynolds number is really low, the effect of lift forces can be neglected. The induced rotation can be clockwise or counter-clockwise according to the position of the cell inside the channel (Figure 2). At low Reynolds number, Re << 1, the angular velocity of a particle (Ω_p) approaches the angular velocity of the fluid (Ω_f), $\Omega_p \approx \Omega_f$ [11]. Furthermore, the angular velocity Ω_p is linearly related to the torque T, and depends upon the cell radius a [12]:

$$\Omega = \frac{T}{8\pi\mu a^3}$$

The torque T is calculated from the velocity by the shear stress $\vec{\tau}$ [13]:

$$\vec{\tau} = \mu \frac{1}{2} (\nabla u + (\nabla u)^T) \vec{n}$$

with u the velocity vector, μ the dynamic viscosity, and $\vec{n}$ the normalized vector normal to the particle surface. The torque T is calculated by multiplying the shear stress $\vec{\tau}$ with the radius a of the considered particle.

5.3 Materials and Methods

5.3.1 Numerical Simulation Analysis

Comsol Multiphysics numerical simulations were performed in order to demonstrate that the angular velocity induced on a sphere depends upon the position across the channel.
In particular, if a cell is perfectly at the center of the channel, no rotation should be induced, due to the fact that the opposite sides of its surface are subjected to about the same velocity value.
A sphere in a cross-square section (70 µm X 70 µm) channel was considered (Figure 3). As already mentioned into the theoretical section, in a shear flow characterized by a low Reynolds number, the rotation of a particle approaches the rotation rate of the surrounding fluid ($\Omega_p \approx \Omega_f$).

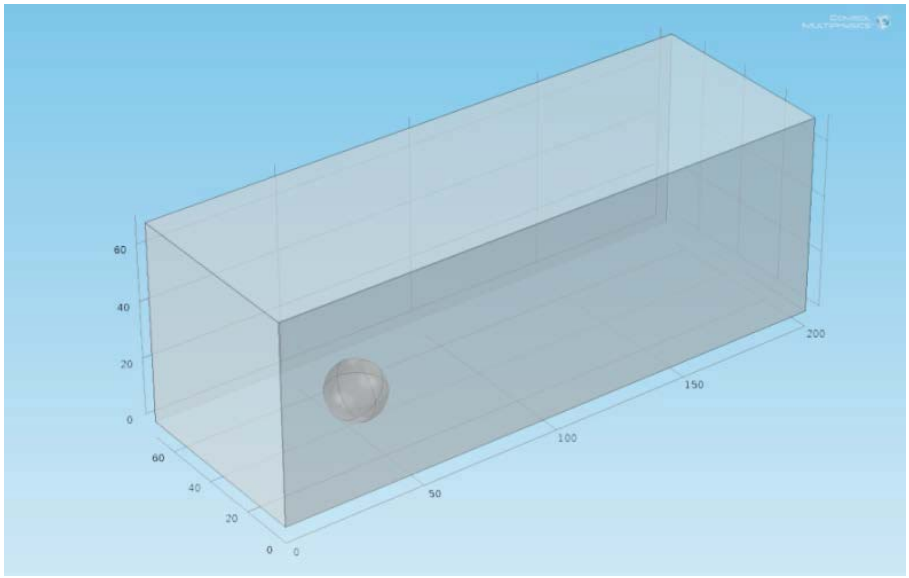

Figure 3: The CAD geometry of the rectangular channel and the sphere used for the COMSOL Multiphysics analysis

The effect of the sphere positions across the channel on the rotation rate has been studied. The analysis was performed considering three different values for the sphere diameter: 5, 10 and 20 µm. The result is reported in Figure 4. It is clear that when the sphere is at the center of the channel, the rotation rate is close to zero, whilst it reaches is maximum value when the sphere is closest to a channel wall.
The observed effect is strictly related to the parabolic velocity profile that characterize a pressure driven flow.
In Figure 5 the velocity distribution in the channel is reported. It can be seen that the velocity intensity goes to zero when the fluid approaches the channel walls, whilst it reaches the maximum at the channel center. As consequence, a particle inside the channel will experience a velocity gradient which intensity depends upon its position.
In Figure 6 it is well represented the velocity distribution on a sphere positioned close to a wall, whilst Figure 7 shows the velocity distribution on a sphere at the center of the channel. It can been seen that in the second case the velocity magnitude is almost uniform on the surface. Therefore, we will observe a rotation only in the first situation, and we will expect to see the sphere travelling without any rotation for the second one.

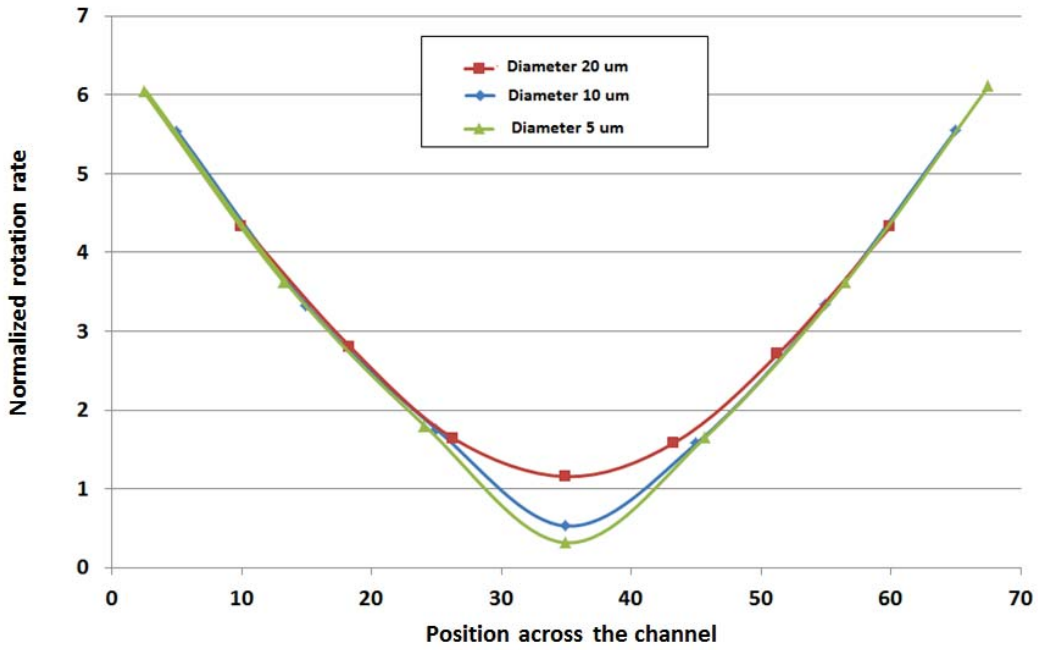

Figure 4: COMSOL simulation results. The rotation rate (number of rotation/s) as a function of the vertical position across the channel. The data referring to three different values for the sphere diameters.

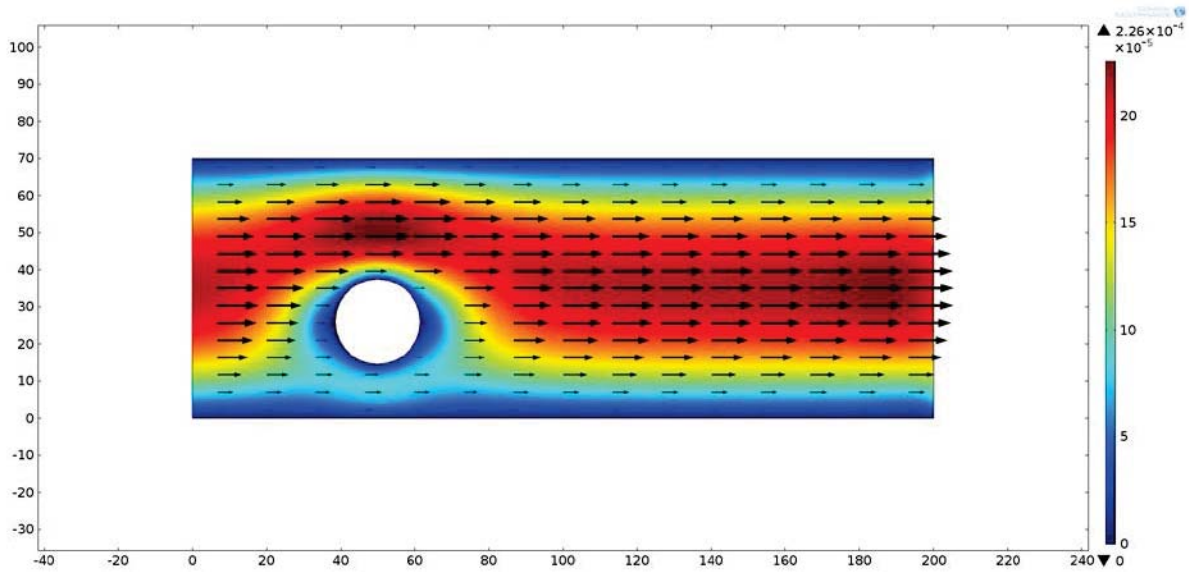

Figure 5: Comsol simulation results. The 2D plot shows the parabolic behavior of the fluid in a pressure driven flow.

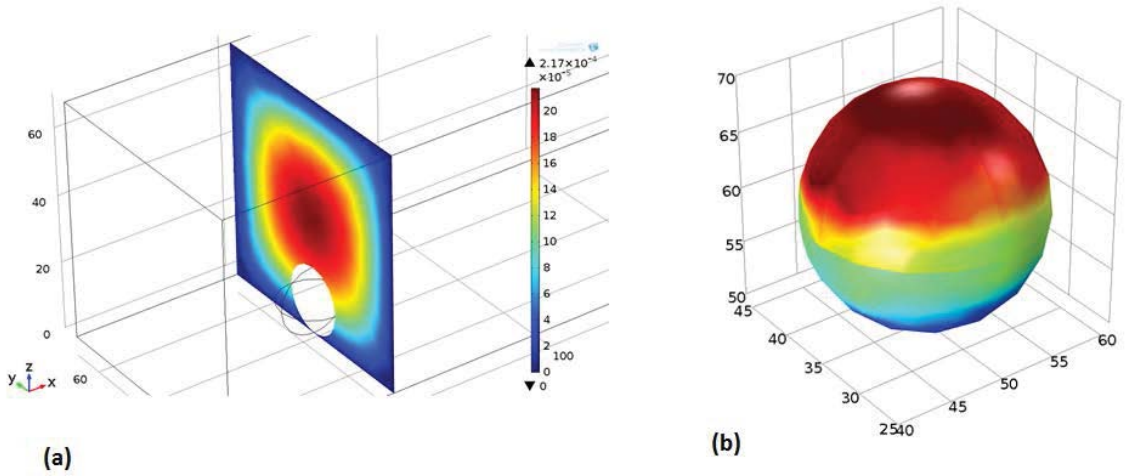

Figure 6: Comsol simulation results. (a) The cut plane shows the parabolic nature of the velocity profile for a pressure driven flow. (b) The surface plot shows the velocity gradient of a sphere that occupies a certain position inside the channel.

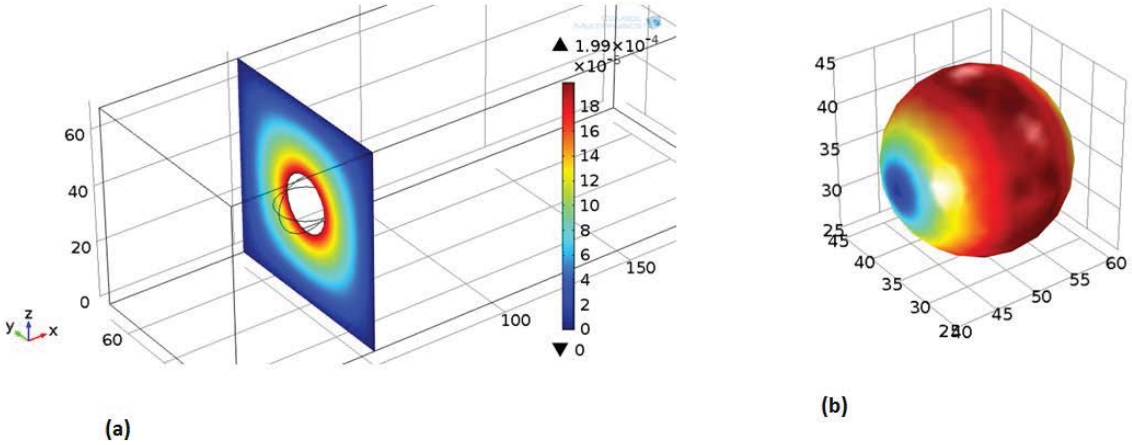

Figure 7: Comsol simulation results. (a) The cut plane shows the parabolic nature of the velocity profile for a pressure driven flow. (b) The surface plot shows the velocity gradient of a sphere at the center of the channel.

Then, we analyzed the rotation rate as a function of the sphere diameters at the same position into the channel. Our results are comparable to the data reported in the paper of Kolb et al. (2014) for the same analysis (Figure 8). The results show that at a fixed sphere position, when the sphere size increases the correspondent rotation rate increases. This could be explained by considering that when the object is bigger in size, the difference between the velocity intensity to which are subjected two opposite sides of its surface is more considerable.

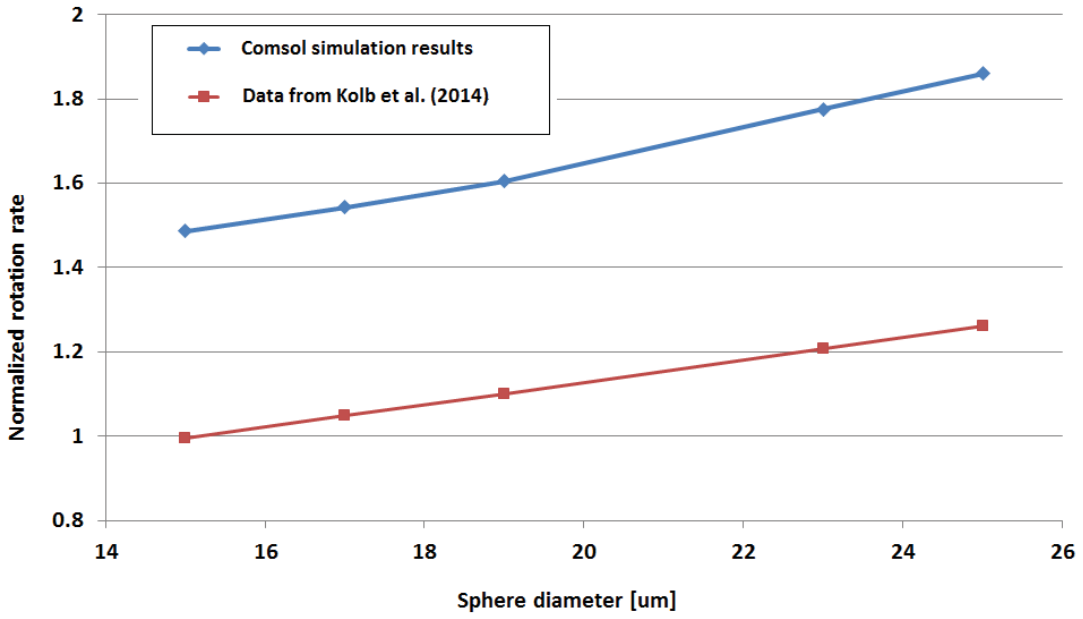

Figure 8: Rotation rate as a function of the sphere diameter. Our COMSOL simulations results are compared to the ones for the same analysis by Kolb et al (2014) [13].

In conclusion, the numerical simulation analysis confirmed our hypothesis, about the possibility to exploit the parabolic nature of the velocity profile inside a microfluidic channel in order to induce cell rotation without the needing of applying any additional external field.

5.3.2 Microfluidic Chip Design and Fabrication

In our device, hydrodynamic focusing is used in order to confine particles close to the channel walls. The designed geometry has two parallel micro-channels, having a common inlet, for the sheath fluid.
Each of them is intersected on one side by an additional channel, transporting the sample fluid (Figure 9). Cells coming from the lateral channel stay confined at the channel wall. The width of the fluid laterally confined depends upon the ratio between the sheath and the sample fluid. The width of the central channel is 30 µm and the lateral ones is 20 µm.

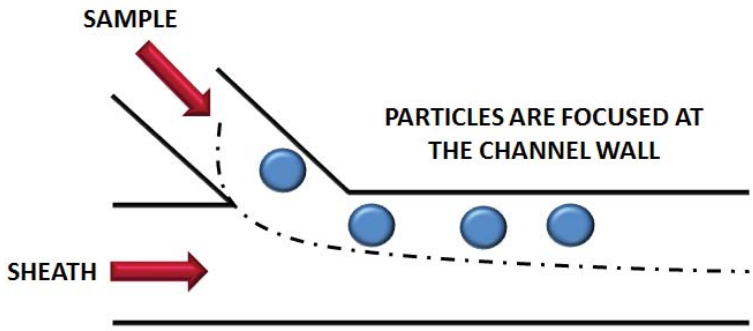

Figure 9: The operating principle of the realized device.

The microfluidic device was realized using the standard PDMS soft-lithography technique. First, a photolithography process was performed in order to obtain a negative master mold of the designed patterns.
A film mask (Figure 10) was used for this step. The SU8-3010 negative photoresist was spinned at 3000 rpm, in order to get a resist thickness of about 10 µm.
A 10:1 mixture of PDMS oligomer and crosslinking agent (Sylgard 184), was poured onto master mold. The polymer was cured in the oven at 80°C for 2 h. The cured PDMS was gently peeled off, cut and holes for the inlet and the outlet were performed. The permanent sealing with a thin glass substrate (166 µm) was obtained through oxygen plasma treatment of both surfaces.

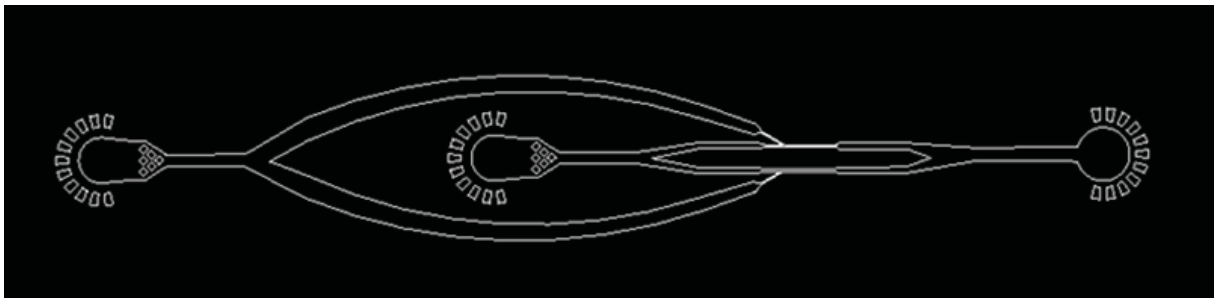

Figure 10: CAD design for the chip mask.

5.3.3 Sample preparation

Experiments were performed by using yeast *Saccharomyces Cerevisiae* cells as target objects to study the hydrodynamic induced rotation effects. S. Cerevisiae is a small, single-celled fungus and thus, like other fungi, it has a rigid cell wall [14]. The motivation to choose these cells to study rotational effect, is due to the fact that they have an asymmetrical shape. Indeed, yeasts, divide by forming a small bud that grows steadily until it separates from the mother cell (Figure 12). In this way it is possible to analyze the change in the object orientation by image processing, against the use of spherical particles or cells.
The sample fluid was prepared by mixing 50 µl of a yeast cells solution with 250 µl of a buffer solution. The latter was made with half DI water and half Bovine Serum Albumin (BSA) solution 40% concentrated. The buffer solution was also used as sheath fluid. A small quantity of yellow food dye was added to the sample fluid. That food dye absorbs the source light wavelength and improves the contrast in the cells images [15].
Once the rotation effect into the device has been validated by using yeast cells, a second experiment has been performed by using B-cell Acute Lymphoid Leukemia (B-ALL) cells. The motivation in choosing this cells are related to the widely diffuse interest among the biology and medical scientist in mapping the spatial distribution of the fluorescence from lymphocyte cancer cells. In this way a better understanding of the cancer phenomena can be achieved, by adding more information to the traditional overall fluorescence intensity signal. In particular, we decided to use cells from the M60 cell line, which diameter is a range of 5-8 µm. The sample for this experiment was prepared by mixing 200 µl of cells solution with the same quantity of a buffer solution.
For both the experiments data have been acquired by using the optical imaging set-up in Figure 11.

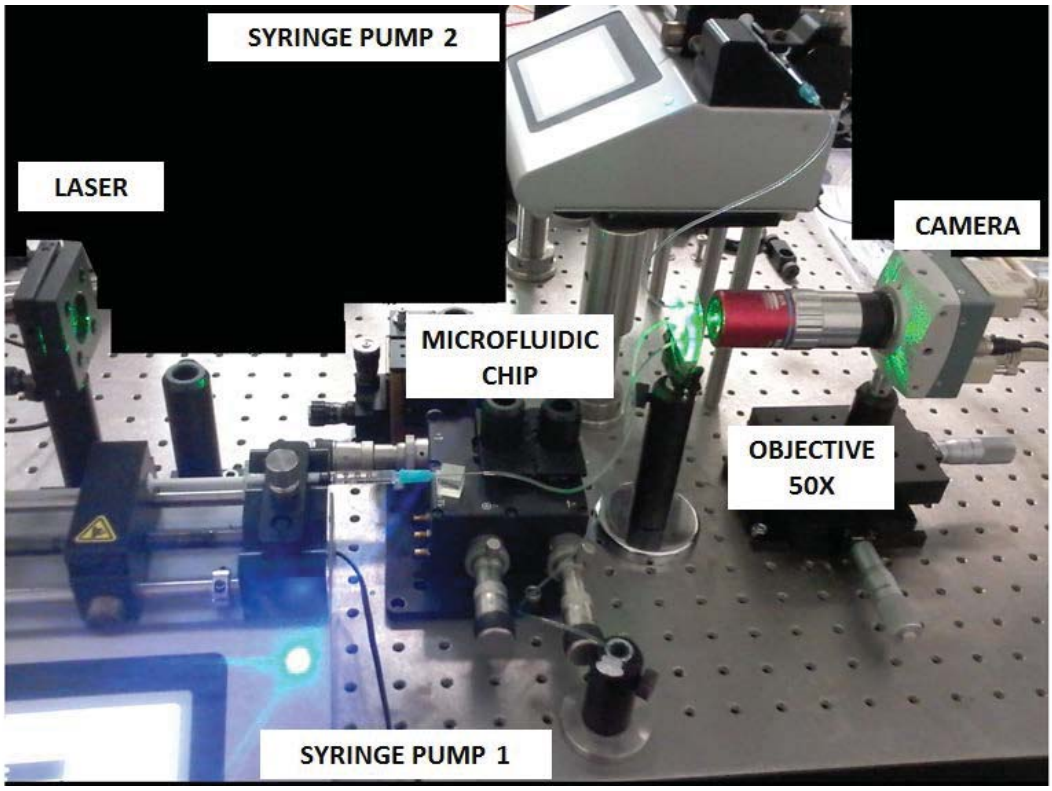

Figure 11: Optical Imaging Set-up used for performing the experiments

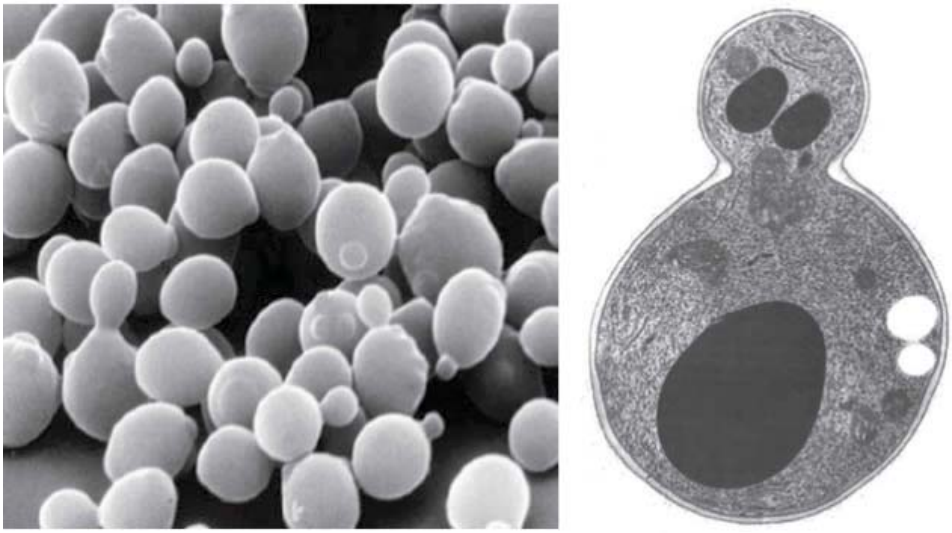

Figure 12: Scanning electron micrograph of yeast cells. Some of them are in the process of dividing, which they do by budding.

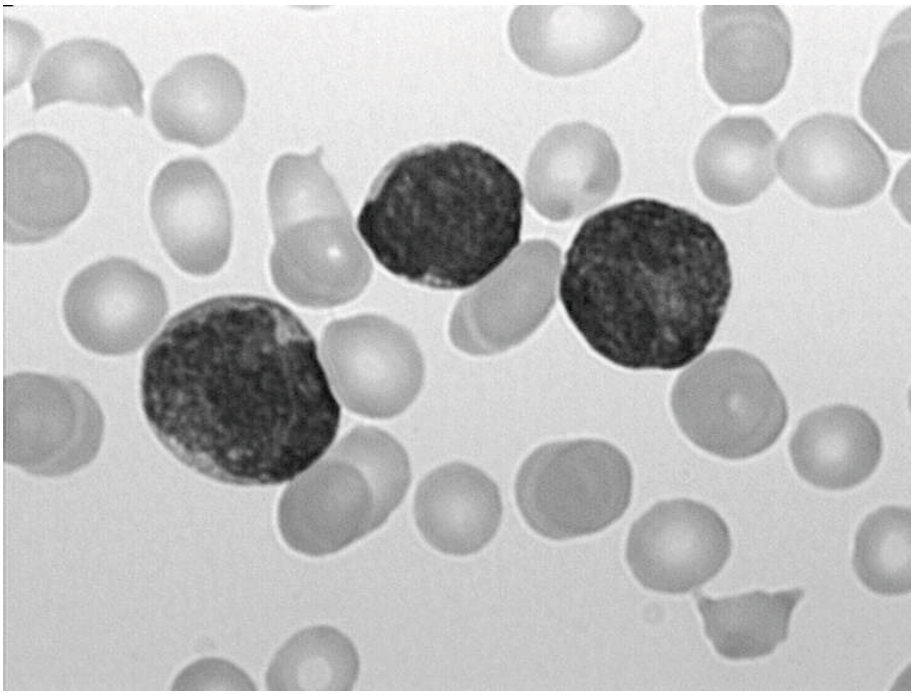

Figure 13: Acute Lymphoblastic Leukemia cells.

5.4 Results and discussion

5.4.1 Yeast cells rotation

Images of the rotating yeast cells were collected by using a CMOS camera (Teledyne DALSA, Inc) and a 40x objective. As source light a 455 nm LED was used. Data were acquired at 1800 frame/s. The flow rate into the device was controlled using two syringe pumps. The flow rate was set to 90 µl/h and 20 µl/h for the sheath and sample fluid respectively.
Through image processing analysis (Matlab, Inc) the cells orientation at each frame of the acquired video is obtained. In order to perform the cells analysis, the acquired images were transformed into binary images. Cell position is defined by the angle between a straight line that follows the cell orientation and a horizontal line (Figure 14). The difference between the angles at two consecutive frames, and the frame rate, allow calculating the angular velocity.

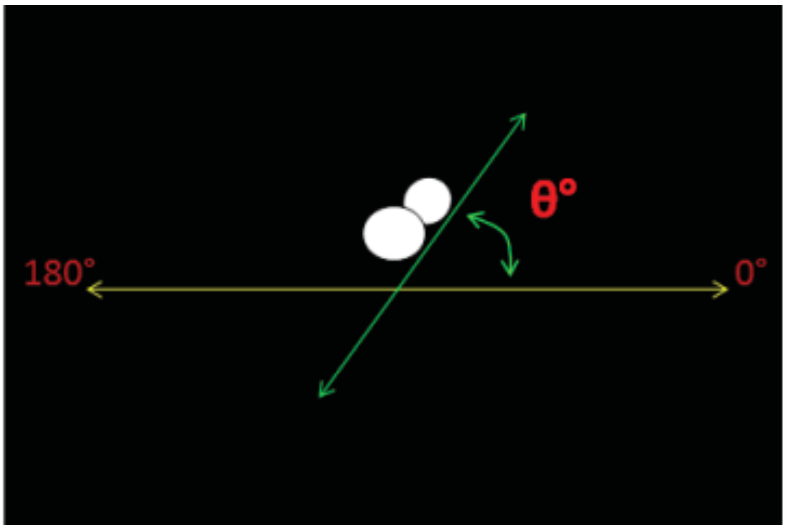

Figure 14: A schematic of how the cell angular orientation has been defined in the Matlab image analysis.

190 videos of 800 frames were analyzed. The number of the captured cells is ≈7000. For each cell the information related to the angular orientation and the centroid position were obtained.
In Figure 15 five frames of an acquired videos are illustrated and rotation induced on a cell that flows close to the channel wall can be observed. As it can be seen from the image, on the back of the cell the fluid is dark. This effect is due to the use of the yellow food dye in the sample solution. Since the yellow dye that we used for the experiment has a big absorption peak at the blue LED wavelength, and so it appears black in the image. On the other hand, the yeast cells do not absorb blue wavelength. In this way, the enhanced contrast between the cell and the background, allows to better delineate the object contours in the image processing phase.
The angular position of each cell has been evaluated analyzing their binary images by means of a Matlab code. In Figure 16 the binary images obtained from those of the Figure 15, are reported. Through the processing analysis we could obtain the information about the cell angular orientation at each frame, and also the position (x,y) into the image field.

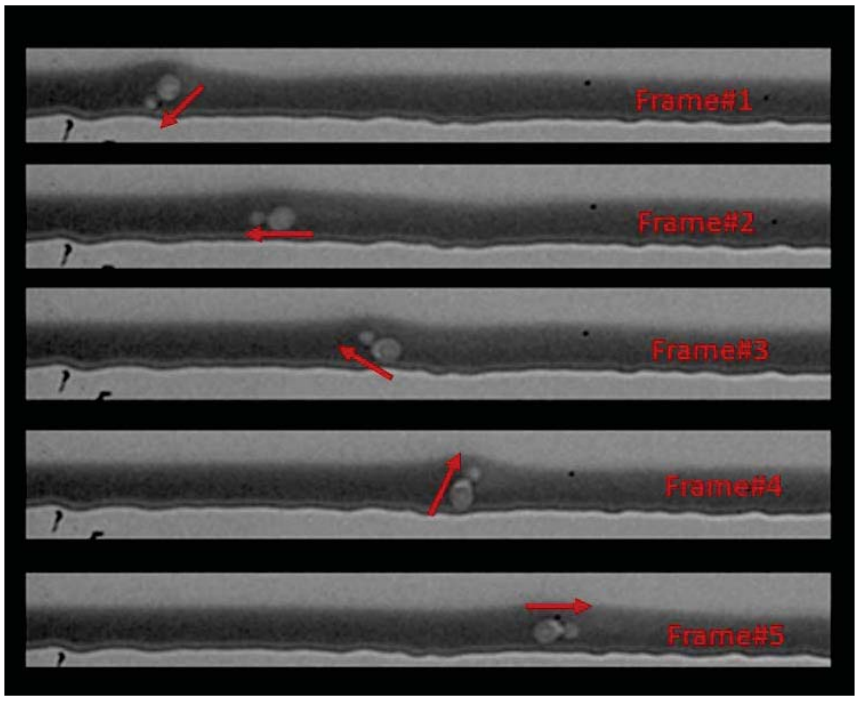

Figure 15: Five frames take out from the acquired videos. A cell close to the channel wall is induced in rotation. The darker background behind the cell is due to the adding o fa dye to the sample fluid, that has a peak of absorption at the wavelength of the illumination source (LED 455 nm).

Figure 16: Binary images of the same frames in Figure 9, obtained by Matlab image processing.

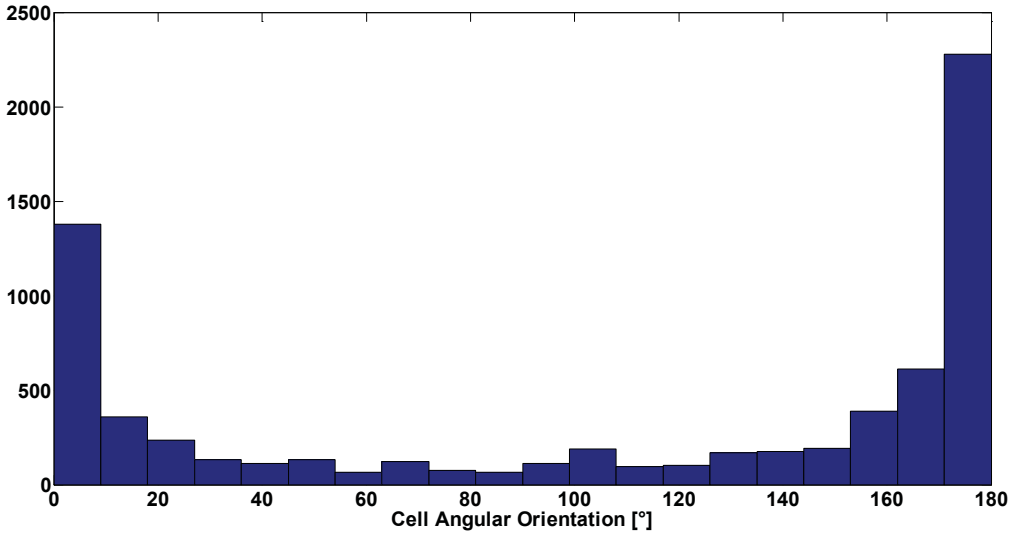

Figure 17: Histogram of the angular orientation of the analyzed cells. It shows that many cells are found in an horizontal position. This could be explained by considering that rotational effects are more easily induced when cells are vertically oriented, since they are experienced by an higher velocity gradient. By contrarily, if they are horizontally oriented they could cross the channel, without being affected by any rotation.

An histogram of the cells angular positions is reported in Figure 17. What we can deduce from this histogram is that a higher number of the collected cells were horizontally orientated (angular orientation close to 0° and 180°). This is an expected result, since when objects are horizontal, its surface is less subjected to velocity gradient compared to the situation in which they are vertically oriented. This means that if cells occupy this position, they tend to flow straight and rarely rotate. So we will find it in the same position in a higher number of frames. By calculating the difference between the values of the angles occupied by cells in two successive frames, the rotation rate can be estimate. First, the obtained data of the cells angular orientation were grouped by considering nine ranges of 10 degrees. Then, rotation rate was calculated by evaluating the change in angular orientation in successive frames. The result (Figure 18) shows that the number of rotation per second, is higher for the cells that occupy a position at 60-140° respect to the fluid direction. This can be explained by considering that if the cell is in a vertical position, respect to an horizontal direction of the fluid flow, the cell surface will experience a higher velocity gradient. For the opposite reason, the angular velocity decreases when the cells occupy an horizontal position (cell angular orientation close to 0° and 180°).

Moreover, from the image processing analysis, the coordinates of the centroids' position for the analyzed cells can be also obtained. Hence, the path of each of them in the flow direction, and therefore the linear velocity, it can be evaluated.

Figure 19 reports the velocity in the flow direction related to the rotation rate. From the plot it can be observed that the cell velocity is almost uniform. The average value for the velocity obtained by the experimental data is $\mu \approx 0.034$ m/s with a variance $\sigma \approx 5x10^{-4}$ m/s. This means that the fluid flow has been well controlled during the experiment.

This result is close to the value that comes out from the theoretical calculation. The flow rate for the sample fluid has been take constant to 20 µl/h, and the lateral channel cross section is ≈ 100 μm^2. By using the simplified relation Velocity = Flow rate / Channel Cross-section, we got a value for the expected linear velocity of ≈ 0.05 m/s.

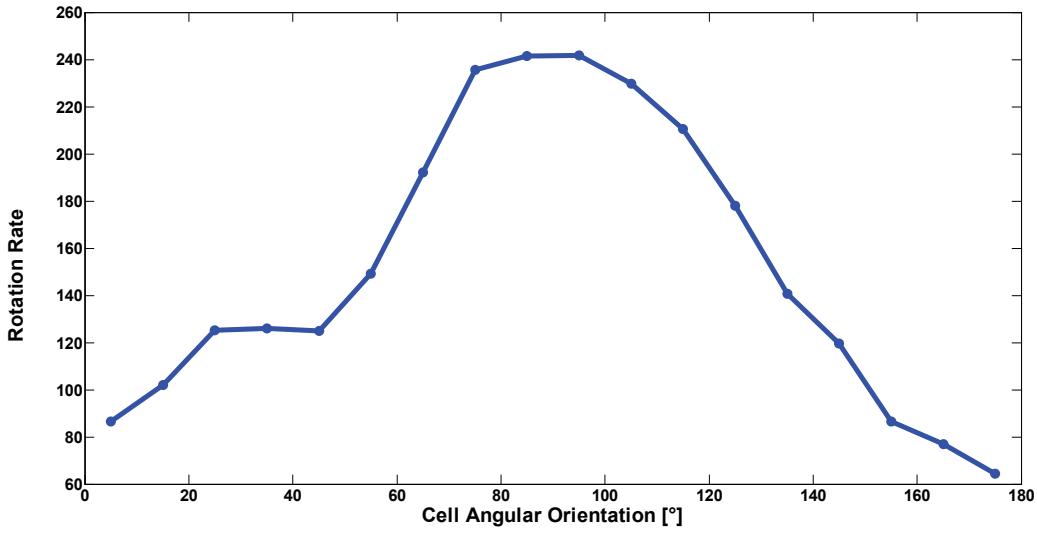

Figure 18: The plot shows the rotation rate (Number of rotation/s) in relation to the angular position of the cell. The first quantity has been calculated for range of 10°, by averaging the values obtained by the image processing analysis of the experimental data.

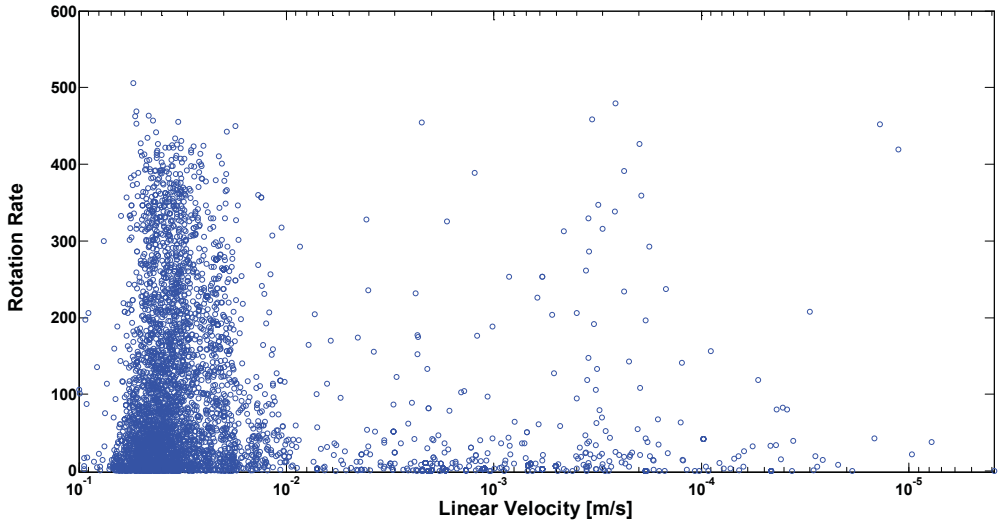

Figure 19: The cells linear velocity vs the Number of Rotation/s. The linear velocity stay is maintained constant during the time of the experiment, since the flow rate has been controlled through syringe pumps. The horizontal axis is in a logarithmic scale.

As already explained before, the ratio between the sample and the sheath flow rate, determines the thickness *t* of the region close to the wall at which cells are focused. Depending on the cell size, it could occupy all the sample fluid band, or, could stay closer to the channel center or to the wall (Figure 20).

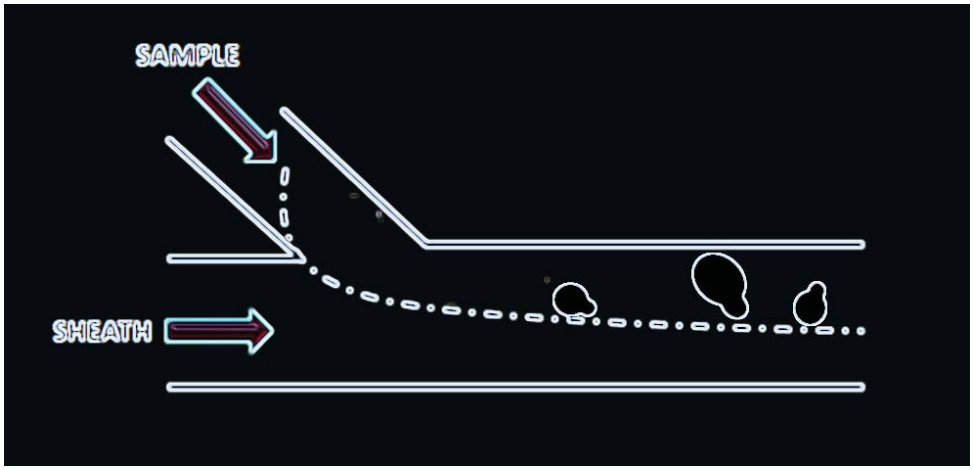

Figure 20: The sheath to sample ratio determines the thickness t of the sample fluid stream focused at the channel width. According to its size the cell can occupy all the fluid band or not.

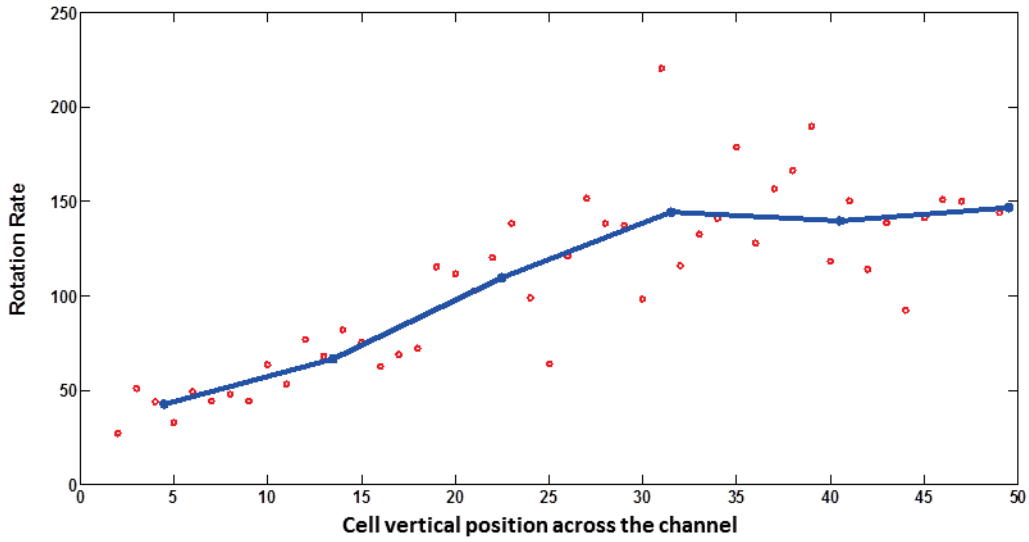

Figure 21: The Rotation Rate (Number of rotation /s) as a function of the vertical cell position across the channel. The values close to zero on the abscissa axis refer to a cell position closer to the center of the channel, and the high ones to a position close to the channel wall. The result is in accordance to the expectation, if the cell is more close to the channel wall, it investigate more velocity gradient and an higher rotation rate. It has to be noticed that the analyzed cells are focused at the channel wall, so the difference in the rotation effect is low

The plot in Figure 21 gives the relation between the rotation rate and the vertical position of the cells across the channel.

The values close to zero on the abscissa axis refer to a cell position closer to the center of the channel, and the high ones to a position close to the channel wall. It has to be noticed that the analyzed data refer to cells focused at the channel wall, so there is only a slight difference in the rotation rate due to the more proximity of

the cell to the center or to the wall . However, the trend reflects the expected behavior: when an object is close to the wall the rotation rate assumes higher values.

5.4.2 Acute Lymphoblastic Leukemia Cells rotation

The experiment described in the previous paragraph allowed us to demonstrate the proper operation of the realized device in the achievement of cell rotation. Then, the same device has been tested by using B-ALL cells from the M60 cell line. Data have been acquired at 1200 frames/s by using a high speed camera (Teledyne DALSA, Inc). A green laser has been used as illumination source. The sample and the sheath flow rate has been controlled by using syringe pumps.

Figure 22 shows six frames of a video in which a M60 cell is rotating while it is flowing (the flow direction is from the right to the left side). In the images sequence the cell side closer to the center of the channel (down in the image) experiences a higher velocity than the side close to the channel wall, and therefore a clock-wise rotation is can be observed.

The imaged cell has an ovoid shape, that is typically observed in ALL-cells from the M60 cell line. Indeed, in comparison to the others ALL cell lines, cells from the M60 are bigger (5-8 μm), they are characterized by a more irregular shape and they have a bi-lobed nucleus [16].

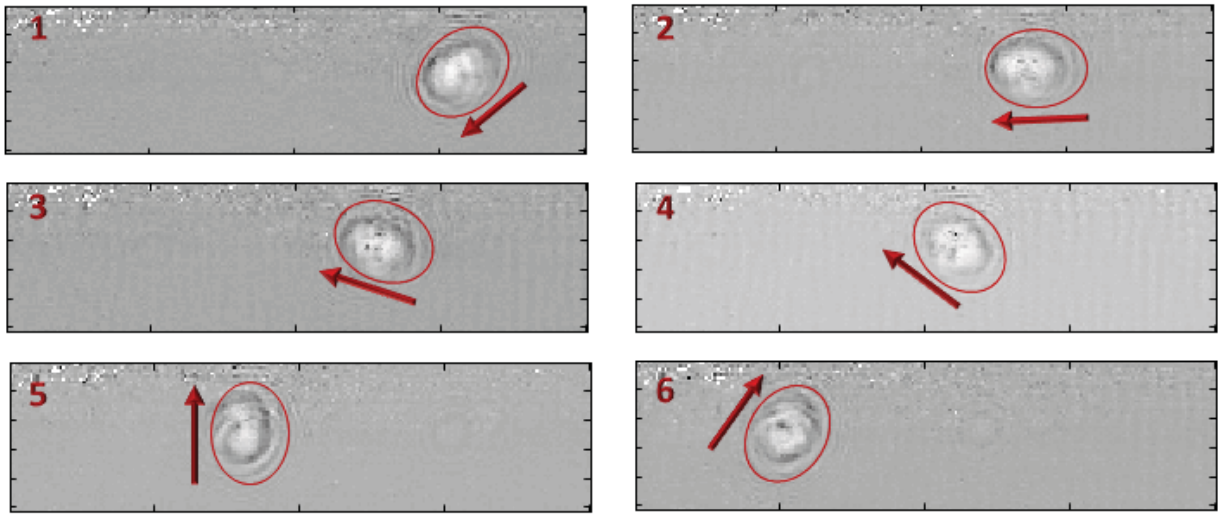

Figure 22: The six consecutive frames show a B-ALL cell from the M60 cell line induced in rotation for hydrodynamic effects in a microfluidic channel.

This means that it will be possible to use the same device for obtaining images of the leukemia cells from different points of view. Therefore, whatever is the initial cell orientation in the microfluidic channel, it will be possible in any case to collect images of different cell sides.
The obtained results allows as to affirm that the proposed approach could considerably improve the existent techniques for imaging cells in flow. It is well known that the challenges associated with imaging cells in flow include achieving sufficient fluorescence sensitivity, producing imagery with high spatial resolution, combining fluorescence imagery with other imaging modes such as brightfield (transmitted light) or darkfield (scattered light), and imaging all of the cells in the flow stream. Moreover, as it has been widely stressed in this chapter, there is the needing of distributing these information in the three-dimensional space.
In clinical practice and in research settings, cellular evaluation by imaging technologies and flow cytometry provides significant information reflecting the particular cellular phenotype, both normal and pathological. Microscopy provides a wealth of information, but data acquisition rates are slow and analysis is generally subjective. For example, a confocal microscope can produce highly detailed fluorescent cell images, including three dimensional cell representations based on multiple stacked images, but it can take as long as several minutes to produce a 3D representation of a single cell. It has been said that the design features associated with confocal microscopy make it well-suited to applications that require the accurate analysis of sub-cellular features in homogeneous samples, but poorly suited to detecting fluorescent probes or evaluating statistically significant numbers of cells within heterogeneous samples. This is the reason why confocal imaging is not widely used in clinical assessment or diagnostics.
On the contrary, flow cytometry allow to get rapid data acquisition, but the data are only intensity-based, thus lacking the morphology that truly lends credence to the analysis.
The proposed microfluidic approach give the basis for the development of a lab-on-chip that can combine both flow cytometry measurements and 3D imaging of flowing cells.

5.5 Conclusions and future trends

In this chapter it has been investigated the possibility to induce cells rotation in a microfluidic device without the needing of additional physic forces. Electric and magnetic field, or optical methods could be used to manipulate cells motion. The adoption of these methods has several disadvantages: the fabrication of the device is more complicated since there is the needing of additional elements (i.e. electrodes); cells could be damaged by the applied forces and the desired information could not be taken out from the experiment.
In our device, cells are induced in rotation taking advantage of the hydrodynamic effects. In a microfluidic channel the velocity profile is parabolic. It assumes the maximum value at the center of the channel, and goes to the minimum close to the channel walls. This means that if an object is confined at the wall, it is effected by a velocity gradient, and a rotation is induced. In order to prove this assumption, in the designed device, the sample fluid is focused to the channel wall through an additional sheath fluid. The operation of the device was tested by using yeast cells, which are characterized by an asymmetrical shape, due to a bud formation during the reproduction phase. The image processing of the acquired data led to the analysis of ≈ 7000 cells. The obtained results demonstrate that cells rotate, and that the rotation rate depends upon the angular orientation of the objects and the position occupied across the channel. Then, the device was tested by using M60 cells, and we have been able to observe rotation effects.
In our experiment, the rotation is generated in the in-plane direction. Since the parabolic velocity profile is three-dimensional in a microfluidic channel, the same effect can be generated if cells are focused at the bottom of the channel.
This means that according to each particular purpose, microfluidic devices can be designed in order to induce cell rotation in the desired direction.

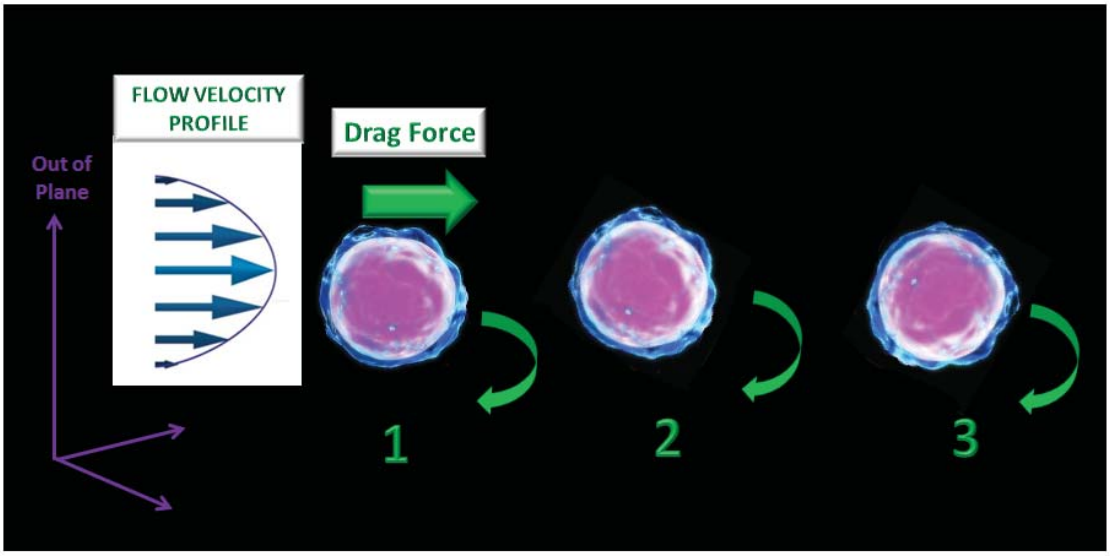

Figure 23: In a microfluidic channel for a pressure driven flow, the velocity profile is parabolic in the 3D domain. Therefore, if cells are focused at the bottom of the channel they will start to rotating in the induced in the out-of-plane direction.

References

1 D. Huh, W. Gu, Y. Kamotani, J.B. Grotberg, and S. Takayama, Microfluidics for flow cytometric analysis of cells and particles, Physiol. Meas. 26, R73 (2005).

2 Simonnet, C.; Groisman, High-throughput and high-Resolution flow cytometry in molded microfluidic devices, A. Anal. Chem. 2006, 78, 5653−5663.

3 N. Watkins, B. M. Venkatesan, M. Toner, W. Rodriguez and R. Bashir, A robust electrical micro-cytometer with 3-dimensional hydrofocusing , Lab Chip, 2009, 9, 3177–3184

4 11 X. Mao, A. A. Nawaz, Sz-Chin S. Lin, M. I. Lapsley, Y. Zhao, J. P. McCoy, W. S. El-Deiry and T. J. Huang, An integrated, multiparametric flow cytometry chip using "microfluidic drifting" based three-dimensional hydrodynamic focusing, Biomicrofluidics, 2012, 6, 024113.

5 E. Schonbrun , R. Malka , G. Caprio , D. Schaak , and J. M. Higgins , Quantitative absorption cytometry for measuring red blood cell hemoglobin mass and volume, Cytometry, Part A. 85(4), 332–338 (2014).

6 S. I. Han, Y. D. Joo, and K. H. Han, An electrorotation technique for measuring the dielectric properties of cells with simultaneous use of negative quadrupolar dielectrophoresis and electrorotation. Analyst, 2013. 138(5): p. 1529-37.

7 M. Zrinyi, M. Nakano, and T. Tsujita, Electrorotation of novel electroactive polymer composites in uniform DC and AC electric fields. Smart Materials and Structures, 2012. 21(6): p. 065022.

8 L. H. Chau, et al., Self-rotation of cells in an irrotational AC E-field in an opto-electrokinetics chip. PLoS ONE, 2013. 8(1): p. e51577

9 G. Carmon and M. Feingold, Rotation of single bacterial cells relative to the optical axis using optical tweezers. Opt Lett, 2011. 36(1): p. 40-2.

10 D. S. Claguea and P. J. Cornelius, The hydrodynamic force and torque on a bounded sphere in Poiseuille flow, Int. J. Numer. Meth. Fluids 2001; 35: 55–70

11 Saffman, P.G.: The lift on a small sphere in a slow shear flow. J. Fluid Mech. 22, 384–400 (1965); and Corrigendum. J. Fluid Mech. 31, 624 (196–8)

12 L. D. Landau and E. M. Lifshitz, Fluid Mechanics, Volume 6 of A Course of Theoretical Physics , 1st Edition Pergamon Press 1959

13 T. Kolb, S. Albert, M. Haug, and G. Whyte, Optofluidic rotation of living cells for single-cell tomography, J. Biophotonics 1–8 (2014)

14 Alberts essential cell biology (book)

15 Schonbrun E, Di Caprio G, Schaak D. Dye exclusion microfluidic microscopy. Opt Exp 2013 ; 21:8793–8798.

16 Cobaleda C, Sánchez-García, B-cell acute lymphoblastic leukaemia: towards understanding its cellular origin, Bioessays. 2009 Jun;31(6):600-9

6. Conclusions

After several years of development, microfluidic devices have testified themselves to be powerful tools for cell-based analysis. Microfluidics offers a set of exciting tools for studying biology. It reduces the time and cost of common bioanalytical assays, and enables technologies to study cells in detail. Moreover, itallows integrating all the functions of a human-scale test laboratory, including transferring samples, drawing off a precise volume of a chemical product, or mixing with reagents, on a system of a few square centimeters. Just imagine a drop of blood simply deposited in a reservoir in a system that can make a complete analysis: minute quantities of that drop are then displaced and injected into several tiny chambers in which different reactions take place.

At the starting phase of the technology, microfluidic fabrication has been developed with two sets of materials: silicon or glass and polymers. Silicon and glass have well-controlled mechanical and chemical properties but they also have high manufacturing costs and high processing complexity, particularly for disposable devices. As the material of choice for microfluidic systems, polymers exhibit advantages over silicon and glass, because they are easy to fabricate, and bio-compatible. In particular, an important breakpoint has been given by the introduction of the soft-lithography technique, combined with the use of PDMS (poly-dimethylsiloxane) as polymeric substrate, that has opened new concrete perspectives in microfluidics.

As it has been discussed in this work, microfluidic technology allows the design of micro-channel networks connecting micro-chambers or interrogation points where analysis or biochemical reaction could take place (*viz*., a miniaturized lab integrated on a chip). The idea is to change the way in which the market of bio-technological instrumentations works: no more expensive benchtop instruments able to perform multiple analysis, but small, cheap and disposable *ad hoc* devices (*i.e.*, lab-on-chips) for each single purpose. An important class of applications concerns cell manipulation. In this case, it is often required to control the position of cells flowing through a fluidic channel. In order to achieve this purpose fabrication of miniaturized cell manipulators has been proposed. The commonly used methods for on-chip cell manipulation can be categorized depending on the manipulating force employed, such as hydrodynamic, magnetic, optical, mechanical, and electrical.

In particular, this thesis work has been focused on the development of microfluidic devices for the manipulation of cell position by using hydrodynamic effects. This approach has the advantage of simplifying the chip fabrication, since there is no needing of introducing additional elements (such as electrodes), and at the same time no effects on the biological samples are induced (*i.e.*, as could happen using electrical fields). Flow cytometry is the most useful and widespread cell-based assay. It is widely applied to diagnose diseases, particularly through counting of various populations of blood cells. Current flow cytometry is restricted to benchtop or full-sized laboratory models. Therefore there is a huge interest in the development of low-cost, miniaturized, portable, easily useable flow cytometer for point-of-care applications, that is, capable of operating outside of a sophisticated biotechnological lab. Lab-on-chip technology represents the answer to this urgent demand.

Cells focusing is the key point for the correct operation of a flow-cytometer. The sample fluid containing cells is hydro-dynamically focused by a surrounding sheath fluid made of a buffer solution. In this way, cells can be confined at the center of the channel in a one single line, and therefore, they will pass one per time through the laser beam in the interrogation region. Several efforts have been made to develop robust, cost-effective, and compact flow cytometers using microfluidic techniques. In most cases, the traditional hydrodynamic focusing mechanism employing sheath fluid is directly translated to the micro-scale. The main drawback in the mentioned approach is that multiple inlets are required. This brings to a high complexity if parallelization is introduced into the device. The advantages of having a parallelized microfluidic structure, and hence multiple channels working simultaneously, has been observed in many research fields, such us DNA sequencing, droplet generation and moreover in micro-cytometers. The

fabrication of multiple cytometers operating in parallel on the same chip leads to a higher throughput, compared to a single channel architecture.

In this work, the limitation related to the needs of multiple inlets for the achievement of hydrodynamic focusing has been overcome by realizing a microfluidic device that exploits only one inlet. This is achieved by introducing a cross-filter into the channel, and in this way the structure can be easily parallelized. The cross-filter is realized through two arrays of pillars, and the gap size between two consecutive pillars determines the size of the pores of the membrane. At the end of the filter region, the *sample fluid* from the center and the *sheath fluid* from the lateral channels, are recombined in what we call *focusing region*. The device has been designed according to the diameter of the target particles. In this way only the fluid can cross the membrane barrier, whilst particles or cells are forced to stay confined at the center. In particular, this work has been focused on the lymphocytes manipulations. This means that the target cell size is in 5-10 μm range. Different cross-filter geometries have been first analyzed by numerical simulations, and then realized and experimentally tested. The geometry of the filter region plays an important role in the value achieved for the diameter of the focused stream, and in particular, we found out that there are mainly three critical parameters: L, the length of the filter region; W_L, the width of the lateral channels; φ, the inclination angle of the pillars array. We found the right combination for these three parameters that allow to well hydro-dynamically focusing Acute Lymphoid Leukemia B-cells from the M60 cell line. Experimental results showed that the geometry, optimal for this application, allows to focus M60 cell in a stream with a width of ≈ 10 μm. Therefore, the realized device allows to make cytometric measurements on multiple channels working simultaneously.

However, conventional flow cytometry uses the total fluorescent signal from the entire cell to characterize the sample and averages over the local distribution and morphology of the signal. Recent advances in imaging flow cytometry enable the collection of fluorescent images of each cell at high speed and therefore add the fluorescent distribution to the available information. Nevertheless, the traditional approach used for imaging cells in microfluidic systems allows to obtain only two-dimensional images, based on the orientation of the cell and the imaging system. A solution to this problem is to make cells rotating as they flow through the channel. In this way, images from multiple points of views can be collected, without the needing of moving the acquisition system. From these acquired data, a cell can be reconstructed in its three-dimensionality using tomographic method. In this thesis work, in complementarity with the micro-cytometer work, the possibility to control cell rotation by only exploiting hydrodynamic forces has been investigated. The main assumption is that in a pressure driven flow the velocity profile is parabolic. In particular, the velocity is minimum at the channel walls and reaches its maximum value at the center of the channel. This means that, if a cell is close to a channel wall, it will experience a velocity gradient on its surface, and therefore a rotation will be induced. Therefore, a parallel microfluidic device that allows to focus cells at the channel wall has been developed. In order to easily test the device operation, shaped asymmetric cells have been used. We decided to use yeast cells since they present a bud formation during their duplication phase. The image processing analysis of the acquired data allowed to evaluate the angular orientation for each captured cell, and therefore to estimate the rotation rate. The obtained results confirmed the hypothesis of a rotation induced by the parabolic velocity profile. Therefore, the new configuration allows a whole and better characterization combining the scatter and fluorescence signals from the cytometric analysis, with the fluorescence distribution obtained by the imaging of rotating cells.

In conclusion, in this thesis it has been laid the foundations for the realization of a new class of microfluidic devices that allows to obtain a whole cell characterization by performing:

a) hydrodynamic focusing in parallel fluidic channels, and
b) cell rotation for complete cell imaging without moving optics.

As a final comment, it has to be underlined that this thesis has been focused on the design and optimization of only the fluidic core, that is one of the subsystems needed for the realization of a fully integrated lab-on-chip for cell assay. In order to completely substitute traditional benchtop instrumentations, additional elements, such as pumps, valves, light sources, detectors, sensors and so on, have to be still integrated into the device.

The common future prospective is that lab-on-chips will enable a more widespread monitoring of health parameters in disease prevention and diagnosis, but even more importantly, daily screening of health parameters in order to extend and improve the quality of life. However, despite the many improvements achieved in the realization of microdevices for bio- sensing and analysis, the ability to assemble and interface individual components in order to achieve high level of integration in complete working systems is still an open challenge.

The future of the biochips industry will depend heavily on the convergence of multiple disciplines such as the biological, physical, chemical, and engineering sciences to bridge the gaps in technology and establish industry standards to support mass commercialization.

7. Appendix: MATLAB Codes

7.1 MATLAB-COMSOL Parametric Analysis

This code has been written in order to perform a parametric analysis by using the Comsol live-link for Matlab. Different cross-filter geometries can be studied thanks to the parametric definition.

(1) Loop Analysis

```
firstpart1='C:\path1';
firstpart2=' C:\path2';

for phi= round(linspace(0,24,5))
    for w=round(linspace(40,100,5))

         if phi==0
             Lmax=1000;
         else
              Lmax=(w+10)/tan(phi*3.14/180);
       end
        for Li=round(linspace(90,900,10));

%DIFINING FILE FOR SAVING THE RESULTS
nomefile1=[firstpart1,'phi',num2str(phi),'w',num2str(w),'Li',num2str(Li),'.txt'];

nomefile2=[firstpart2,'phi',num2str(phi),'w',num2str(w),'Li',num2str(Li),'.txt'];

out = comsol_parametric_analysis (Li,w,phi,nomefile1,nomefile2);

        end
    end
  end
end
```

(2) Comsol parametric analysis function

```
function out = comsol_parametric_analysis (Li,w,phi,nomefile1,nomefile2)

import com.comsol.model.*
import com.comsol.model.util.*

model = ModelUtil.create('Model');

model.modelPath('C:\...path_model);

model.name('matlabresult3.mph');

%PARAMETERS DEFINITION

model.param.set('sample_flow_rate', '100[ul/h]');
model.param.set('Li', [num2str(Li),' [um]']);
model.param.set('l', '50[um]');
model.param.set('L', 'Lc+l');
model.param.set('delta', '0');
model.param.set('Lc', 'Li+delta');
model.param.set('w', [num2str(w),'[um]']);
model.param.set('wc', '100[um]');
model.param.set('wL', 'wc+2*w', 'definisce l''altezza del rettangolo centrale');
model.param.set('yc', '25[um]', 'coordinata simmetria y della struttura');
model.param.set('post_size', '15[um]');
model.param.set('gap_size', '5[um]');
model.param.set('N', 'Lc/(gap_size+post_size)');
```

```
model.param.set('phi', [num2str(phi)]);
model.param.set('xpillar', '-200[um]-Lc+gap_size');
model.param.set('y1', 'tan((phi*3.14)/180)*(-195[um]-xpillar)+50[um]');
model.param.set('hpillar', 'y1');


%GEOMETRY

model.modelNode.create('comp1');
model.geom.create('geom1', 3);
model.geom('geom1').lengthUnit([native2unicode(hex2dec({'00'    'b5'}),    'unicode')
'm']);
model.geom('geom1').feature.create('wp1', 'WorkPlane');
model.geom('geom1').feature.create('ext1', 'Extrude');
model.geom('geom1').feature('wp1').geom.feature.create('r1', 'Rectangle');
model.geom('geom1').feature('wp1').geom.feature.create('b1', 'BezierPolygon');
model.geom('geom1').feature('wp1').geom.feature.create('mir2', 'Mirror');
model.geom('geom1').feature('wp1').geom.feature.create('r3', 'Rectangle');
model.geom('geom1').feature('wp1').geom.feature.create('r4', 'Rectangle');
model.geom('geom1').feature('wp1').geom.feature.create('mov27', 'Move');
model.geom('geom1').feature('wp1').geom.feature.create('b3', 'BezierPolygon');
model.geom('geom1').feature('wp1').geom.feature.create('mir5', 'Mirror');
model.geom('geom1').feature('wp1').geom.feature.create('r5', 'Rectangle');
model.geom('geom1').feature('wp1').geom.feature.create('arr1', 'Array');
model.geom('geom1').feature('wp1').geom.feature.create('uni3', 'Union');
model.geom('geom1').feature('wp1').geom.feature.create('rot2', 'Rotate');
model.geom('geom1').feature('wp1').geom.feature.create('mov28', 'Move');
model.geom('geom1').feature('wp1').geom.feature.create('mir3', 'Mirror');
model.geom('geom1').feature('wp1').geom.feature.create('b4', 'BezierPolygon');
model.geom('geom1').feature('wp1').geom.feature.create('mir6', 'Mirror');
model.geom('geom1').feature('wp1').geom.feature.create('r6', 'Rectangle');
model.geom('geom1').feature('wp1').geom.feature.create('mir7', 'Mirror');
model.geom('geom1').feature('wp1').geom.feature.create('uni4', 'Union');
model.geom('geom1').feature('wp1').geom.feature.create('b5', 'BezierPolygon');
model.geom('geom1').feature('wp1').geom.feature.create('mir8', 'Mirror');
model.geom('geom1').feature('wp1').geom.feature.create('uni5', 'Union');
model.geom('geom1').feature('wp1').geom.feature.create('r7', 'Rectangle');
model.geom('geom1').feature('wp1').geom.feature.create('mir9', 'Mirror');
model.geom('geom1').feature('wp1').geom.feature.create('uni6', 'Union');
model.geom('geom1').feature('wp1').geom.feature.create('dif1', 'Difference');
model.geom('geom1').feature('wp1').set('unite', 'on');
model.geom('geom1').feature('wp1').geom.feature('r1').set('pos', {'-200' '0'});
model.geom('geom1').feature('wp1').geom.feature('r1').set('size', {'520' '50'});
model.geom('geom1').feature('wp1').geom.feature('b1').set('p',  {'-55'  '-40'  '-200'
'-200' '-55'; '75' '75+w' '75+w' '75' '75'});
model.geom('geom1').feature('wp1').geom.feature('b1').set('degree',  {'1'  '1'  '1'
'1'});
model.geom('geom1').feature('wp1').geom.feature('b1').set('w', {'1' '1' '1' '1' '1'
'1' '1' '1'});
model.geom('geom1').feature('wp1').geom.feature('mir2').set('keep', true);
model.geom('geom1').feature('wp1').geom.feature('mir2').set('axis', {'0' '1'});
model.geom('geom1').feature('wp1').geom.feature('mir2').set('pos', {'0' '25'});
model.geom('geom1').feature('wp1').geom.feature('mir2').selection('input').set({'b1
'});
model.geom('geom1').feature('wp1').geom.feature('r3').set('base', 'center');
model.geom('geom1').feature('wp1').geom.feature('r3').set('pos',      {'-200-(Lc/2)'
'25'});
model.geom('geom1').feature('wp1').geom.feature('r3').set('size', {'Lc' 'wL'});
model.geom('geom1').feature('wp1').geom.feature('r4').set('pos', {'-300-Li' '0'});
model.geom('geom1').feature('wp1').geom.feature('r4').set('size', {'100' '50'});
model.geom('geom1').feature('wp1').geom.feature('mov27').set('displx', '-delta');
model.geom('geom1').feature('wp1').geom.feature('mov27').selection('input').set({'r
4'});
model.geom('geom1').feature('wp1').geom.feature('b3').set('p',  {'-55'  '0'  '160'  '-
40'; '75' '50' '50' '75+w'});
```

```
model.geom('geom1').feature('wp1').geom.feature('b3').set('degree', {'1' '1' '1'});
model.geom('geom1').feature('wp1').geom.feature('b3').set('w', {'1' '1' '1' '1' '1'
'1'});
model.geom('geom1').feature('wp1').geom.feature('mir5').set('keep', true);
model.geom('geom1').feature('wp1').geom.feature('mir5').set('axis', {'0' '1'});
model.geom('geom1').feature('wp1').geom.feature('mir5').set('pos', {'0' '25'});
model.geom('geom1').feature('wp1').geom.feature('mir5').selection('input').set({'b3
'});
model.geom('geom1').feature('wp1').geom.feature('r5').set('pos',          {'xpillar'
'hpillar'});
model.geom('geom1').feature('wp1').geom.feature('r5').set('size',       {'post_size'
'post_size'});
model.geom('geom1').feature('wp1').geom.feature('arr1').set('type', 'linear');
model.geom('geom1').feature('wp1').geom.feature('arr1').set('size', 'N');
model.geom('geom1').feature('wp1').geom.feature('arr1').set('displ',
{'post_size+gap_size' '0'});
model.geom('geom1').feature('wp1').geom.feature('arr1').selection('input').set({'r5
'});
model.geom('geom1').feature('wp1').geom.feature('uni3').name('posts');
model.geom('geom1').feature('wp1').geom.feature('uni3').selection('input').set({'ar
r1'});
model.geom('geom1').feature('wp1').geom.feature('rot2').set('rot', '-phi');
model.geom('geom1').feature('wp1').geom.feature('rot2').set('pos',       {'-200[um]'
'hpillar+7.5[um]'});
model.geom('geom1').feature('wp1').geom.feature('rot2').selection('input').set({'un
i3'});
model.geom('geom1').feature('wp1').geom.feature('mov28').set('disply',            '-
hpillar+50[um]');
model.geom('geom1').feature('wp1').geom.feature('mov28').selection('input').set({'r
ot2'});
model.geom('geom1').feature('wp1').geom.feature('mir3').set('keep', true);
model.geom('geom1').feature('wp1').geom.feature('mir3').set('axis', {'0' '1'});
model.geom('geom1').feature('wp1').geom.feature('mir3').set('pos', {'0' '25'});
model.geom('geom1').feature('wp1').geom.feature('mir3').selection('input').set({'mo
v28'});
model.geom('geom1').feature('wp1').geom.feature('b4').set('p',  {'-200'  '-33'  '-55'
'-200' '-200'; '65' '65' '75' '75' '65'});
model.geom('geom1').feature('wp1').geom.feature('b4').set('degree',  {'1'  '1'  '1'
'1'});
model.geom('geom1').feature('wp1').geom.feature('b4').set('w', {'1' '1' '1' '1' '1'
'1' '1' '1'});
model.geom('geom1').feature('wp1').geom.feature('mir6').set('keep', true);
model.geom('geom1').feature('wp1').geom.feature('mir6').set('axis', {'0' '1'});
model.geom('geom1').feature('wp1').geom.feature('mir6').set('pos', {'0' '25'});
model.geom('geom1').feature('wp1').geom.feature('mir6').selection('input').set({'b4
'});
model.geom('geom1').feature('wp1').geom.feature('r6').set('pos', {'-200' '50'});
model.geom('geom1').feature('wp1').geom.feature('r6').set('size', {'5' '15'});
model.geom('geom1').feature('wp1').geom.feature('mir7').set('keep', true);
model.geom('geom1').feature('wp1').geom.feature('mir7').set('axis', {'0' '1'});
model.geom('geom1').feature('wp1').geom.feature('mir7').set('pos', {'0' '25'});
model.geom('geom1').feature('wp1').geom.feature('mir7').selection('input').set({'r6
'});
model.geom('geom1').feature('wp1').geom.feature('uni4').set('edge', 'all');
model.geom('geom1').feature('wp1').geom.feature('uni4').set('intbnd', false);
model.geom('geom1').feature('wp1').geom.feature('uni4').selection('input').set({'b1
' 'b3' 'b4' 'mir2' 'mir5' 'mir6' 'mir7' 'mov27' 'r1' 'r3'  ...
'r6'});
model.geom('geom1').feature('wp1').geom.feature('b5').set('p',  {'-33'  '0'  '-33';
'50' '50' '65'});
model.geom('geom1').feature('wp1').geom.feature('b5').set('degree', {'1' '1'});
model.geom('geom1').feature('wp1').geom.feature('b5').set('w', {'1' '1' '1' '1'});
model.geom('geom1').feature('wp1').geom.feature('mir8').set('keep', true);
model.geom('geom1').feature('wp1').geom.feature('mir8').set('axis', {'0' '1'});
model.geom('geom1').feature('wp1').geom.feature('mir8').set('pos', {'0' '25'});
```

```
model.geom('geom1').feature('wp1').geom.feature('mir8').selection('input').set({'b5
'});
model.geom('geom1').feature('wp1').geom.feature('uni5').set('edge', 'all');
model.geom('geom1').feature('wp1').geom.feature('uni5').set('intbnd', false);
model.geom('geom1').feature('wp1').geom.feature('uni5').selection('input').set({'b5
' 'mir8' 'uni4'});
model.geom('geom1').feature('wp1').geom.feature('r7').set('pos', {'-40' '50'});
model.geom('geom1').feature('wp1').geom.feature('r7').set('size', {'7' '15'});
model.geom('geom1').feature('wp1').geom.feature('mir9').set('keep', true);
model.geom('geom1').feature('wp1').geom.feature('mir9').set('axis', {'0' '1'});
model.geom('geom1').feature('wp1').geom.feature('mir9').set('pos', {'0' '25'});
model.geom('geom1').feature('wp1').geom.feature('mir9').selection('input').set({'r7
'});
model.geom('geom1').feature('wp1').geom.feature('uni6').set('edge', 'all');
model.geom('geom1').feature('wp1').geom.feature('uni6').set('intbnd', false);
model.geom('geom1').feature('wp1').geom.feature('uni6').selection('input').set({'mi
r9' 'r7' 'uni5'});
model.geom('geom1').feature('wp1').geom.feature('dif1').selection('input2').set({'m
ir3' 'mov28'});
model.geom('geom1').feature('wp1').geom.feature('dif1').selection('input').set({'un
i6'});
model.geom('geom1').feature('ext1').setIndex('distance', '20', 0);
model.geom('geom1').feature('ext1').selection('input').set({'wp1'});

model.geom('geom1').feature.create('boxsel1', 'BoxSelection');
model.geom('geom1').feature('boxsel1').set('entitydim', '2');
model.geom('geom1').feature('boxsel1').set('zmax', '10');
model.geom('geom1').feature('boxsel1').set('xmin', '320');
model.geom('geom1').feature('boxsel1').set('ymin', '10');
model.geom('geom1').feature('boxsel1').set('xmax', '320');
model.geom('geom1').feature('boxsel1').set('zmin', '5');
model.geom('geom1').feature('boxsel1').set('ymax', '40');


model.geom('geom1').run
%
model.view.create('view3', 2);
model.view.create('view4', 2);
model.view.create('view5', 2);
model.view.create('view6', 2);
model.view.create('view7', 2);
model.view.create('view8', 'geom1');

model.material.create('mat1');
model.material('mat1').propertyGroup('def').func.create('eta', 'Piecewise');
model.material('mat1').propertyGroup('def').func.create('Cp', 'Piecewise');
model.material('mat1').propertyGroup('def').func.create('rho', 'Piecewise');
model.material('mat1').propertyGroup('def').func.create('k', 'Piecewise');
model.material('mat1').propertyGroup('def').func.create('cs', 'Interpolation');

model.physics.create('spf', 'LaminarFlow', 'geom1');
model.physics('spf').feature.create('inl1', 'Inlet', 2);
model.physics('spf').feature('inl1').selection.set([1]);
model.physics('spf').feature.create('out1', 'OutletBoundary', 2);
model.physics('spf').feature('out1').selection.named('geom1_boxsel1');

%MESH

model.mesh.create('mesh1', 'geom1');
model.mesh('mesh1').feature.create('ftet1', 'FreeTet');

% MATERIAL DEFINITION

model.material('mat1').name('Water');
```

```
model.material('mat1').propertyGroup('def').func('eta').set('pieces',      {'273.15'
'413.15'         '1.3799566804-0.021224019151*T^1+1.3604562827E-4*T^2-4.6454090319E-
7*T^3+8.9042735735E-10*T^4-9.0790692686E-13*T^5+3.8457331488E-16*T^6';      '413.15'
'553.75' '0.00401235783-2.10746715E-5*T^1+3.85772275E-8*T^2-2.39730284E-11*T^3'});
model.material('mat1').propertyGroup('def').func('eta').set('arg', 'T');
model.material('mat1').propertyGroup('def').func('Cp').set('pieces',       {'273.15'
'553.75'   '12010.1471-80.4072879*T^1+0.309866854*T^2-5.38186884E-4*T^3+3.62536437E-
7*T^4'});
model.material('mat1').propertyGroup('def').func('Cp').set('arg', 'T');
model.material('mat1').propertyGroup('def').func('rho').set('pieces',      {'273.15'
'553.75' '838.466135+1.40050603*T^1-0.0030112376*T^2+3.71822313E-7*T^3'});
model.material('mat1').propertyGroup('def').func('rho').set('arg', 'T');
model.material('mat1').propertyGroup('def').func('k').set('pieces',        {'273.15'
'553.75' '-0.869083936+0.00894880345*T^1-1.58366345E-5*T^2+7.97543259E-9*T^3'});
model.material('mat1').propertyGroup('def').func('k').set('arg', 'T');
model.material('mat1').propertyGroup('def').func('cs').set('table',  {'273'  '1403';
'278' '1427'; '283' '1447'; '293' '1481'; '303' '1507'; '313' '1526'; '323' '1541';
'333' '1552'; '343' '1555'; '353' '1555';  ...
'363' '1550'; '373' '1543'});
model.material('mat1').propertyGroup('def').func('cs').set('interp',
'piecewisecubic');
model.material('mat1').propertyGroup('def').set('dynamicviscosity',
'eta(T[1/K])[Pa*s]');
model.material('mat1').propertyGroup('def').set('ratioofspecificheat', '1.0');
model.material('mat1').propertyGroup('def').set('electricconductivity',      {'5.5e-
6[S/m]' '0' '0' '0' '5.5e-6[S/m]' '0' '0' '0' '5.5e-6[S/m]'});
model.material('mat1').propertyGroup('def').set('heatcapacity',
'Cp(T[1/K])[J/(kg*K)]');
model.material('mat1').propertyGroup('def').set('density', 'rho(T[1/K])[kg/m^3]');
model.material('mat1').propertyGroup('def').set('thermalconductivity',
{'k(T[1/K])[W/(m*K)]'    '0'    '0'    '0'    'k(T[1/K])[W/(m*K)]'    '0'    '0'    '0'
'k(T[1/K])[W/(m*K)]'});
model.material('mat1').propertyGroup('def').set('soundspeed', 'cs(T[1/K])[m/s]');
model.material('mat1').propertyGroup('def').addInput('temperature');


%%%PHYSICS DEFINITION

model.physics('spf').prop('CompressibilityProperty').set('Compressibility',
'Incompressible');
model.physics('spf').feature('inl1').set('V0', 'sample_flow_rate');
model.physics('spf').feature('inl1').set('LaminarInflowOption', 'V0');
model.physics('spf').feature('inl1').set('BoundaryCondition', 'LaminarInflow');


%% MESH RUN

model.mesh('mesh1').feature('size').set('table', 'cfd');
model.mesh('mesh1').run;


model.frame('material1').sorder(1);
model.study.create('std1');
model.study('std1').feature.create('stat', 'Stationary');

model.sol.create('sol1');
model.sol('sol1').study('std1');
model.sol('sol1').attach('std1');
model.sol('sol1').feature.create('st1', 'StudyStep');
model.sol('sol1').feature.create('v1', 'Variables');
model.sol('sol1').feature.create('s1', 'Stationary');
model.sol('sol1').feature('s1').feature.create('fc1', 'FullyCoupled');
model.sol('sol1').feature('s1').feature.create('d1', 'Direct');
model.sol('sol1').feature('s1').feature.remove('fcDef');
```

```
model.study('std1').feature('stat').set('initstudyhide', 'on');
model.study('std1').feature('stat').set('initsolhide', 'on');
model.study('std1').feature('stat').set('notstudyhide', 'on');
model.study('std1').feature('stat').set('notsolhide', 'on');

model.result.dataset.create('cpl1', 'CutPlane');
model.result.export.create('data1', 'Data');

model.sol('sol1').attach('std1');
model.sol('sol1').feature('st1').name('Compile Equations: Stationary');
model.sol('sol1').feature('st1').set('studystep', 'stat');
model.sol('sol1').feature('v1').set('control', 'stat');
model.sol('sol1').feature('s1').set('control', 'stat');

model.sol('sol1').feature('s1').feature('fc1').set('initstep', '0.01');
model.sol('sol1').feature('s1').feature('fc1').set('minstep', '1.0E-6');
model.sol('sol1').feature('s1').feature('d1').set('linsolver', 'pardiso');
model.sol('sol1').runAll;

model.result.dataset('cpl1').set('quickx', '-40');

%Cut plan Export

model.result.export('data1').set('data', 'cpl1');
model.result.export('data1').set('location', 'grid');
model.result.export('data1').set('gridx2', 'range(-(wL-50)/2,0.25,-15)');
model.result.export('data1').set('header', false);
model.result.export('data1').set('descr', {'Velocity magnitude'});
model.result.export('data1').set('gridy2', 'range(0,0.25,20)');
model.result.export('data1').set('filename', nomefile2);
model.result.export('data1').set('unit', {'m/s'});
model.result.export('data1').set('expr', {'spf.U'});
model.result.export('data1').run;

model.result.export('data1').set('data', 'cpl1');
model.result.export('data1').set('location', 'grid');
model.result.export('data1').set('gridx2', 'range(0,0.25,50)');
model.result.export('data1').set('header', false);
model.result.export('data1').set('descr', {'Velocity magnitude'});
model.result.export('data1').set('gridy2', 'range(0,0.25,20)');
model.result.export('data1').set('filename', nomefile1);
model.result.export('data1').set('unit', {'m/s'});
model.result.export('data1').set('expr', {'spf.U'});
model.result.export('data1').run;

out = model;
```

7.2 Particle Image Velocimetry Analysis (PIV)

The following Matlab code has been written in order to perform a Particle Image Velocimetry Analysis (PIV), the technique that allows to measure instantaneous velocity fields using images of particles moving into the field.

```
% IMPORT DATA
v=importdata('C:\...path');
v.dat=squeeze(v.dat);
[R C Nframe]=size(v.dat);

ts=(v.t(end)-v.t(1))/Nframe;

dp=7.4; %PIXEL SIZE OF THE CAMERA SENSOR
```

```
Magn=10; %OBJECTIVE USE DFOR THE EXPERIMENT
dp_obj=dp/Magn;

%TIME BETWWEN TO CONSECUTIVE FRAMES
for i=1:Nframe-1
dt(i)=v.t(i+1)-v.t(i);
end

%IMAGE BACKGROUND DEFINITION
bck=sum(v.dat,3)./Nframe;

%BACKGROUND SUBCTRACTION
for i=1:Nframe
    f(:,:,i)=1-double(v.dat(:,:,i))./bck;
end

%FIELD UNDER ANALYIS
y1=1;y2=480; x1=1;x2=640;

for i=1:Nframe
    fr(:,:,i)=f(y1:y2,x1:x2,i);
end

%DEFINITION OF THE NUMBER OF BOXES IN WHICH THE TOTAL FIELD OF VIEW IS DIVIDED
N=20; p=round((y2-y1)/N);
ms=14; M=round((x2-x1)/ms);

l=1; m=1;j=1;

for h=1:2*N-1
    a=1;
    l=1;
for r=1:2*M-1
     ccs=zeros(2*p+1,2*ms-1);
 for i=1:Nframe-1
       f1=fr(m:m+p,a:a+ms-1,i);
       f2=fr(m:m+p,a:a+ms-1,i+1);

    %CROSS_CORRELATION MATRIX
    cc=xcorr2(f2,f1);

ccs=cc+ccs;

end

mcc=ccs./(Nframe-1);
 [vmaxc pmaxc(j,l)]=max(max(mcc));
 mcc1=mcc';
[vmayc pmayc(j,l)]=max(max(mcc1));

l=l+1;
 a=a+(ms)/2;

end
m=m+((p+1)/2);
j=j+1;

end

[R1 C1]=size(cc);
 c0=[(C1-1)/2,(R1-1)/2];

%PARTCLES DISPLACEMENT ESTIMATION
dx=pmaxc-c0(1);
dy=pmayc-c0(2);
```

```
%PARTCLES VELOCITY ESTIMATION

vmx=(dx*dp_obj)/mean(dt);
vmy=(dy*dp_obj)/mean(dt);
```

7.3 Particles Position Analysis

The following Matlab code has been written in order to evaluate particles or cells position in the analyzed images.

```
%IMPORT DATA
 v=VideoReader('C:\path');

fps=1200;ts=1/fps;%%%frame rate

a=read(v);b=squeeze(a(:,:,1,:));b=double(b);
nframe=size(b);
Nframe=nframe(3);

%BACKGROUND DEFINITION
bck=sum(b,3)./Nframe;

for i=1:Nframe
    f(:,:,i)=1-(b(:,:,i))./bck;
end

%FIELD UNDER ANALYIS
y1=1; y2=480;
x1=1; x2=640;

[Row,Col]=size(bck);


%MAKE BINARY EACH FRAME
h=1;

for i=1:Nframe

[junk, threshold] = edge(f(y1:y2,x1:x2,i), 'Canny');
fudgeFactor1 =5;

if threshold(2)*fudgeFactor1>1
     threshold(2)=0.999/fudgeFactor1;
 end

BWs1(:,:,h)= edge(f(y1:y2,x1:x2,i),'Canny', threshold*fudgeFactor1 );
BWs2(:,:,h)= bwareaopen(BWs1(:,:,h),50);

se90 = strel('line',2, 90);
se0 = strel('line',2, 0);

BWsdil1(:,:,h) = imdilate(BWs1(:,:,h), [se90 se0]);

BWdfill1(:,:,h)= imfill(BWsdil1(:,:,h), 'holes');
BWnobord(:,:,h) = imclearborder(BWdfill1(:,:,h), 4);
BWdfill2(:,:,h)=bwareaopen(BWnobord(:,:,h),50);

h=h+1;

end
```

```
%ANALYZE THE BINARY IMAGES AND FIND THE CENTROIDS OF THE OBJECTS
l=1;
sumbeads=0;

for i=1:1500

    f1=BWdfill2(:,:,i);

    b_count1=regionprops(f1,'basic','Centroid');

    [n1,z]=size(b_count1);

    s_beads1(i)=n1;

    sumbeads=sumbeads+n1;

    if n1~=0
        for g=1:n1
            vposy(l,1)=b_count1(g).Centroid(1);
            vposy(l,2)=b_count1(g).Centroid(2);
         vposy(l,3)=i;
        l=l+1;
        end

     if n1~=0
        angular=regionprops(f1,'Orientation');
        for g=1:n1
            vangle(l,1)=i;
            vangle(l,2)=angular(g).Orientation;

        l=l+1;
        end


    end
```